

**Development of target antigen-displaying virus-like
particles (VLPs) for the generation of antibodies
using hybridoma technology**

Von der Naturwissenschaftlichen Fakultät der Gottfried Wilhelm Leibniz
Universität Hannover

zur Erlangung des Grades
Doktorin der Naturwissenschaften (Dr. rer. nat.)

genehmigte Dissertation
von
Stefanie Schatz, M. Sc. RWTH

2024

Referent:	Prof. Dr. rer. nat. Thomas Scheper
Koreferent:	Prof. Dr. rer. nat. Sascha Beutel
Koreferent	Prof. Dr. phil. nat. Jörn Stitz
Tag der Promotion:	19. Januar 2024

Abstract

Formaldehyde-fixed, paraffin-embedded (FFPE) cell and tissue samples are of great importance for immunohistochemical studies of histological specimens. However, antibodies for FFPE samples pose a challenge to antibody discovery as current immunization strategies rely predominantly on soluble proteins that cannot adequately reflect the changes in target antigens during the FFPE process. Enveloped virus-like particles (VLPs) allow for the presentation of membrane-anchored target antigens on the VLP surface and elicit a strong target antigen-specific antibody response after immunization. This proof-of-concept study presents a novel FFPE-like fixation methodology for VLP preparation aiming at the generation of FFPE-compatible monoclonal antibodies (mAbs). Human 293-F-derived VLP-producing suspension cell pools were established to produce human immunodeficiency virus (HIV)-like particles decorated with the truncated human low affinity nerve growth factor receptor (trNGFR) as model antigen. The trNGFR antigen was efficiently incorporated into VLPs with an average of 284 ± 24 trNGFR molecules per VLP. To develop a fixation protocol applicable to VLPs, trNGFR-expressing cells were subjected to a variety of fixation treatments. Changes in epitopes introduced by fixation were monitored using two mAbs recognizing either an epitope present in native NGFR or an epitope present in native and FFPE NGFR. The novel simplified fixation procedure consisted of only formaldehyde and 90 °C heat fixation (FF90). Transmission electron microscopic and dynamic light scattering analysis of FF90 VLPs revealed that the fixed VLPs withstood the FF90 treatment and showed no morphological changes, allowing for the FF90 trNGFR-VLPs to be used to immunize mice for hybridoma cell generation.

Hybridoma clones were screened for mAbs specifically recognizing native, FF90 and FFPE trNGFR-expressing cells in a flow cytometric assay. The isolated hybridoma mAbs did not recognize native epitopes but were reactive with FF90 and FFPE epitopes. The use of FF90-trNGFR VLPs for immunization led to the discovery of nine FFPE-NGFR-specific mAbs. This proof-of-concept study demonstrated that FF90-treated VLPs decorated with a membrane-anchored target antigen are suitable antigens to preferentially generate FFPE-compatible mAbs. The FF90-VLP platform should be useful for the future discovery of specific mAbs directed against a variety of FFPE cell surface antigens.

Keywords: virus-like particle, VLP, antibody discovery, formalin-fixed paraffin-embedded, FFPE, hybridoma, antigen display

Kurzfassung

Formaldehyd-fixierte, Paraffin-eingebettete (FFPE) Zell- und Gewebeproben sind für die immun-histochemische Untersuchung histologischer Präparate von großer Bedeutung. Die Entwicklung neuer Antikörper für FFPE-Proben stellt jedoch eine Herausforderung dar. Die gegenwärtigen Immunisierungsstrategien basieren hauptsächlich auf löslichen Proteinen, die die Veränderungen der Zielantigene während des FFPE-Prozesses jedoch nur ungenügend abbilden können. Umhüllte virusartige Partikel (VLPs) ermöglichen die Präsentation von membranverankerten Zielantigenen auf der VLP-Oberfläche und rufen nach Immunisierung eine starke zielantigenspezifische Antikörperreaktion hervor. In der vorliegenden Arbeit wird eine neuartige FFPE-ähnliche Fixierungsmethode für VLP-basierte Antigene zur Generierung von FFPE-kompatiblen monoklonalen Antikörpern (mAb) vorgestellt.

Von humanen 293-F-abgeleitete, VLP-produzierende Suspensionszellen wurden hergestellt, um humane Immundefizienz-Virus (HIV)-basierte VLPs zu produzieren, die mit dem Modellantigen trunkierter humaner Nervenwachstumsfaktor-Rezeptor (trNGFR) dekoriert waren. Die VLPs präsentierten durchschnittlich 284 ± 24 trNGFR-Moleküle pro VLP. Zur Entwicklung eines vereinfachten Fixierungsprotokolls wurden trNGFR-exprimierende Zellen verschiedenen Fixierungsbehandlungen unterzogen. Die durch die Fixierung hervorgerufenen Veränderungen an trNGFR wurden mit zwei mAbs überwacht, von denen einer spezifisch für ein natives Epitop ist und der andere ein Epitop erkennt, das sowohl im nativen als auch FFPE-Antigen vorkommt. Das neue vereinfachte Fixierungsprotokoll besteht lediglich aus Formaldehydfixierung mit anschließender 90 °C-Hitzefixierung (FF90). Elektronenmikroskopische und dynamische Lichtstreuungsanalysen der VLPs zeigten, dass die VLPs gegenüber der FF90-Behandlung stabil waren und keine morphologischen Veränderungen aufwiesen, so dass die FF90-trNGFR-VLPs zur Immunisierung von Mäusen zur Generierung von Hybridomzellen verwendet werden konnten.

Die Hybridom-Klone wurden in einem durchflusszytometrischen Verfahren auf mAbs untersucht, die spezifisch native, FF90- und FFPE-trNGFR-exprimierende Zellen erkennen. Die untersuchten Hybridom-mAbs erkannten keine nativen Epitope, waren aber reaktiv gegenüber FF90- und FFPE-Epitopen. Die Verwendung von FF90-trNGFR-VLPs zur Immunisierung führte zur Entdeckung von neun FFPE-NGFR-spezifischen mAbs. Dieser Konzeptnachweis hat gezeigt, dass FF90-behandelte VLPs, die mit einem membranverankerten Zielantigen dekoriert sind, geeignet sind, um FFPE-kompatible mAbs zu erzeugen. Die FF90-VLP-Plattform sollte für die zukünftige Entwicklung von spezifischen mAbs gegen eine Vielzahl von FFPE-Zelloberflächenantigenen nützlich sein.

Schlagwörter: virusartige Partikel, VLP, Antikörperentwicklung, formalin-fixiert paraffin-eingebettet, FFPE, Hybridoma, Antigenpräsentation

Table of Contents

Abstract	iii
Kurzfassung	iv
Table of Contents	v
List of Abbreviations	viii
1. Introduction and Aim	1
2. Theoretical Background	4
2.1. Antibody discovery technologies	4
2.1.1. <i>In vitro</i> display technologies	4
2.1.2. Immunization-dependent mAb discovery	6
2.2. Basics of adaptive immune responses	8
2.3. Antigen formats	10
2.3.1. Soluble antigens	11
2.3.2. Particulate antigens	11
2.4. Virus-like particles (VLPs)	12
2.4.1. Structure and morphology	13
2.4.2. Gag assembly and VLP formation	14
2.4.3. VLPs as immunogens	15
3. Results	18
3.1. Establishment and characterization of VLP producer cell pools	18
3.1.1. 293-F/Mos1.Gag/trNGFR, 293-F/Mos1.Gag and 293-F cells express NGFR	18
3.1.2. Recombinant trNGFR but not wild-type NGFR is incorporated into HIV- derived VLPs	19
3.2. Development of a fixation protocol for antigen preparation	22
3.2.1. Formaldehyde and heat fixation induces a loss of epitope recognition by the "native" anti-NGFR mAb while maintaining recognition by the corresponding FFPE-compatible mAb	23

Table of Contents

3.2.2. FF90 treatment induces the appearance of epitopes recognizable by FFPE-compatible antibodies	24
3.2.3. FF90 VLPs maintain their integrity and morphology after formaldehyde and heat fixation at 90 °C	26
3.3. Generation and screening of monoclonal antibodies	27
3.3.1. Screening strategy for antibodies	27
3.3.2. FF90 trNGFR-VLP immunization elicits blood IgG antibodies that bind to FF90 3T3/Gag/trNGFR cells	28
3.3.3. FF90 trNGFR-VLP immunization generates hybridoma antibodies that recognize FF90 3T3/Gag/trNGFR cells	30
3.3.4. The majority of generated hybridoma antibodies is also specific for FFPE 3T3/Gag/trNGFR cells	33
4. Discussion	36
5. Materials and Methods	42
5.1. Materials	42
5.1.1. List of chemicals and consumables	42
5.1.2. List of antibodies	45
5.1.3. Equipment and software list	47
5.1.4. Compositions of buffers and solutions	48
5.2. Plasmids	49
5.2.1. Design of the transposase expression vectors	49
5.2.2. Design of the transposon donor vectors	51
5.3. Cell culture	52
5.3.1. Cell lines, media and culture conditions	52
5.3.2. Establishment of stable recombinant cells	53
5.3.3. VLP production, concentration and storage	54
5.4. Fixation of cells and VLPs	55
5.4.1. Formaldehyde, ethanol and heat treatment of single cells	55
5.4.2. Formaldehyde-fixed paraffin-embedded single cell preparation	55
5.4.3. Preparation of formaldehyde-fixed and 90 °C-fixed VLPs	56
5.5. Characterization of cells and VLPs	56
5.5.1. Flow cytometric analysis of cells	56
5.5.2. Protein quantitation	57
5.5.3. VLP capture assay	58
5.5.4. Western blotting	59
5.5.5. Dynamic light scattering measurement	59

Table of Contents

5.5.6. Transmission electron microscopic imaging	59
5.5.7. Statistics	60
5.6. Generation and screening of antibodies	60
5.6.1. Immunization of mice	60
5.6.2. Generation of hybridoma cells	60
5.6.3. Flow cytometric screening	61
6. References	63
List of Figures	81
List of Tables	83
Appendix	84
A. Supplementary data	85
A.1. Plasmid maps	85
A.2. NGFR staining of recombinant cells	87
A.3. IgM antibodies in blood samples	88
A.4. Results of positive hybridoma supernatants identified in the first screening	89
B. Standard lab protocols	99
B.1. SDS-PAGE	99
B.2. Blotting	103
C. Acknowledgements	105
D. Curriculum vitae	106
E. List of publications	108

List of Abbreviations

APCy	allophycocyanin	FITC	fluorescein isothiocyanate
APC	antigen-presenting cell	FSC-A	forward scatter area
BCR	B cell receptor	Gag	group-specific antigen
BSA	bovine serum albumin	HAT	hypoxanthine-aminopterin-thymidine
CA	capsid	HIV	human immunodeficiency virus
CD	cluster of differentiation	HRP	horseradish peroxidase
CDS	coding sequence	hyPBase	hyperactive <i>piggyBac</i> transposase
CFSN	cell-free supernatant	IHC	immunohistochemistry
DC	dendritic cell	Ig	immunoglobulin
DLS	dynamic light scattering	IN	integrase
EDTA	ethylenediaminetetraacetic acid	IVS	synthetic intron
ELISA	enzyme-linked immunosorbent assay	IRES	internal ribosomal entry site
ESCRT	endosomal sorting complexes required for transport	MA	matrix
Fab	antigen-binding fragment	mAb	monoclonal antibody
FBS	fetal bovine serum	MCS	multiple cloning site
FDC	follicular dendritic cell	MFI	mean fluorescent intensity
FF90	formaldehyde- and 90 °C-fixed	MHC	major histocompatibility complex
FFPE	formaldehyde-fixed paraffin-embedded	Mos1.Gag	mosaic Gag
		NGFR	nerve growth factor receptor

NC	nucleocapsid	SB	<i>Sleeping Beauty</i>
p55-Gag	Gag precursor polyprotein	scFv	single chain variable fragment
PB	<i>piggyBac</i>	SDS-PAGE	sodium dodecyl sulphate-polyacrylamide gel electrophoresis
PBMCs	peripheral blood mononuclear cells	SI	stain index
PCR	polymerase chain reaction	SOP	standard operating procedure
PdI	polydispersity index	SSC-A	side scatter area
PE	phycoerythrin	TCR	T cell receptor
PEI	polyethylenimine	TEM	transmission electron microscopy
PI(4,5)P₂	phosphatidylinositol-(4,5)-bisphosphate	TLR	toll-like receptor
PR	viral protease	trNGFR	truncated human low affinity nerve growth factor receptor
PRR	pattern recognition receptor	TIR	terminal inverted repeat
PVDF	polyvinylidene fluoride	VCD	viable cell density
RRID	research resource identifier	VLP	virus-like particle
RT	reverse transcriptase	WPRE	woodchuck hepatitis virus post transcriptional element
PAMP	pathogen-associated molecular pattern		

1. Introduction and Aim

For decades, antibodies represent the leading protein class of biopharmaceuticals [Walsh 2018; Walsh and Walsh 2022] and are important reagents in many fields of science and medicine. Their ability to specifically bind to a wide range of biomolecules renders them invaluable tools for therapeutic, diagnostic and research purposes. For most diagnostic and therapeutic applications monoclonal antibodies (mAbs) that recognize a specific epitope present on a single antigen are preferred to polyclonal antibodies consisting of a heterogeneous mixture of undefined mAbs.

Diagnostic mAbs are used for the specific detection and quantitation of target antigens in, for example, immunoassays, flow cytometry and immunohistochemical (IHC) examinations of histological specimens such as tumor biopsies [Gao et al. 2018]. These specimens are often preserved as formaldehyde-fixed paraffin-embedded (FFPE) tissues in paraffin blocks and represent an enormous source of material for research studies [Gaffney et al. 2018; Tucker et al. 2019]. However, many mAbs are designed for living cells and native conditions and therefore may not work in applications involving FFPE antigens as recently demonstrated [Haverkamp et al. 2019]. Therapeutic mAbs specific for the native Middle East Respiratory Syndrome coronavirus spike protein were examined for their ability to recognize their respective antigen in FFPE tissue samples. Of the eight mAbs tested, only three mAbs bound specifically to FFPE-treated spike proteins [Haverkamp et al. 2019].

Tissues and samples subjected to the FFPE process are first fixed using formaldehyde solution, followed by a step-wise dehydration in alcohol solutions, clearing in xylene and embedding in paraffin wax. The FFPE procedure leads to chemical modifications of amino acids introduced by formaldehyde, cross-linking of proteins and formation of protein aggregates [Werner et al. 2000; Thavarajah et al. 2012]. These modifications result in the generation of new epitopes and the masking of pre-existing epitopes so that many antibodies instrumental in the staining of native tissues lose their ability to recognize their epitope in FFPE tissues. Therefore, there is a great need to develop FFPE-compatible mAbs.

Commonly used strategies to generate FFPE-compatible murine mAbs for diagnostic and research applications are based on immunization of mice using denatured soluble proteins and subsequent hybridoma generation [Wang et al. 2005; O'Shannessy et al. 2011; Hatano et al. 2014; Hatano

et al. 2019; Kurokawa and Yamamoto 2022; Suzuki et al. 2023]. Although several suitable mAbs have been identified using this approach, the use of soluble antigens requires many immunizations and often extensive screening. The formulation of soluble antigens poses particular challenges for weak immunogens and complex membrane-anchored surface antigens [Dodd et al. 2018]. The latter can only be solubilized by deletion or truncation of the hydrophobic domains frequently mutilating the structure of the antigen. Enveloped virus-like particles (VLPs) offer an attractive solution as they facilitate the incorporation of conformationally authentic cell surface antigens into the VLP membrane. Furthermore, VLPs are known to be highly immunogenic and effective in eliciting an antibody response against the displayed target antigen [Deml et al. 2005; Nooraei et al. 2021; Gonelli et al. 2021]. Consequently, VLPs presenting cell surface antigens at high densities and subjected to FFPE-like fixation prior to immunization could be instrumental in the generation of FFPE-compatible mAbs using hybridoma technology.

This thesis aimed at the development of a novel FFPE-like VLP-based cell surface antigen delivery system to discover FFPE-compatible mAbs in a proof of concept study. To achieve this, the following objectives were pursued:

1. For the production of human immunodeficiency virus (HIV)-derived VLPs decorated with the model target antigen truncated human low affinity nerve growth factor receptor (trNGFR), recombinant 293-F VLP producer suspension cells were established using transposon vector-mediated gene transfer of HIV-1 group-specific antigen (Gag)- and trNGFR-encoding donor vectors. The generated cell pools were analyzed for VLP formation and trNGFR expression using flow cytometry as well as Gag- and NGFR-specific enzyme-linked immunosorbent assays (ELISAs). In addition, trNGFR incorporation into VLPs was assessed employing a VLP capture assay.
2. As the preparation of FFPE-fixed VLPs is very challenging and paraffin embedding and subsequent extraction of VLPs is not possible, a simplified fixation methodology for FFPE-like antigen preparation had to be developed. For this purpose, different treatments mimicking steps of the FFPE procedure were assessed using 293-F cells expressing trNGFR and two mAbs recognizing either the native target antigen or both, the native and FFPE antigen. The effect of the tested fixation protocols on mAb reactivity was monitored using flow cytometric analysis of the fixed cells. The identified novel fixation protocol was further evaluated for additional antigens present on peripheral blood mononuclear cells (PBMCs). To investigate the effect of the fixation treatment on VLP morphology and integrity, native and fixed VLP preparations were compared using dynamic light scattering (DLS) measurement and transmission electron microscopy (TEM).

3. The suitability of formaldehyde- and 90 °C-fixed (FF90) trNGFR-VLP antigens for the generation of FFPE-compatible mAbs was assessed by immunization of mice with three and four doses of FF90 trNGFR-VLPs, respectively. The antibody response in blood plasma was analyzed for native and FF90-reactive immunoglobulin (Ig)G and IgM antibodies before hybridoma cells were generated. The hybridoma clones were screened for mAbs specifically recognizing native, FF90 and FFPE trNGFR-expressing screening cells employing flow cytometry.

2. Theoretical Background

2.1. Antibody discovery technologies

Basically, two main strategies to mAb discovery can be distinguished: a) immunization-independent *in vitro* technologies relying on the generation of antibody display libraries and b) immunization-dependent *in vivo* technologies based on the isolation of animal- or human-derived B cells (Figure 2.1). Immunization-dependent strategies can be further separated into the single B cell technology and the traditional hybridoma technology.

2.1.1. *In vitro* display technologies

Display technologies allow for the construction of very large libraries in which various antibodies or fragments thereof are displayed on cell- or virus-derived particles and screened for reactivity to a specific antigen. Phage libraries arose as the first platform in the early 1990s displaying antibody fragments [McCafferty et al. 1990; Breitling et al. 1991; Barbas et al. 1991]. Antibody display libraries are classified as universal or immune libraries [Valldorf et al. 2022]. Universal libraries consist of either antibody fragment coding sequences (CDSs) derived from natural sources representing animal or human antibody repertoires (naïve libraries), *in silico* constructed sequences (synthetic libraries) or a combination of both (semi-synthetic libraries), whereas immune libraries are generated from pre-immunized animals or humans after antigen exposure [Nagano and Tsutsumi 2021]. Universal libraries offer an enormous diversity resulting from the shuffling of heavy and light chains derived from separate parental mAbs, and thus include heavy and light chain pairs that form antibodies directed against self-antigens and antigens that are highly toxic or of low immunogenicity. Immune libraries on the other hand benefit from the *in vivo* affinity maturation of the antigen-specific antibodies before library generation, but are restricted to the isolation of antigen-binding molecules targeted to a single antigen.

Depending on the choice of the display platform, different library sizes are available. For example, phage display enables library sizes of up to 10^{12} unique clones, mammalian and yeast display of up to 10^9 and ribosome display of even up to 10^{15} unique clones [Valldorf et al. 2022]. Besides the supported library size, the platforms may foster different antibody formats (Figure 2.2). Mammalian display platforms can be used to present complete Ig molecules including post-translational

2. Theoretical Background

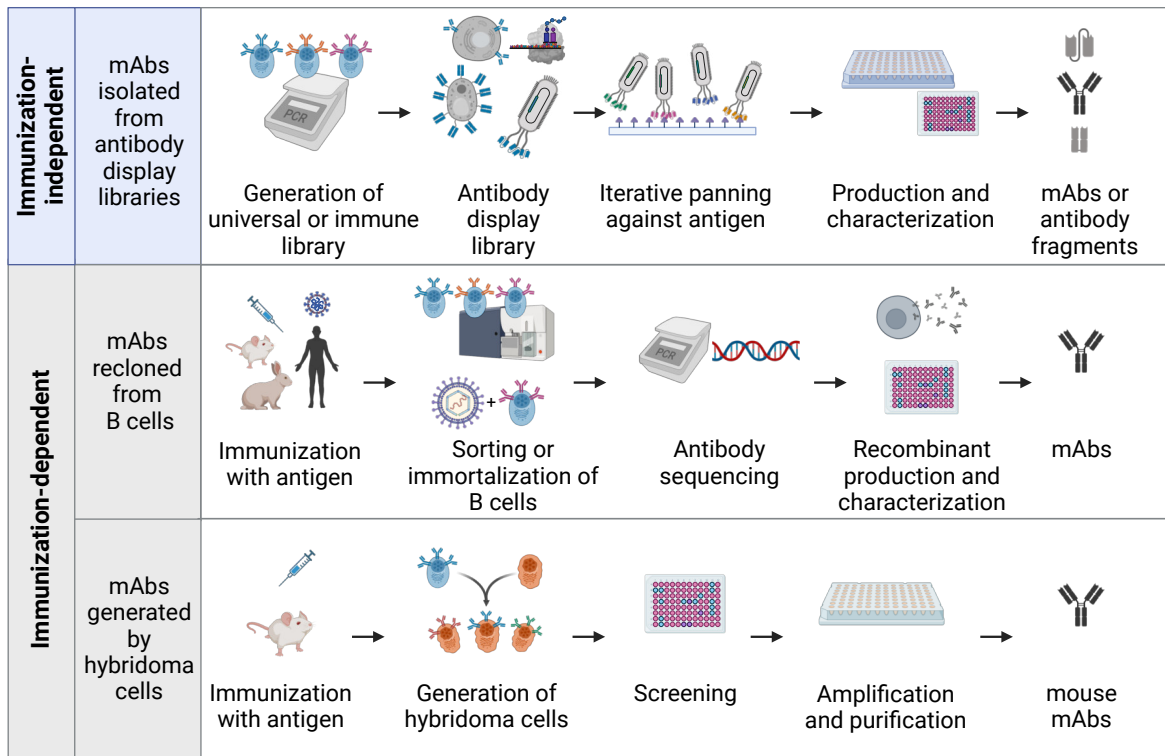


Figure 2.1. Overview on different monoclonal antibody (mAb) discovery technologies. Immunization-independent strategies are based on antibody library screens, whereas immunization-dependent strategies rely on isolated B cells after immunization with the target antigen. Adapted from [Laustsen et al. 2021] (CC BY 4.0; <https://creativecommons.org/licenses/by/4.0/>); „Monoclonal Antibodies Production“ and „Blank Panels (Layout 4x1) 2“ by BioRender.com (2023) [Biorender.com 2023].

modifications, whereas phage display platforms usually display only antibody fragments such as single chain variable fragments (scFvs) and antigen-binding fragments (Fabs). Each clone harbors the CDS of the antibody (fragment) that is displayed on its surface (genotype-phenotype coupling). Suitable antigen-specific antibodies are selected from the library by *in vitro* panning. Panning consists of iterative cycles of incubation of the display library with the (immobilized) antigen, removal of unbound individuals and amplification of antigen-specific candidates resulting in a smaller sublibrary of enriched antigen-specific binders ready for the next cycle. The genotype-phenotype coupling of the display platforms facilitates the easy recovery of cognate CDSs, and thus the recombinant production of soluble mAbs or antibody fragments for further characterization.

In contrast to immunization-dependent strategies, *in vitro* display libraries are rapidly screened for suitable antibodies and universal libraries are commercially available. A drawback of display platforms is the random pairing of the variable heavy and light chains that may lead to undesirable properties such as reduced stability and aggregation [Lehmann et al. 2015; Ma et al. 2020].

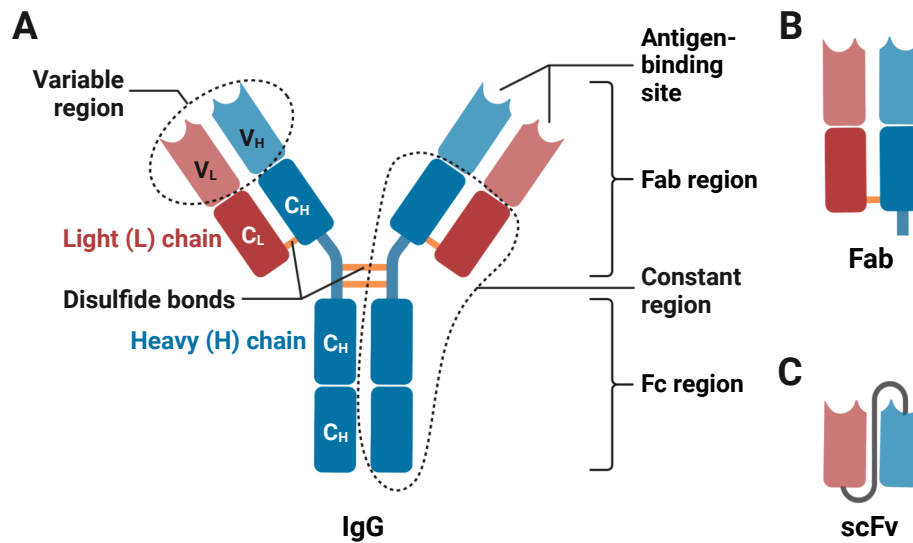


Figure 2.2. Schematic illustration of antibody formats. **(A)** Immunoglobulin G (IgG) structure. **(B)** The antigen-binding fragment (Fab) consists of the Fab region of an immunoglobulin. **(C)** The single chain variable fragment (scFv) is a fusion protein consisting of the variable region of an immunoglobulin connected by a linker peptide. Abbreviations: V_{H/L} = variable domain of the heavy/light chain; C_{H/L} = constant domain of the heavy/light chain; Fc = fragment crystallizable region. Adapted from „Immunoglobulin G (IgG) Structure“ by BioRender.com (2023) [Biorender.com 2023].

In addition, the lack of affinity maturation of antibodies may result in antibodies with a lower binding affinity to their cognate antigen compared to antibodies discovered utilizing immunization-dependent technologies [Sorouri et al. 2014]. However, *in vitro* affinity maturation strategies for phage and yeast display employing mutagenesis techniques exist and were successfully used to generate high affinity antibodies [Gram et al. 1992; McConnell et al. 2012; Wellner et al. 2021].

2.1.2. Immunization-dependent mAb discovery

The *in vivo* approach to antibody discovery is based on the isolation of animal- or human-derived B cells after exposure of the individual to the target antigen. Basically, the technology can be separated into antibodies produced by hybridoma cell generation and antibodies recloned directly from either immortalized B cells (for example by Epstein-Barr virus infection) or from primary B cells (Figure 2.1).

Köhler and Milstein established the first expression system for the production of mAbs named hybridoma technology in 1975 [Köhler and Milstein 1975]. The generation of hybridoma cells can be summarized in five steps: (1) Development and generation of the immunogenic antigen (Chapter 2.3), (2) immunization of the host, (3) isolation of antibody-producing B cells and fusion to myeloma cells, (4) screening and selection of hybridoma cells producing antigen-specific anti-

2. Theoretical Background

bodies, and (5) amplification of hybridoma cells and purification of mAbs [Zaroff and Tan 2019]. Immunization of the host animal, usually mice, is conducted over a duration of several weeks using repetitive injections of the antigen. The initial priming of the host's immune system does usually result in an increase in antigen-specific B cells. A second injection of the antigen called boost increases antibody levels and additional boosts yield antibodies with high affinity to the antigen [Greenfield 2022].

For hybridoma preparation, short-lived antibody-producing B cells are isolated from the lymphoid organs, such as the spleen, and fused with immortalized myeloma cells to generate immortal antibody-producing hybridoma cells. Fusion of the two cell types is mediated by polyethylene glycol or pulsed electric fields [Karsten et al. 1985; Wu et al. 2022]. Murine myeloma cells such as the Sp2/0-Ag14 cell line are capable of producing Igs but do not produce Igs by themselves and the cells are sensitive to hypoxanthine-aminopterin-thymidine (HAT) selection [Shulman et al. 1978]. The HAT medium is used to select for hybridomas from a mixture of unfused cells. The enzyme inhibitor aminopterin blocks nucleotide synthesis and cells not capable of synthesizing nucleotides using hypoxanthine die. In contrast to B cells, myeloma cells lack the *hgprt* gene required for the salvage pathway for nucleotide synthesis [Parray et al. 2020]. Unfused B cells are short-lived and die during the HAT selection process. The surviving hybridoma cell clones are subsequently screened to select for cell clones producing antigen-specific antibodies. Positive clones are further expanded and used for the production of murine mAbs. The whole hybridoma protocol takes approximately 4 to 6 months [Pedrioli and Oxenius 2021].

Although an old method, hybridoma technology is still a useful and preferred method, especially for generating murine mAbs for analytic applications [Zaroff and Tan 2019; Parray et al. 2020]. Over the years, other species than mice were used to generate hybridoma cells. Rabbits and chicken, for example, were instrumental in the generation of mAbs against human epitopes that are not immunogenic in mice [Lillehoj et al. 1994; Spieker-Polet et al. 1995; Rief et al. 1998]. However, the success of these non-murine hybridoma cells was limited due to the unavailability of suitable fusion partners for B cells and insufficient stability of the generated hybridoma cells [Parray et al. 2020]. Consequently, single B cell strategies were increasingly employed for the generation of mAbs from these species.

Single B cell technologies avoid the generation of hybridoma cells or immortalization of B cells. Antigen-specific B cells are isolated either from PBMCs of human or animal donors or from the spleen of experimental animals followed by molecular cloning of the Ig variable region cDNAs and recombinant production of mAbs [Babcook et al. 1996]. Multi-parameter cell sorting relies on the specific interaction of membrane-bound Igs, the B cell receptors (BCRs), with the cognate

fluorescent dye-labeled antigen and additional fluorescent antibodies, e.g. for memory B cell labeling [Perry et al. 2019]. Sorted single B cells are either directly subjected to cell lysis, mRNA isolation and reverse transcription polymerase chain reaction (PCR) to obtain the Ig variable region cDNAs or cultivated in single cell cultures to further analyze secreted mAbs before reverse transcription PCR is performed [Pedrioli and Oxenius 2021]. Starkie and colleagues isolated antigen-specific IgG⁺ memory B cells originating from murine spleen and rabbit PBMCs using multi-parameter cell sorting [Starkie et al. 2016]. The authors generated cDNA PCR products and transfected them directly into HEK-293 cells for transient expression of mAbs specific for their cognate antigen [Starkie et al. 2016]. The entire procedure took only one week. Other single B cell technologies rely on the screening of secreted mAbs utilizing microfluidic systems and other miniaturized devices [Pedrioli and Oxenius 2021; Gaa et al. 2021].

In summary, immunization-dependent technologies benefit from *in vivo* antibody generation and affinity maturation resulting in antibodies with high affinities for the target antigen. In addition and in contrast to *in vitro* display libraries, hybridoma as well as single B cell technologies maintain the natural pairing of the variable heavy and light chain domains of the Igs.

2.2. Basics of adaptive immune responses

For the elicitation of antigen-specific antibodies as part of the adaptive immune response to a foreign antigen, antigen presentation as well as B and T cell activation is required (Figure 2.3). Dendritic cells (DCs), macrophages and B cells are considered professional antigen-presenting cells (APCs) and internalize particulate and soluble antigens efficiently through macropinocytosis, phagocytosis and endocytosis [Roche and Furuta 2015]. Receptors involved in phago- and endocytosis include pattern recognition receptors (PRRs), complement and Fc receptors as well as the antigen-specific BCRs. PRRs such as toll-like receptors (TLRs) and scavenger receptors bind to pathogen-associated molecular patterns (PAMPs), Fc receptors interact with immune complexes consisting of antibody-labeled antigens, whereas complement receptors recognize antigens opsonized with complement factors.

After internalization, antigens are delivered to endo-lysosomal compartments, in which proteases, e.g. of the cathepsin family, process the antigens into peptides [Hsing and Rudensky 2005]. The peptide fragments of the processed antigens are loaded onto major histocompatibility complex (MHC) class II molecules, transported to the cell surface of APCs and displayed as MHC-II-peptide complexes. Among APCs, DCs are the most efficient activators of T cells [Kleindienst and Brocker 2005; Jong et al. 2006]. Upon antigen uptake and processing, immature DCs develop into

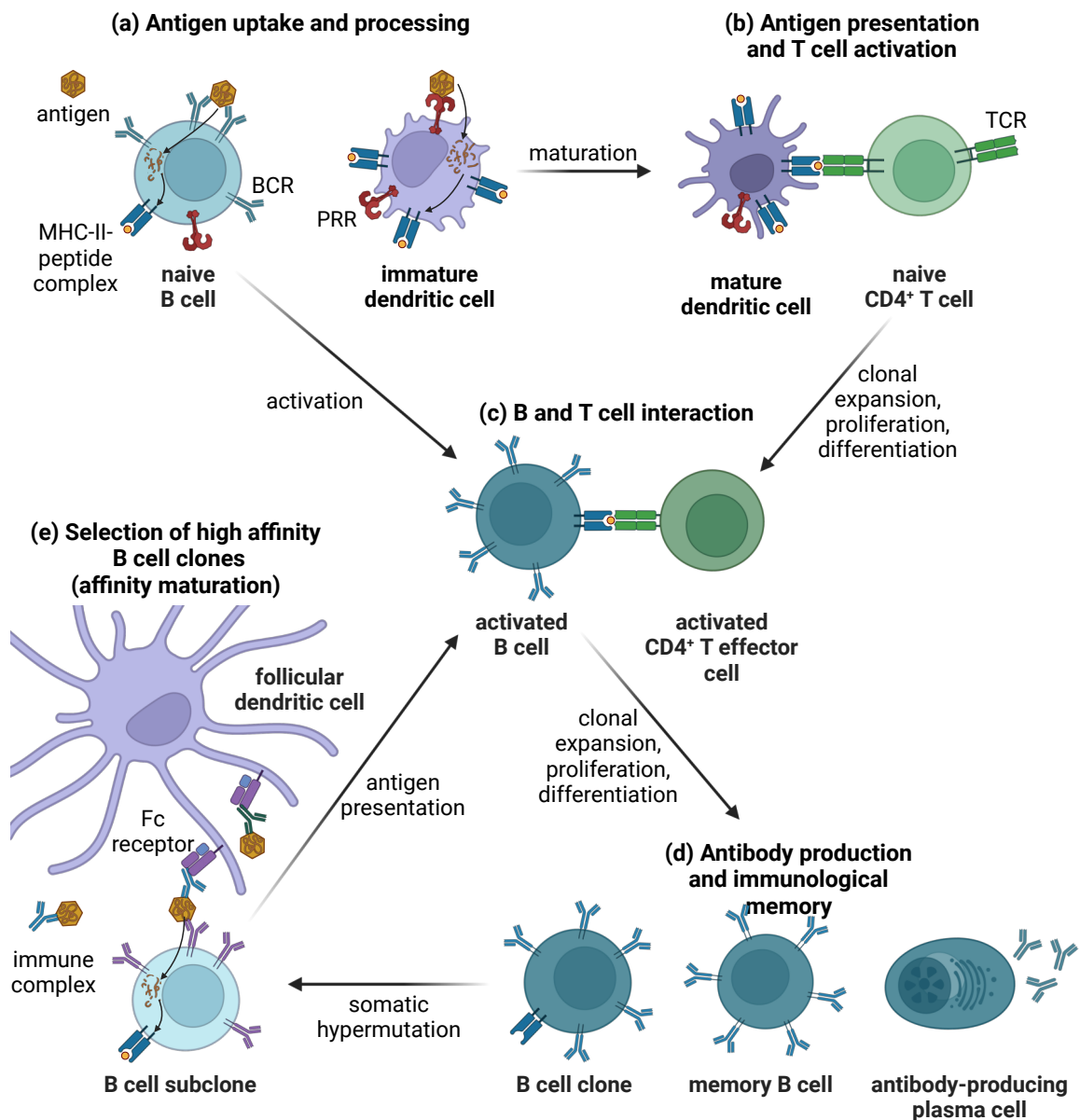


Figure 2.3. Illustration of the key steps involved in the elicitation of antigen-specific antibodies. **(a)** Antigens are recognized through cell surface receptors such as pattern recognition (PRRs) and B cell receptors (BCRs). The antigen is processed into antigenic peptide fragments, which are loaded onto major histocompatibility complex (MHC) class II molecules and displayed as MHC-II-peptide complexes. **(b)** Mature dendritic cells activate CD4⁺ T cells expressing the T cell receptor (TCR) specific for the MHC-II-displayed antigenic peptide. Activated CD4⁺ T cells proliferate and differentiate into CD4⁺ T effector cells. **(c)** Antigen-activated B cells present antigen-derived peptides to CD4⁺ T effector cells. The interaction between B and T cells is essential for clonal expansion, proliferation and differentiation of antigen-specific B cells. **(d)** Upon T cell stimulation, B cells proliferate generating B cell clones and differentiate into memory B cells and antibody-producing plasma cells. Some B cell clones undergo somatic hypermutation of the *bcr* genes resulting in B cell subclones with different affinities for their target antigen. **(e)** Antigen persistence on follicular dendritic cells (FDCs) as immune complexes enables the selection of B cell subclones with high antigen affinity. B cells acquire membrane-tethered antigen from FDCs and present the antigenic peptides to T cells entering a new cycle of clonal expansion. This process is called affinity maturation. Created with Biorender.com.

mature DCs and migrate into secondary lymphoid organs, that is lymph nodes and the spleen, to present antigenic peptides to T cells. Naïve cluster of differentiation (CD)4⁺ T cells recognize the MHC-II-peptide complex through antigen-specific T cell receptor (TCR) interaction. After activation, the antigen-specific CD4⁺ T cells proliferate (clonal expansion), differentiate into CD4⁺ T effector cells and migrate towards B cell-rich regions.

In contrast to the TCR that exclusively recognizes antigenic peptides loaded onto MHC-II molecules, the BCR binds to unprocessed antigens enabling the BCR to recognize complex structural epitopes. Naïve B cells encounter their cognate antigen in the follicles of lymphoid organs. Antigens smaller than 200 nm can travel as free antigens through lymphatic vessels, whereas larger antigens are transported in a cell-dependent manner [Ikomi et al. 1999; Sixt et al. 2005; Manolova et al. 2008; Bachmann and Jennings 2010]. DCs, macrophages and follicular dendritic cells (FDCs) can display membrane-tethered unprocessed antigens for B cell presentation [Carrasco and Batista 2007; Heath et al. 2019]. FDCs are pivotal for affinity maturation. The non-phagocytic FDCs are located in the germinal center of B cell follicles and retain unprocessed antigens in the form of immune complexes [Qin et al. 2000]. Following BCR-mediated antigen recognition and uptake, the antigen is processed into peptides and presented at the B cell surface as a MHC-II-peptide complex. Upon antigen-specific interaction with CD4⁺ T effector cells, the activated B cell proliferates (clonal expansion) and differentiates into memory B cells and antibody-producing plasma cells. In addition, the cooperation between T effector cells and B cells enables antibody-producing cells to switch the Ig class, for example from IgM to IgG, as well as to enter the affinity maturation process. Somatic hypermutation of the *bcr* genes results in B cell subclones expressing BCRs with modified antigen-binding variable regions, and thus different affinities for the antigen. High affinity B cells can acquire antigens from FDCs, process and present the antigens to T effector cells that convey survival and proliferation signals to the B cell subclone and thereby selecting for high affinity antibodies [Batista et al. 2001; Wang et al. 2011; Abd El-Aleem et al. 2022].

2.3. Antigen formats

The choice of the antigen format for immunization is crucial for the successful development of novel mAbs and is often neglected during antibody discovery [Ebersbach and Geisse 2012]. Folding and structure of the antigen during immunization and screening should as closely as possible resemble the target antigen structure occurring in the application which the mAb is developed for.

2.3.1. Soluble antigens

Soluble proteins are commonly used as immunogens for the development of therapeutic as well as analytic mAbs. Soluble antigens comprise purified protein preparations and short synthetic peptides. Synthetic peptides are usually 8 to 20 amino acids long and can be synthesized in high purity [Trier et al. 2012]. The selection of the right amino acid sequence of the peptide is fundamental in antibody development. The secondary structures of the synthetic peptide as well as the accessibility and location of the sequence within the protein are important factors in isolating mAbs that recognize the complete antigen [Trier et al. 2012; Ramos-Vara and Miller 2014]. Peptide antigens can be used to direct the immune response to a specific epitope, but due to the short amino acid sequence it can be challenging to isolate mAbs that recognize structural epitopes [Dodd et al. 2018]. In addition, peptides by themselves often show poor immunogenicity and require the use of carrier proteins such as keyhole limpet hemocyanin and adjuvants to induce an immune response [Trier et al. 2012].

Fusion proteins, full-length proteins and polypeptide chains are produced in suitable prokaryotic and eukaryotic host cells or derived from cell or tissue lysates. In contrast to synthetic peptides, these proteins can fold in three-dimensional structures and include post-translational modifications. However, soluble antigens may not be suitable immunogens when the target antigen is a membrane protein. Removing the hydrophobic transmembrane region and using the purified, soluble extracellular domain may work for some membrane proteins, but this approach might not be suitable for membrane proteins that form complex three-dimensional structures and consist of several transmembrane regions [Dodd et al. 2018]. In addition, soluble antigens often require adjuvants such as aluminium salts, Freund's adjuvant or PRR agonists to efficiently stimulate immune responses [Burakova et al. 2018; Lee and Suresh 2022]. Moreover, some adjuvants such as aluminium salts and antigen formulations may negatively affect the structure and conformation of the antigen [Fox et al. 2013; Barinova et al. 2017]. In some cases, the weak immunogenicity of soluble antigens can be improved using particle-based formulations for antigen delivery [Bezbaruah et al. 2022].

2.3.2. Particulate antigens

Insoluble or particulate antigens include bacteria, viruses, whole cells but also nanoparticles such as liposomes, lipid nanoparticles and VLPs. Particulate antigens are usually better immunogens than soluble proteins. The similar dimensions of particulate antigens to pathogens as well as the often hydrophobic, charged and receptor-interacting surface structures facilitate antigen uptake, processing and presentation by APCs [Bachmann and Jennings 2010].

For the discovery of mAbs directed against cell-surface antigens, whole cells displaying either naturally occurring or recombinantly expressed membrane proteins are suitable for immunization [Tuekprakhon et al. 2018; Dodd et al. 2018]. Since the membrane proteins are expressed in their native environment and embedded into a lipid bilayer membrane, the target antigens are presented in their native conformation enabling the elicitation of conformation-specific mAbs [Asgarov et al. 2017]. Moreover, cells can be fixed with formaldehyde and subsequently embedded in paraffin to generate cells that display FFPE antigens [Knudsen et al. 2009]. However, extensive screening is necessary to identify target antigen-specific antibodies, because whole cells contain many host cell proteins potentially distracting the immune response away from the desired target antigen [Jones et al. 2016; Dodd et al. 2018]. In competition with the host cell proteins, the immunogenicity and relative abundance of the target antigen greatly influences the success of antibody discovery [Dodd et al. 2018].

Enveloped VLPs generated by co-expression of viral structural proteins and the target surface antigen represent an alternative to cells for the presentation of membrane proteins. VLPs can display and efficiently deliver linear and conformational antigens to APCs. The advantage of VLPs originates from their inherent immunogenicity combined with a better ratio of target antigen to host cell proteins as only a limited number of distracting host cell proteins are incorporated into VLPs [Ebersbach and Geisse 2012].

2.4. Virus-like particles (VLPs)

VLPs are nanoparticles that self-assemble into structures similar to the cognate parental virus, but VLPs lack the viral genome. Based on their structure, they can be divided into enveloped and non-enveloped VLPs. Non-enveloped VLPs consist of one or multiple types of viral proteins. Examples for non-enveloped VLPs include approved vaccines against hepatitis B and human papilloma viruses [Valenzuela et al. 1982; Harper et al. 2006]. Enveloped VLPs are formed by one or multiple viral proteins and are surrounded by a lipid bilayer derived from the host cell membrane. Examples of enveloped VLPs include retrovirus- and influenza-like particles. VLPs are produced recombinantly using different expression platforms such as prokaryotes, yeast, insect, mammalian and plant cells [Fuenmayor et al. 2017]. However, for efficient production of retrovirus-derived enveloped VLPs, such as HIV-like particles, mammalian and insect expression systems are predominantly used [Cervera et al. 2019]. Retrovirus-derived VLPs can be utilized as nanoscale cargo vessels that function as scaffolds for the delivery of proteins and nucleic acids and as vaccine candidates [Link et al. 2006; Kaczmarczyk et al. 2011; Knopp et al. 2018; Lu et al. 2019; Fontana et al. 2021; Nooraei et al. 2021].

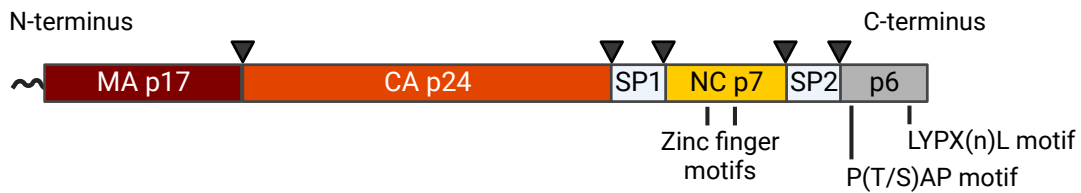


Figure 2.4. Schematic illustration of the HIV-1 Gag precursor polyprotein (p55-Gag). The p55-Gag protein consists of three structural subunits: the matrix (MA, p17-Gag), capsid (CA, p24-Gag) and the nucleocapsid (NC, p7-Gag) domains as well as two spacer peptides (SP1 and SP2) and the p6 domain each separated by protease cleavage sites (represented as triangles). Located at the N-terminus of MA, a myristic acid group anchors Gag to the plasma membrane of the host cell. The NC domain harbors two zinc finger motifs responsible for binding the viral RNA genome. P(T/S)AP and LPX_nL are conserved late assembly domains that interact with cellular proteins. Created with Biorender.com.

2.4.1. Structure and morphology

The retroviral Gag proteins are the structural core proteins responsible for the formation of particles. The HIV-1 Gag precursor polyprotein (p55-Gag) consists of several subunits: the matrix (MA), the capsid (CA) and the nucleocapsid (NC) domains flanked by two spacer peptides (SP1 and SP2) and the C-terminal p6 domain (Figure 2.4). Each domain is separated by protease cleavage sites and involved in key steps in the formation of viral and virus-like particles (Chapter 2.4.2).

Figure 2.5 illustrates the main commonalities and differences of the HI virion and HIV p55-Gag-formed VLPs. Both particles are spherical and surrounded by a lipid bilayer membrane derived from the host cell. The average diameter of the virions ranges from 110 nm to 128 nm, whereas the diameter of VLPs is slightly increased and ranges from 132 nm to 146 nm [Gentile et al. 1994; Martin et al. 2016]. On average 14 ± 7 viral envelope glycoprotein trimers are embedded in the lipid bilayer membrane of the virion mediating fusion and entry of the virion into the host cell [Zhu et al. 2006]. The p55-Gag proteins of the mature virion are processed by the viral protease (PR) into the three structural proteins MA, CA and NC. The MA subunit is anchored to the membrane envelope via a myristic acid group present at the N-terminus. The CA proteins form the conically shaped capsid containing the viral RNA genome, reverse transcriptase (RT), integrase (IN) and the NC proteins stabilizing the genome. VLPs formed by Gag proteins alone lack the Pol proteins that are responsible for maturation of the particle by Gag precursor cleavage. Therefore, the p55-Gag proteins remain unprocessed and are ordered concentrically below the VLP membrane [Wright et al. 2007; Martin et al. 2016]. In contrast to the virion, the VLP is devoid of the viral RNA genome and therefore is non-infectious. Recombinant co-expression of p55-Gag proteins and a membrane target protein enables the formation of VLPs displaying the target antigen on the surface of the VLPs (antigen-decorated VLPs).

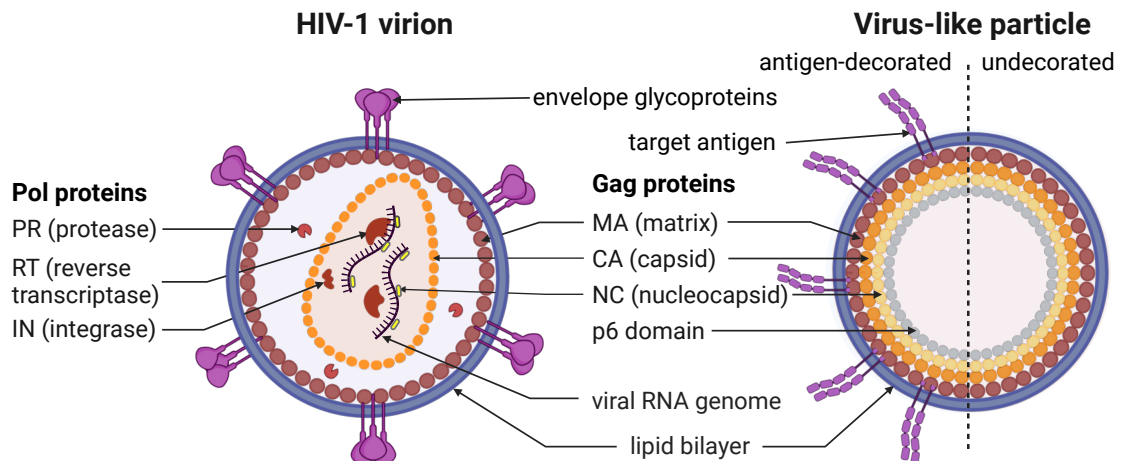


Figure 2.5. Simplified structures of a HIV-1 virion and a HIV-like particle (VLP). Both particles are spherical and surrounded by a lipid bilayer. Trimers of envelope glycoproteins are embedded in the membrane of the mature virion, whereas the VLP can be decorated with a recombinant target antigen. The Gag precursor polyproteins (p55-Gags) of the mature virion are processed into the three structural proteins matrix (MA), capsid (CA) and nucleocapsid (NC) by the viral protease (PR). The CA proteins form the capsid containing the viral RNA genome, reverse transcriptase (RT), integrase (IN) and the NC proteins. As the VLP lacks the Pol proteins, the p55-Gag proteins remain unprocessed and are ordered concentrically below the VLP membrane. VLPs can be decorated with recombinantly expressed membrane proteins as target antigens for immunization or remain undecorated. Adapted from „HIV-1 Structure“ by BioRender.com (2023) [BioRender.com 2023].

2.4.2. Gag assembly and VLP formation

Although the recombinant expression of the HIV p55-Gag alone is sufficient to mediate the formation of VLPs, the process of assembly, budding and release of the particles depends heavily on the interaction of Gag subunits with cellular proteins, lipids and RNA. HIV assembles at cholesterol-rich cell membrane micro-domains called lipid rafts. The N-terminal MA domain recruits Gag proteins to the plasma membrane and anchors them in the lipid bilayer via a myristoylation signal [Saad et al. 2007; Li et al. 2007]. Studies revealed that Gag binding to the cell membrane induces the coalescence of lipid rafts and tetraspanin-enriched microdomains and reduces the diffusion of cholesterol, phosphatidylinositol-(4,5)-bisphosphate (PI(4,5)P₂) and tetraspanin at assembly sites [Krementsov et al. 2010; Hogue et al. 2011; Favard et al. 2019]. The trapping of these components and the manipulation of the lipid environment at viral assembly sites provides budded particles with a rigid, and thus robust enveloping membrane.

The interaction of highly basic regions present in the MA domain with acidic membrane phospholipids such as PI(4,5)P₂ and cellular RNAs regulates the localization of assembly sites [Murray et al. 2005; Mücksch et al. 2017; Gaines et al. 2018]. In particular, the binding of cellular tRNA^{Lys} prevents targeting of Gag to intracellular membranes [Alfadhli et al. 2009; Alfadhli et al. 2011;

Gaines et al. 2018; Thornhill et al. 2019]. Upon binding of the MA domain to PI(4,5)P₂ and simultaneous binding of NC domain to viral RNA, the Gag protein refolds into an extended conformation promoting the formation of Gag multimers [Datta et al. 2011; Chen et al. 2020b]. In the absence of viral RNA cellular RNA serves as a scaffold for VLP assembly and is packaged into VLPs [Rulli et al. 2007; Pitoiset et al. 2017]. The growing Gag multimer bends the membrane and forms a spherical particle that is still connected to the cell membrane. The conserved sequences of the late assembly domains P(T/S)AP and LPX_nL present in the p6 domain of Gag recruit adapter proteins for endosomal sorting complexes required for transport (ESCRT) components [Baumgärtel et al. 2011; Weiss and Göttlinger 2011; Votteler and Sundquist 2013]. The assembled ESCRT machinery finally mediates membrane fission and releases the VLP from the cell membrane.

As the Gag proteins interact closely with cellular molecules, host-derived proteins and RNAs are incorporated into the particles during the formation of VLPs. Membrane proteins present at lipid rafts are usually embedded in the membrane envelope and displayed on the VLP surface. The incorporation of most membrane proteins is regarded as a passive process, but some proteins are actively concentrated within or excluded from incorporation into retroviral particles [Hammarstedt et al. 2000; Hammarstedt and Garoff 2004]. Examples of displayed membrane proteins include cell adhesion molecules such as intercellular adhesion molecule 1 (CD54), integrins and complement regulatory proteins that confer protection against the host organism's complement system [Montefiori et al. 1994; Beausejour and Tremblay 2004; Segura et al. 2008; Jalaguier et al. 2015; Hu et al. 2010].

2.4.3. VLPs as immunogens

The immunogenicity of VLPs originates from their particulate virus-like structure, their small size and the highly repetitive structure of densely presented surface antigens. As VLPs resemble the structure of their parental virus, VLPs are identified through the same mechanisms, for example PAMPs recognized by PRRs, responsible for the detection of viruses [Nooraei et al. 2021]. These features enable efficient activation of DCs, B cells and T cells resulting in a strong cellular and humoral immune response [Buonaguro et al. 2006; Sailaja et al. 2007; Bachmann and Jennings 2010].

The nanometer size of VLPs ranging from 20 nm to 200 nm enables traveling of VLPs through the lymph vessels as free antigens independent of cell-mediated transport [Ikomi et al. 1999; Sixt et al. 2005; Manolova et al. 2008; Bachmann and Jennings 2010]. As a consequence, VLPs rapidly enter the lymphatic organs and interact with immune cells residing in these organs. Macrophages present in the lymph nodes or the spleen gather small particles such as viruses and VLPs and translocate these particular antigens to follicular B cells and FDCs [Aichele et al. 2003; Junt et al.

2. Theoretical Background

2007; Carrasco and Batista 2007; Matter and Ochsenbein 2008; Link et al. 2012]. In a study comparing the soluble Q β antigen and its particulate form, the Q β -VLP, Link and colleagues identified complement and natural IgM as responsible agents for capture, transport and deposit of VLPs in the spleen [Link et al. 2012]. Natural antibodies exist unrelated to the encounter of a cognate antigen and are often cross-reactive for a variety of antigens including bacterial and viral antigens [Ochsenbein and Zinkernagel 2000]. Natural antibodies and complement components support the clearance of antigens from the blood, as they opsonize and label foreign antigens for immune cells with the cognate receptors [Matter and Ochsenbein 2008; Link et al. 2012].

The repetitive arrangement of antigens present on the surface of VLPs facilitates the cross-linking of BCRs, which is a strong activation signal for B cells and already sufficient to induce an early T cell-independent IgM antibody response – mostly also in the absence of adjuvants [Bachmann et al. 1993; Jegerlehner et al. 2002]. Although T cell-independent activation of B cells is possible, the isotype switch from IgM to IgG depends on the high epitope density displayed and the ability of the VLPs to recruit T cells to promote B cell differentiation, isotype switch and affinity maturation [Jegerlehner et al. 2002; Chen et al. 2020c].

The envelope of VLPs allows for the conformational adequate display of complete membrane proteins for immunization. The possibility to functionalize VLPs with a variety of antigens, for example viral envelope glycoproteins, tetraspanning membrane proteins and other cell surface markers, renders retrovirus-derived VLPs attractive candidates for immunization [Chua et al. 2013; Schneider et al. 2018; Fontana et al. 2021; Boix-Besora et al. 2022]. Furthermore, VLPs facilitate immunization with self-antigens and can induce an auto-antibody response mediated by the repetitive structure of the self-antigen on the VLP surface that can break B cell tolerance [Bachmann et al. 1993; Schneider et al. 2018; Chen et al. 2020c]. After uptake of the self-antigen-decorated VLP, the B cell processes the VLP and presents peptides derived from the viral structural core proteins on MHC-II molecules. T cells specific for the virus-derived antigens recognize the presented peptides and stimulate the antigen-presenting and self-antigen-specific B cell to proliferate and differentiate resulting in a strong auto-antibody response [Chen et al. 2020c].

The formation of target antigen-decorated VLPs can be achieved by co-overexpression of Gag structural core proteins and the target antigen in appropriate VLP producer cells [Cervera et al. 2019]. However, display of the target antigens on the VLP surface depends on the presence of the protein in lipid rafts. General mechanisms that target proteins to lipid raft microdomains are post-translational modifications such as lipidation, glycosylphosphatidylinositol (GPI)-anchors, palmitoylation, myristoylation and sterol-conjugation as well as other structural features of trans-membrane domains [Legler et al. 2005; Levental et al. 2010; Lorent and Levental 2015; Yurtsever

2. Theoretical Background

and Lorent 2020]. These mechanisms can be exploited to genetically modify proteins that do not naturally occur at lipid rafts accordingly and thereby facilitate their incorporation into VLPs [Kueng et al. 2007; Deo et al. 2014; Deo et al. 2016]. Some lipid raft-associated membrane proteins are not included into the VLP envelope due to steric hindrance of a long cytoplasmic domain of the protein. In this case, truncation of the cytoplasmic tail can be a solution [Schnierle et al. 1997; Henriksson et al. 1999; Stitz et al. 2000; Christodoulouopoulos and Cannon 2001].

3. Results

3.1. Establishment and characterization of VLP producer cell pools

Stable human 293-F VLP producer cell pools were generated using transposon vector-mediated gene transfer. 293-F cells were co-transfected with the *piggyBac* (PB) transposase expression construct and the transposon donor vector pPB-mos1.gag-lpW encoding for the mosaic Gag (Mos1.Gag) protein consisting of synthetically shuffled Gag sequences originating from different HIV variants [Fischer et al. 2007; Langedijk et al. 2019]. Four days post transfection, puromycin was added to the culture medium to initiate the selection of stably transfected cells. Cells were subjected to increasing concentrations of puromycin to establish the stable VLP producer cell pool 293-F/Mos1.Gag producing undecorated VLPs [Rosengarten et al. 2022b]. For the production of truncated human low affinity nerve growth factor receptor (trNGFR)-decorated VLPs, the 293-F/Mos1.Gag/trNGFR VLP producer cell pool was subsequently generated. The 293-F/Mos1.Gag cells were co-transfected with the *Sleeping Beauty* (SB) transposase expression construct and the transposon donor vector pSB-trNGFR-lhW encoding for the trNGFR (Figure 5.1). The trNGFR differs from the wild-type nerve growth factor receptor (NGFR) in the length of the cytoplasmic tail. The C-tail of the trNGFR comprises only 8 amino acids, whereas the C-tail of the wild-type NGFR is 155 amino acids long. Three days post transfection, cells stably expressing Mos1.Gag and trNGFR were selected using increasing concentrations of hygromycin. Stable VLP producer cells were investigated for the expression of Gag proteins and trNGFR as well as VLP formation and antigen incorporation into VLPs.

3.1.1. 293-F/Mos1.Gag/trNGFR, 293-F/Mos1.Gag and 293-F cells express NGFR

For the detection of cell surface expression of trNGFR, cells were stained using the phycoerythrin (PE)-conjugated anti-NGFR mAb REA844. Matching isotype control antibodies served as negative controls. The expression of NGFR was investigated using flow cytometric analysis of the antibody-labeled cells. As shown in Figure 3.1, NGFR was detected in 293-F/Mos1.Gag/trNGFR cells, 293-F/Mos1.Gag cells and 293-F cells, albeit for the latter two at lower expression levels as compared to 293-F/Mos1.Gag/trNGFR cells. As the PB-derived transposase expression construct harbors the reporter gene *trngfr*, the detection of NGFR in 293-F/Mos1.Gag cells might have resulted from random stable integration of the plasmid into the genome. However, the very similar

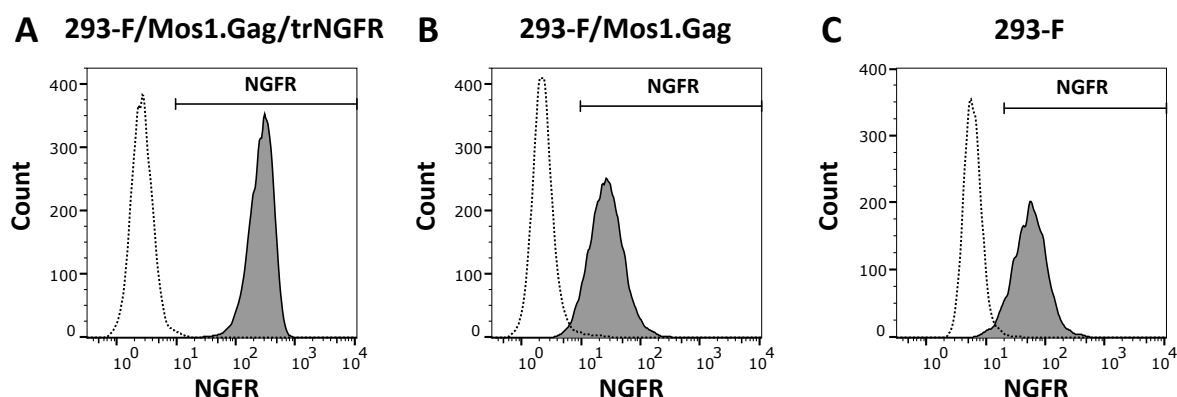


Figure 3.1. Flow cytometric results of cell surface expression of nerve growth factor receptor (NGFR) in the recombinant virus-like particle (VLP) producer cell pools 293-F/Mos1.Gag and 293-F/Mos1.gag/trNGFR, and the parental 293-F cell line. Cells were stained using the PE-conjugated anti-NGFR monoclonal antibody REA844 (grey, solid line) and a matching isotype control antibody (white, dotted line). **(A)** 293-F/Mos1.Gag/trNGFR cells, **(B)** 293-F/Mos1.Gag cells, **(C)** 293-F cells.

NGFR expression of 293-F and 293-F/Mos1.Gag cells as well as the comparable stain indices of 9.4 and 9.9, respectively (Figure 3.1, Table S1), strongly indicated an endogenous expression of wild-type NGFR rather than a residual expression of trNGFR originating from the transposase expression construct. In contrast, 293-F/Mos1.Gag/trNGFR cells showed pronounced NGFR expression and a stain index of 63.0 (Figure 3.1A and Table S1). Thus, the successful and high expression of the recombinant trNGFR at the cell membrane was confirmed – a prerequisite for efficient VLP incorporation.

3.1.2. Recombinant trNGFR but not wild-type NGFR is incorporated into HIV-derived VLPs

The formation of VLPs and the incorporation of the trNGFR and wild-type NGFR, respectively, into VLPs was first investigated utilizing Gag- and NGFR-specific ELISAs. Biological replicates of VLP producer cell cultures were seeded at a viable cell density (VCD) of 0.5×10^6 viable cells/mL in 20 mL culture medium. Three days after inoculation, cell-free supernatants (CFSNs) were harvested from cell cultures and analyzed for their p24-Gag content. CFSN harvested from 293-F/Mos1.Gag cultures contained on average 180 ± 59 ng/mL p24-Gag, whereas CFSN of 293-F/Mos1.Gag/trNGFR cell cultures produced on average 53 ± 7 ng/mL p24-Gag. Gag protein was not detectable in CFSN of 293-F cells (data not shown). Subsequently, 15 mL of CFSN of the VLP producer cell cultures was subjected to ultracentrifugation to pellet VLPs formed by the Gag proteins. The pelleted VLP samples were analyzed for their p24-Gag content. Gag was found in all samples demonstrating the successful formation of VLPs (Table 3.1). An independent two-sample *t*-test showed a significant difference between the amount of VLPs produced by

3. Results

Table 3.1. Gag content of VLP samples produced by 293-F/Mos1.Gag and 293-F/Mos1.Gag/trNGFR cell pools. Cells were seeded at a VCD of 0.5×10^6 viable cells/mL. After three days, 15 mL CFSN was harvested from the cultures and subjected to ultracentrifugation to isolate VLPs. The VLP pellets were analyzed using a p24-Gag-specific ELISA. Data shown represent mean \pm standard deviation of biological replicates.

VLP producer cell pools	Total pelleted Gag	Replicates
293-F/Mos1.Gag	535 \pm 59 ng	n=3
293-F/Mos1.Gag/trNGFR	55 \pm 19 ng	n=4

293-F/Mos1.Gag and the 293-F/Mos1.Gag/trNGFR cell pools ($t=15.605$, $df=5$, $p=0.00002$). The 293-F/Mos1.Gag cultures produced approximately 10-fold more VLPs (535 \pm 59 ng Gag) than the 293-F/Mos1.Gag/trNGFR cultures (55 \pm 19 ng Gag; Table 3.1).

In addition, the CFSNs harvested from 293-F, 293-F/Mos1.Gag and 293-F/Mos1.Gag/trNGFR cell cultures were examined for the presence of NGFR proteins including both wild-type NGFR and trNGFR. The CFSNs of the VLP producer cell pools were normalized to a p24-Gag concentration of 45 ng/mL before determining the NGFR concentrations. No NGFR was detectable in the CFSN of the 293-F cell culture demonstrating that full-length wild-type NGFR was not secreted into the cell culture medium as a soluble protein (Table 3.2). NGFR was also absent in CFSNs of the VLP producer cell pool 293-F/Mos1.Gag strongly suggesting that wild-type NGFR is not incorporated into VLPs. In contrast, NGFR was readily detected in the CFSNs derived from the 293-F/Mos1.Gag/trNGFR cell cultures indicating that the detected NGFR was trNGFR incorporated into VLPs. The mean relative trNGFR amount of 99.60 ± 8.50 ng per 1 μ g p24-Gag revealed a Gag to trNGFR mass ratio of approximately 10:1 in CFSNs (Table 3.2). The average number of trNGFR molecules was calculated at 284 ± 24 trNGFR molecules per VLP.

Table 3.2. NGFR content of CFSNs harvested from 293-F, 293-F/Mos1.Gag and 293-F/Mos1.Gag/trNGFR cell cultures. NGFR concentrations were determined using an NGFR-specific ELISA and normalized to p24-Gag concentrations. Data shown represent mean \pm standard deviation of biological triplicates, if not otherwise stated. Reproduced from [Schatz et al. 2023b] (CC BY 4.0; <https://creativecommons.org/licenses/by/4.0/>).

Cells	trNGFR per 1 μ g Gag	Replicates
293-F	<0.08 ng	n=1
293-F/Mos1.Gag	<0.08 ng	n=3
293-F/Mos1.Gag/trNGFR	99.60 \pm 8.50 ng	n=3

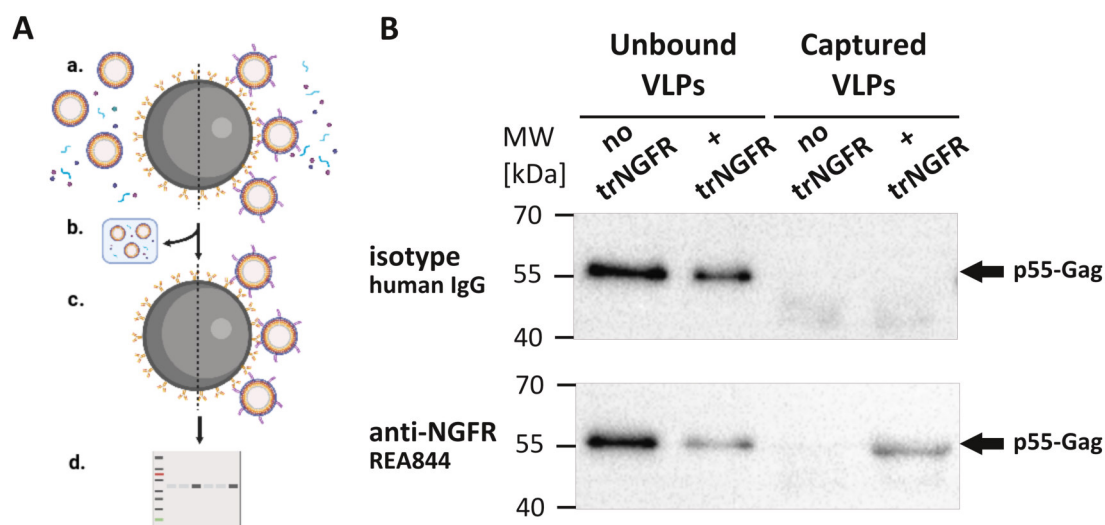


Figure 3.2. Indirect detection of NGFR displayed on VLPs employing a VLP capture assay followed by an anti-Gag Western blot analysis. **(A)** Schematic illustration of the experimental set-up of the VLP capture assay. a.) VLP samples are incubated with anti-NGFR-coated magnetic beads. VLPs not displaying trNGFR do not bind to the beads (left), whereas trNGFR-displaying VLPs are captured by anti-NGFR mAbs (right). b./c.) The supernatant containing unbound VLPs is separated from the beads and the beads are subsequently washed. d.) Finally, the beads are subjected to a Gag-specific Western blot to detect VLPs captured by the anti-NGFR-coated beads. **(B)** VLPs were immunoprecipitated using the anti-NGFR mAb REA844 immobilized on the surface of magnetic beads. Beads coated with isotype control antibodies served as negative controls. Unbound VLPs were taken from the supernatant of samples after incubation with antibody-coated beads. Unbound and captured VLP samples were subsequently subjected to Western blot analysis for the detection of Gag precursor polyprotein (p55-Gag) proteins using primary antibodies directed against Gag. The trNGFR-free VLPs were produced by 293-F/Mos1.Gag cells, which expressed only Gag proteins, whereas the trNGFR-VLPs were produced by 293-F/Mos1.Gag/trNGFR cells expressing Gag proteins and human trNGFR. The VLP samples used for the capture assay contained up to 25 ng Gag protein per sample. The positions of the molecular weight marker (MW) in kilodaltons (kDa) is depicted on the left. The arrows indicate the expected position of p55-Gag proteins. Adapted from [Schatz et al. 2023b] (CC BY 4.0; <https://creativecommons.org/licenses/by/4.0/>).

To demonstrate that the trNGFR detected in the CFSN of 293-F/Mos1.Gag/trNGFR cell pools was VLP-associated, an NGFR-specific VLP capture assay was performed (Figure 3.2A, [Rosengarten et al. 2022a]). Magnetic beads were coated with anti-NGFR mAbs and isotype control antibodies that served as negative control, respectively. VLPs devoid of trNGFR display and produced by 293-F/Mos1.Gag cells as well as trNGFR-VLPs produced by 293-F/Mos1.Gag/trNGFR cells were incubated with the antibody-coated beads. After incubation, the supernatant and the beads were separated in a magnetic field and samples taken from the supernatant were analyzed for unbound VLPs. The beads were washed extensively and subjected to p55-Gag Western blot analysis for the detection of Gag-formed VLPs. As visible in Figure 3.2B, comparable amounts of unbound VLPs were detected in trNGFR-free and trNGFR-VLP samples after incubation with

isotype control antibody-coated beads, whereas slightly less Gag was detected after incubation of the trNGFR-VLP sample with anti-NGFR-coated beads compared to the trNGFR-free VLP sample. The anti-NGFR-coated beads did not capture trNGFR-free VLPs. In contrast, trNGFR-VLPs were precipitated using anti-NGFR-coated beads demonstrating that the trNGFR detected in the CFSNs of the trNGFR-VLP producer cell pools was particle-associated and trNGFR is incorporated into VLPs. No VLPs were precipitated using isotype control antibodies demonstrating that capturing of VLPs was entirely mediated by the anti-NGFR mAbs. These results supported the previous data obtained from the NGFR-specific ELISA showing that the wild-type NGFR present on the surface of the 293-F/Mos1.Gag cells was not incorporated into VLPs, whereas the C-terminally truncated variant trNGFR decorated the HIV-derived VLPs.

3.2. Development of a fixation protocol for antigen preparation

Since the trNGFR-VLPs were intended to be used for immunization of mice to generate antibodies directed against the formaldehyde-fixed paraffin-embedded (FFPE) target antigen, a fixation technique for VLPs had to be developed to generate VLPs presenting FFPE-like trNGFR proteins. FFPE tissue processing includes the initial fixation of the tissue using formaldehyde (typically in a concentration of 4%), followed by dehydration using graded alcohol solutions, clearing in xylene and final embedding in liquid paraffin at 50 °C to 70 °C. This procedure introduces changes in the protein 3D structure, chemical modification of amino acids, cross-linking of proteins and formation of protein aggregates [Werner et al. 2000; Thavarajah et al. 2012]. Hence, new epitopes are generated and pre-existing epitopes are masked during the fixation and embedding procedure. To develop a fixation protocol suitable to form FFPE-like epitopes that are potentially able to elicit an antibody response against FFPE antigens in mice, NGFR was chosen as a model antigen and changes induced during fixation were monitored using two antibodies with a different NGFR recognition profile. The anti-NGFR mAb C40-1457 is routinely used in flow cytometry applications and for immunohistochemistry (IHC) staining of FFPE tissue sections [Lin et al. 2018; Fujii et al. 2022]. The anti-NGFR mAb REA844 is applicable for flow cytometric analysis of native cells and for IHC staining of acetone- and formaldehyde-fixed tissue sections but not for FFPE samples [Miltényi Biotec undated; Personal communication 2021], and thus not recognizing FFPE NGFR. The aim was to develop a fixation procedure that leads to the loss of epitope recognition by the „native“ mAb REA844 while still preserving the binding of the FFPE-compatible mAb C40-1457. The fixation protocol was developed using the 293-F/Mos1.Gag/trNGFR cells instead of VLPs to avoid time-consuming separation of liquids and VLPs employing ultracentrifugation. In addition, ultracentrifugation is accompanied with a loss of VLPs at every centrifugation step. Therefore, the fixation protocol was developed minimizing centrifugation steps and keeping it as simple as possible.

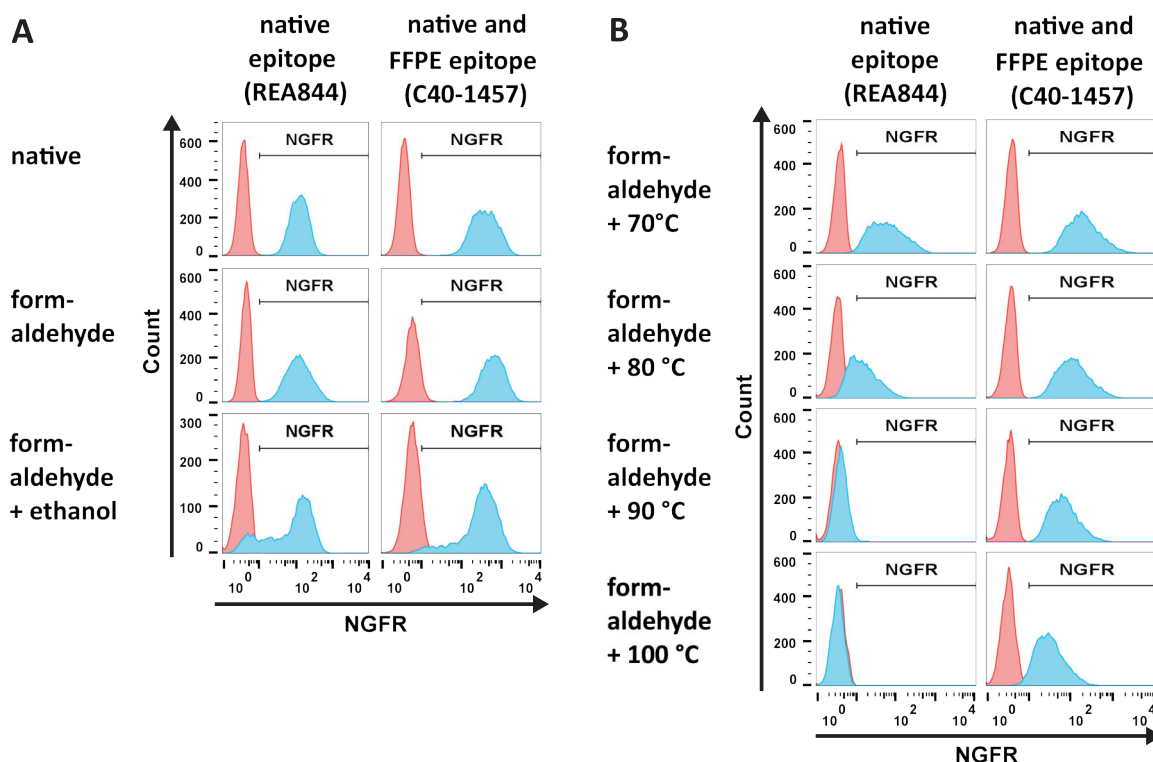


Figure 3.3. Flow cytometric results of NGFR staining of 293-F/Mos1.Gag/trNGFR cells after employing different fixation strategies. Cells were stained using the PE-conjugated anti-NGFR mAbs REA844 and C40-1457 (shown in blue) and matching isotype control antibodies as negative control (shown in red). The REA844 antibody recognizes a native epitope, whereas the C40-1457 antibody also recognizes an formaldehyde-fixed paraffin-embedded (FFPE) epitope. **(A)** Cells were chemically fixed using different substances. Panel 1: Native cells were freshly harvested from cell cultures without fixation. Panel 2: Formaldehyde-fixed cells were incubated in 4% formaldehyde for 1 h (middle). Panel 3: Cells were first fixed in formaldehyde and afterwards incubated in ascending ethanol concentrations (50%, 70% and 90% for 20 min, respectively). **(B)** Heat denaturation: After formaldehyde fixation, cells were incubated in hot PBS for 1 h at different temperatures including 70 °C, 80 °C, 90 °C and 100 °C. Adapted from [Schatz et al. 2023b] (CC BY 4.0; <https://creativecommons.org/licenses/by/4.0/>).

3.2.1. Formaldehyde and heat fixation induces a loss of epitope recognition by the "native" anti-NGFR mAb while maintaining recognition by the corresponding FFPE-compatible mAb

293-F/Mos1.Gag/trNGFR cells were harvested, subjected to different fixation steps, stained using the two anti-NGFR mAbs REA844 and C40-1457, and analyzed employing flow cytometry. Matching isotype control antibodies were used as negative controls. As shown in Figure 3.3A, both anti-NGFR antibodies bound to native cells as well as cells that were fixed using 4% formaldehyde solution. As formaldehyde fixation alone did not change the recognition profile of the antibodies, an additional fixation step using alcohol was introduced to test the potential influence of dehydration

of proteins. Cells were first fixed using formaldehyde solution, washed and subjected to increasing concentrations of ethanol (50 %, 70 % and 90 %). Only minor effects of the ethanol fixation on the recognition profile of the antibodies were observed. Both antibodies showed a partial loss of binding but remained reactive to the majority of cells.

Next, the combination of formaldehyde fixation and heat denaturation was investigated. 293-F/-Mos1.Gag/trNGFR cells were fixed using 4 % formaldehyde solution. After fixation, cells were incubated in hot PBS at different temperatures ranging from 70 °C to 100 °C. Incubation at 70 °C hardly influenced the NGFR binding capacity of the anti-NGFR mAbs (Figure 3.3B). In contrast, incubation at 80 °C caused a drastic decrease in NGFR recognition of the mAb REA844 while not affecting the reactivity of mAb C40-1457. At 90 °C and 100 °C the fluorescent signal intensity mediated by the native mAb REA844 was similar to the isotype control staining. Although the overall signal intensity decreased with increasing temperatures and was lowest at 100 °C, the FFPE mAb C40-1457 was still able to bind to the 293-F/Mos1.Gag/trNGFR cells.

3.2.2. FF90 treatment induces the appearance of epitopes recognizable by FFPE-compatible antibodies

The combination of formaldehyde fixation and subsequent heat treatment at 90 °C, hereafter called FF90, was further evaluated using native and FF90 human PBMCs stained with antibodies directed against four different CD markers, namely CD3, CD4, CD8 and CD20. For each CD, a mAb recognizing only the native epitope but not the FFPE epitope (as proclaimed by the manufacturer) and *vice versa* was used.

Native PBMCs (no fixation) from two healthy donors were stained with the fluorophor-conjugated mAbs and analyzed using flow cytometry (Figure 3.4A). All antibodies recognizing the native epitope of their respective antigen bound to distinct subpopulations of native PBMCs: CD3⁺, CD8⁺ and CD20⁺ cells showed a single subpopulation, whereas CD4⁺ cells occurred as two subpopulations of PBMCs. In contrast, the antibodies recognizing an FFPE epitope of their respective antigen did not recognize any subsets of the native PBMCs. Only the FFPE-compatible anti-CD8 mAb showed a slight recognition of some cells above the background signal.

PBMCs from the same donors were subjected to FF90 fixation and subsequently stained using the same antibody set (Figure 3.4B). FF90 PBMCs stained with the native anti-CD3 mAb showed a weak increase in the overall fluorescent intensity of the whole PBMC population indicating an unspecific labeling with the anti-CD3 antibodies rather than a specific staining of CD3⁺ cells. The native anti-CD4 and the anti-CD8 mAbs did not recognize CD4⁺ and CD8⁺ FF90 PBMCs. In contrast, the native anti-CD20 mAb was still able to label CD20⁺ FF90 PBMCs.

3. Results

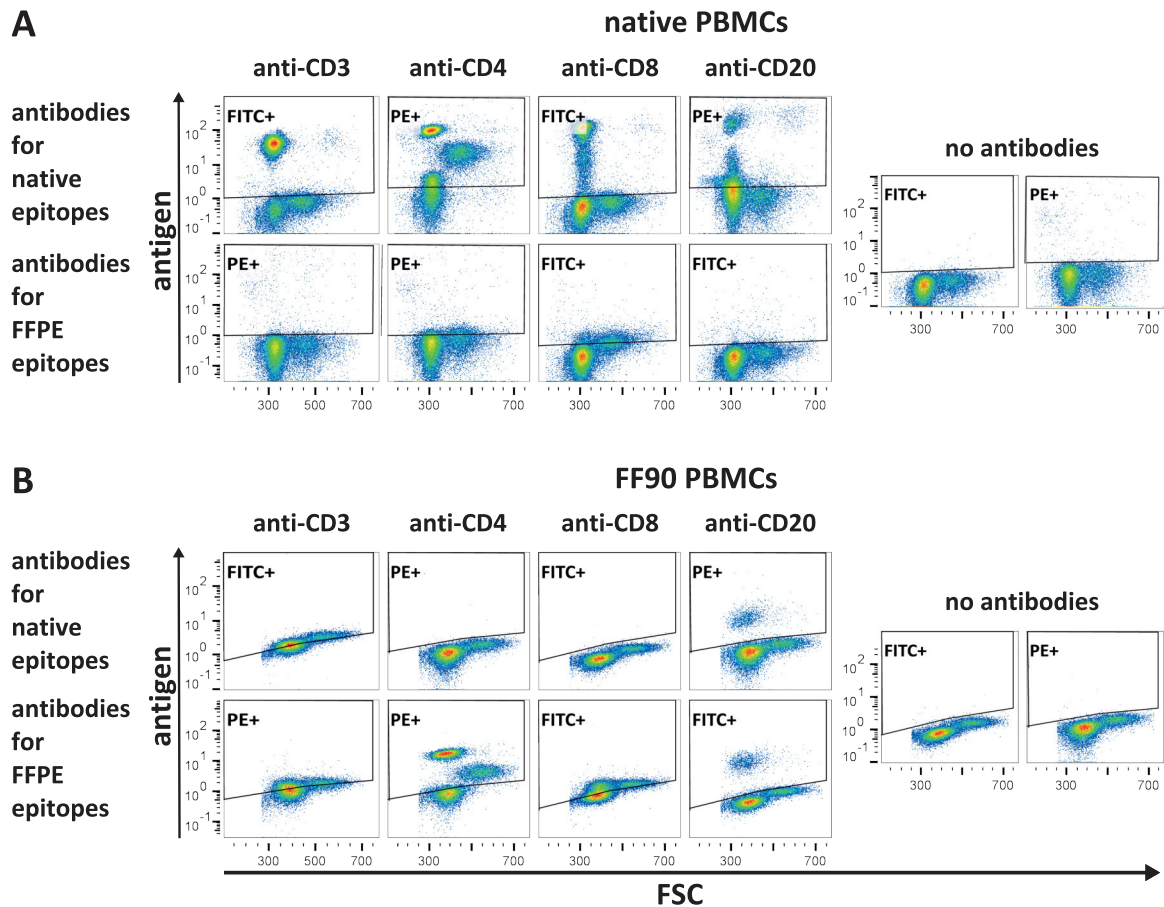


Figure 3.4. Representative flow cytometric results of native and formaldehyde- and 90 °C-fixed (FF90) peripheral blood mononuclear cells (PBMCs) from a healthy donor stained with different PE- or fluorescein isothiocyanate (FITC)-conjugated cluster of differentiation (CD) marker antibodies recognizing either native epitopes or formaldehyde-fixed paraffin-embedded (FFPE) epitopes. **(A)** Native PBMCs from a healthy donor. **(B)** PBMCs from the same donor stained after fixation in formaldehyde and subsequent heat-fixation at 90 °C (FF90 PBMCs). Cells not incubated with antibodies were used for gating to determine the unstained population.

Staining of FF90 PBMCs with the FFPE-compatible anti-CD3 mAb facilitated a similar weak increase in the overall fluorescent intensity of the FF90 PBMC population as the anti-CD3 mAb for the native epitope indicating unspecific binding. The FFPE anti-CD4 mAb exhibited the same pattern of CD4⁺ lymphocytes as the native anti-CD4 mAb when staining native PBMCs, whereas the FFPE anti-CD8 antibody showed a shift in fluorescent intensity similar to the one of the FFPE anti-CD3 mAb. The FFPE anti-CD20 mAb recognized a CD20⁺ subpopulation of FF90 PBMCs alike the native anti-CD20 antibody.

In summary, FF90 fixation almost completely reversed the staining pattern of the antibodies under investigation. Except for the native anti-CD20 mAb, no distinct FF90 PBMCs subpopulations were

3. Results

stained using the native anti-CD3, anti-CD4 and anti-CD8 mAbs. The FFPE mAbs anti-CD4 and anti-CD20 both labeled a subset of FF90 PBMCs similar to the native subpopulations stained with the respective antibodies specific for native epitopes. Encouraged by these results, the FF90 treatment was chosen for preparation of VLPs.

3.2.3. FF90 VLPs maintain their integrity and morphology after formaldehyde and heat fixation at 90 °C

VLPs for later immunization of mice were treated following the FF90 fixation procedure and subjected to ultracentrifugation to pellet the FF90 VLPs. In order to evaluate whether FF90 VLPs were still intact after the FF90 treatment, the pelleted FF90 VLP samples were assessed for their Gag content employing p24-Gag-specific ELISA and Gag-specific Western blot analysis. Gag proteins were not detectable using the antibody-based assays (data not shown). It appears feasible to assume that the formaldehyde fixation masked the epitopes recognized by the Gag-specific antibodies. However, transmission electron microscopic (TEM) imaging of native and FF90 VLPs revealed intact VLPs and a comparable morphology of both, native as well as FF90, VLPs (Figure 3.5A). The observed VLPs were spherical with the typical concentric ring of ordered immature Gag molecules below the VLP envelope [Wright et al. 2007; Martin et al. 2016]. Dynamic

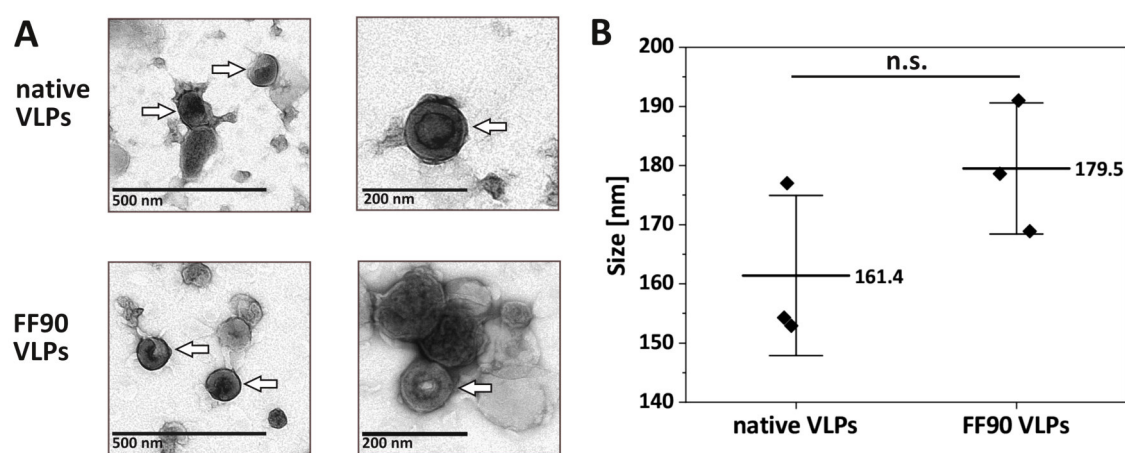


Figure 3.5. Morphology of VLPs before and after fixation. Native VLP samples were harvested from VLP producer cell pools and concentrated using ultracentrifugation. FF90 VLPs were obtained from formaldehyde and heat fixation of native VLPs at 90 °C. **(A)** Negative stain transmission electron microscopic images of native and FF90 VLPs. The arrows indicate VLPs. Scale bars shown represent 200 nm and 500 nm, respectively. **(B)** Determination of the average size of native and FF90 trNGFR-VLPs using dynamic light scattering measurement. Data are represented as mean \pm standard deviation from $n = 3$ individual VLP preparations and significance was calculated using independent two-sample t -test (not significant (n.s.): $p > 0.05$). Adapted from [Schatz et al. 2023b] (CC BY 4.0; <https://creativecommons.org/licenses/by/4.0/>).

light scattering (DLS) analysis of three individual VLP preparations showed that the average size of native VLPs was 161.4 ± 13.5 nm, whereas the diameter of FF90 VLPs was slightly bigger with an average size of 179.5 ± 11.1 nm (Figure 3.5B). No significant difference between the diameter of native and FF90 VLP preparations was observed using an independent two-sample *t*-test ($t=-1.793$, $df=4$, $p=0.147$). In addition, the samples were monodisperse as indicated by the low polydispersity indices (PDI) of native VLPs (0.110 ± 0.027) and FF90 VLPs (0.163 ± 0.021).

3.3. Generation and screening of monoclonal antibodies

Hybridoma technology was utilized to generate mAbs directed against fixed NGFR. For this purpose, two mice were immunized intravenously with FF90 VLPs displaying human trNGFR. As summarized in Figure 3.6, three doses of FF90 trNGFR-VLPs (9.5 μ g total protein) were administered at intervals of 14 days. Two days after the third injection, the blood was analyzed for NGFR-specific antibodies. The first mouse was sacrificed and hybridoma cell fusion was performed on day 31 (MZ34). The second mouse received a fourth dose of FF90 trNGFR-VLPs (3.2 μ g total protein) on day 56. Again, the blood was analyzed and splenocytes isolated from mouse 2 were fused with Sp2/0-Ag14 myeloma cells to generate hybridoma cells (MZ35).

3.3.1. Screening strategy for antibodies

For screening of blood and hybridoma antibodies, the 3T3/Gag/trNGFR screening cell line was generated using transposon vector-mediated gene transfer. Murine 3T3/Gag cells were co-transfected with the SB transposase expression construct (pSB100x-trNGFR-SEAP) and the transposon donor vector pSB-trNGFR-lhW encoding for the human trNGFR. Starting three days post transfection, the selection of stably transfected cells was initiated using increasing concentrations of hygromycin. At a final concentration of 400 μ g/mL hygromycin, single cells highly expressing trNGFR were isolated from the stable cell pool employing cell sorting and limiting dilution to establish the clonal screening cell line 3T3/Gag/trNGFR H6 (hereafter referred to as 3T3/Gag/trNGFR; Figure S3).

The screening strategy was based on flow cytometric analysis of a mixture of native and FF90 3T3/Gag/trNGFR cells. The increased autofluorescence of fixed 3T3/Gag/trNGFR cells at 450/50 nm allowed for separation between native and fixed cells during analysis. A representative example of the gating strategy for flow cytometric screening is shown in Chapter 5.6.3, Figure 5.2. The cell mixture was first incubated with the putative murine antibodies present in blood plasma samples or hybridoma cell culture supernatants and subsequently labeled using fluorophor-conjugated anti-mouse Ig secondary antibodies.

3. Results

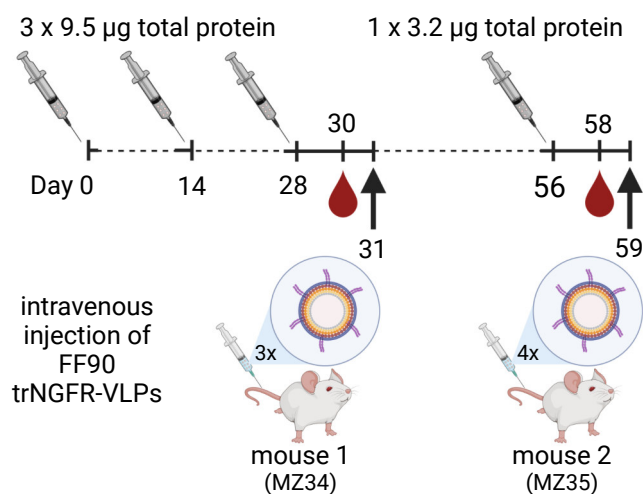


Figure 3.6. Immunization schedule. Two mice were immunized on day 0, 14 and 28 using 9.5 µg total protein of formaldehyde- and 90 °C heat-fixed trNGFR-VLPs (FF90 trNGFR-VLPs). The second mouse received a fourth dose consisting of FF90 trNGFR-VLPs (3.2 µg total protein) on day 56. Blood samples were taken two days after the last dose and hybridoma cell fusion was performed on the following day (indicated by the arrow). Adapted from [Schatz et al. 2023b] (CC BY 4.0; <https://creativecommons.org/licenses/by/4.0/>) and created with BioRender.com.

3.3.2. FF90 trNGFR-VLP immunization elicits blood IgG antibodies that bind to FF90 3T3/Gag/trNGFR cells

Two days after the third and fourth immunization, respectively, blood samples were taken and analyzed for antibodies binding to the murine 3T3/Gag/trNGFR screening cell line, which expressed the human trNGFR. Plasma samples from mice that did not receive any immunizations served as a negative controls. No IgG antibodies specific to native and FF90 3T3/Gag/trNGFR cells were detected in the plasma sample of the negative control mouse (Figure 3.7A). In contrast, IgG binding to FF90 3T3/Gag/trNGFR cells was present in the blood of mice immunized with FF90 trNGFR-VLPs. Immunization with the FF90 trNGFR-VLPs elicited only a weak IgG response to native 3T3/Gag/trNGFR cells. The fluorescent intensity of the IgG signal of mouse 1 was slightly more intense than the IgG signal of mouse 2. Hence, mouse 1 was chosen for the generation of hybridoma cells (fusion MZ34). Noteworthy, analysis of IgM antibodies revealed that IgM antibodies able to recognize epitopes of the FF90 3T3/Gag/trNGFR were already present in mice not immunized with the FF90 trNGFR-VLPs (Figure S4). Therefore, generated hybridoma cells were only screened for IgG antibodies. Mouse 2 was boosted with a fourth dose of FF90 trNGFR-VLPs (3.2 µg total protein) at day 56. Two days later, the blood was analyzed for antibodies binding to 3T3/Gag/trNGFR cells. The administration of the additional VLP boost induced an increase in IgG antibodies binding to FF90 as well as to native 3T3/Gag/trNGFR cells (Figure 3.7B). The IgM antibodies remained unchanged (Figure S4).

3. Results

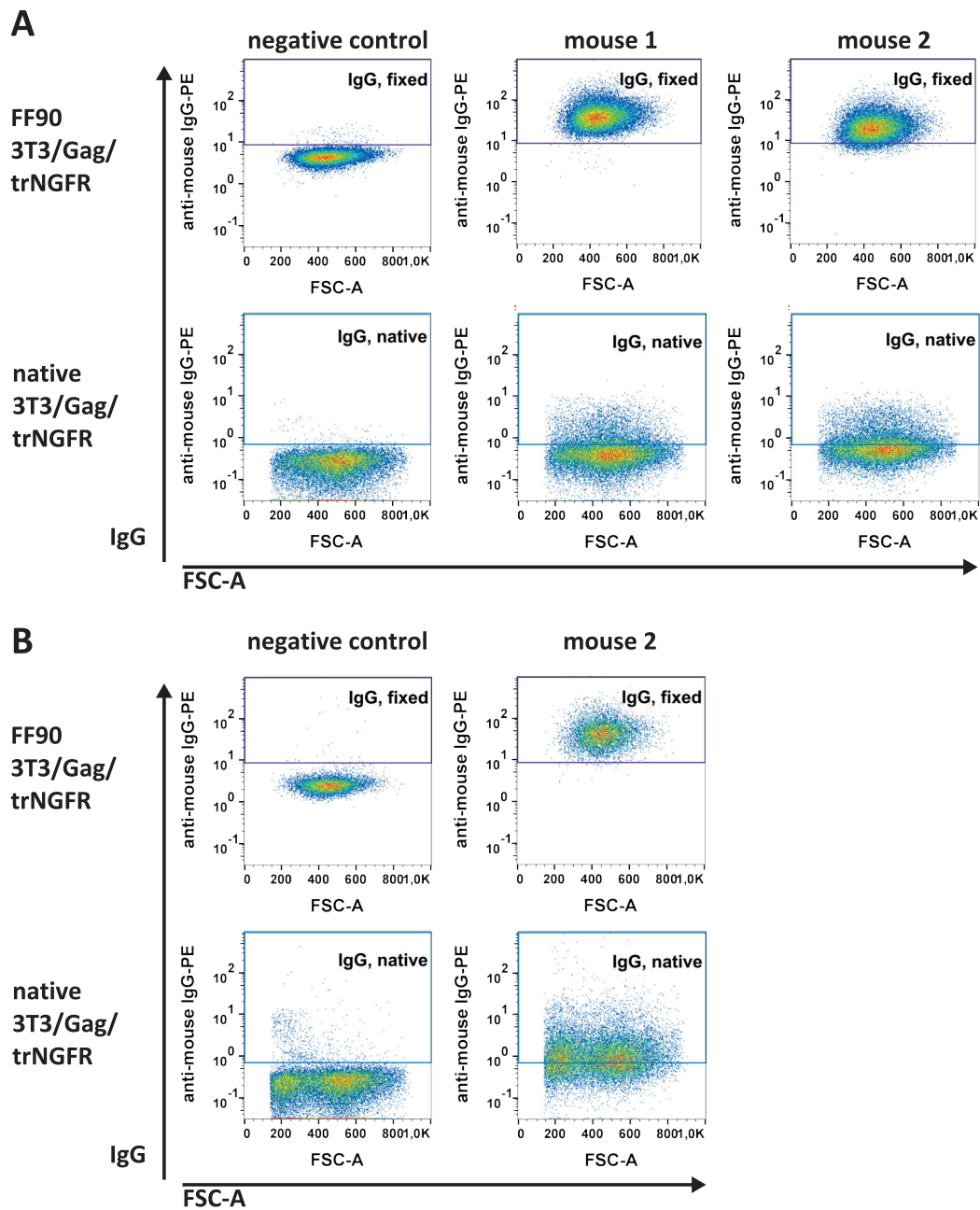


Figure 3.7. Flow cytometric results of murine IgG antibodies present in blood plasma. The 3T3/Gag/-trNGFR screening cell line was incubated with blood plasma samples. The murine IgG antibodies were subsequently labeled with PE-conjugated anti-mouse IgG1 and IgG2ab secondary antibodies. **(A)** Blood plasma samples drawn from mouse 1 and mouse 2 on day 30 and from a negative control mouse not immunized with the VLP immunogen. Mouse 1 and 2 received three immunizations. The screening cells were incubated with 35 μ L of plasma. **(B)** Plasma sample taken from mouse 2 on day 58 and from a negative control mouse not immunized with the VLP immunogen. Mouse 2 received a fourth dose of FF90 trNGFR-VLPs. The screening cells were incubated with 25 μ L of plasma. Adapted from [Schatz et al. 2023b] (CC BY 4.0; <https://creativecommons.org/licenses/by/4.0/>).

3.3.3. FF90 trNGFR-VLP immunization generates hybridoma antibodies that recognize FF90 3T3/Gag/trNGFR cells

After fusion of splenocytes and Sp2/0-Ag14 myeloma cells, culture supernatants of hybridoma cell cultures showing one or more clusters of cells were initially screened for reactivity with native and FF90 3T3/Gag/trNGFR cells employing flow cytometry. Cultures were defined as positive when at least 90 % of the native or FF90 screening cells were labeled with fluorophore-conjugated anti-mouse IgG1 or IgG2ab secondary antibodies, respectively. Table 3.3 summarizes the results of the screening. The first hybridoma cell fusion MZ34 using splenocytes isolated from mouse 1, which received three VLP immunizations, yielded in total 698 hybridoma cell clones. Of these clones, only 3 reactive clones were identified as producers of FF90 3T3/Gag/trNGFR-reactive antibodies (0.4 % of tested supernatants). Two antibodies belonged to the Ig class IgG1 and one antibody to class IgG2ab. In contrast, hybridoma cell fusion MZ35 performed with splenocytes of mouse 2, which was immunized with four doses, resulted in 975 hybridomas of which 35 clones produced FF90 3T3/Gag/trNGFR-reactive mAbs (3.6 % of tested supernatants). Only one antibody bound to an epitope present in native as well as FF90 cells (Figure S22). Among the 35 identified MZ35 clones, 26 clones (74.3 %) produced IgG2ab antibodies and 9 clones (25.7 %) were IgG1 producers. This observation is in accordance with the reported property of VLPs to preferentially stimulate the differentiation of B cells into IgG2a-secreting cells [Zhang et al. 2009; Lee et al. 2017]. The respective dot plots of the flow cytometric screening results of the positive hybridomas are appended in Chapter A.4, Figures S5-S23.

Table 3.3. Summary of the flow cytometric screening results of hybridoma cell cultures for FF90 NGFR reactivity and specificity. In the first screening, hybridoma supernatants were tested for reactivity with native and FF90 3T3/Gag/trNGFR cells. In the second screening, hybridoma supernatants were tested for specificity to NGFR employing NGFR-negative FF90 human peripheral blood mononuclear cells (PBMCs). Adapted from [Schatz et al. 2023b] (CC BY 4.0; <https://creativecommons.org/licenses/by/4.0/>).

ID	Immunization	Screening	Cells used for screening	Reactive mAbs/ tested mAbs
MZ34	3 x FF90 trNGFR-VLPs	1st	native and FF90 3T3/Gag/trNGFR ⁺	3/698 (0.4 %) ^a
		2nd	FF90 PBMCs (NGFR ⁻)	2/2 (100.0 %) ^b
MZ35	4 x FF90 trNGFR-VLPs	1st	native and FF90 3T3/Gag/trNGFR ⁺	35/975 (3.6 %) ^a
		2nd	FF90 PBMCs (NGFR ⁻)	4/13 (30.8 %) ^b

^a Number of positive individual hybridoma supernatants (supernatant from a single well) out of total number of screened hybridoma supernatants.

^b Number of reactive, that is NGFR-unspecific, individual hybridoma supernatants out of tested positive hybridoma supernatants identified in the 1st screening.

3. Results

Positive cultures were expanded and single subclones were generated by limiting dilution of cultures containing more than one cell cluster. The hybridoma supernatants were frequently retested during cultivation and approximately half of the initially positive cultures lost their ability to produce antibodies or stopped growing. Finally, 15 hybridoma antibody candidates were successfully expanded and further tested for their specificity to FF90 NGFR.

The VLPs used for immunization were produced in human 293-F/Mos1.Gag/trNGFR cells, and thus some human host cell proteins were co-incorporated into the VLPs along with the target antigen trNGFR. Consequently, the hybridoma supernatants were tested for reactivity with FF90 human PBMCs and in parallel with FF90 3T3/Gag/trNGFR cells as control. Human PBMCs were chosen for specificity testing to identify hybridoma antibodies that unspecifically recognize human host cell proteins. Noteworthy, NGFR expression was reported on approximately 20% of PBMCs [Morgan et al. 1989] and associated with CD20⁺-positive B lymphocytes [Brodie et al. 1996]. Therefore, the FF90 PBMCs were co-stained with an anti-CD20 mAb to exclude CD20⁺ cells from the specificity analysis. Stain indices (SIs) for each antibody were calculated as the difference between the mean fluorescent intensity (MFI) of the tested antibody and the isotype control antibody divided by 2-fold the standard deviation of the isotype control's MFI. Antibodies that showed a SI > 1.0 were considered as reactive.

All fifteen tested hybridoma antibodies were confirmed as FF90 3T3/Gag/trNGFR binders. With the exception of the mAb 3H6 (SI: 3.5), the SIs of the other fourteen mAbs were above 15 (Figure 3.8A+B). In contrast, the SIs of the FF90 PBMC staining ranged from 0 to 228. The two hybridoma mAbs 11D6.44 and 14B4.7.2 from fusion MZ34 as well as four of the thirteen tested mAbs from fusion MZ35, namely 8B6, 12D1, 19B3 and 20G3, bound to NGFR-negative FF90 PBMCs (all revealing SIs > 1.0) and therefore were classified as non-specific to FF90 NGFR (Table 3.3, Figure 3.8A). Figure 3.8C shows representative examples of anti-mouse IgG versus forward scatter area (FSC-A) dot plots of FF90 PBMCs at four different SIs. Noteworthy, the anti-NGFR mAb C40-1457 exhibited an unspecific staining of NGFR-negative FF90 PBMCs, too.

In summary, no antibodies derived from fusion MZ34 were FF90 NGFR-specific, but nine mAbs – namely 3H6, 5G10, 6E7, 6G8, 16D8.1, 18F10, 19C5, 19H2 and 20A9 – derived from fusion MZ35 showed specificity for FF90 NGFR as these mAbs did not bind to the NGFR-negative FF90 PBMCs.

3. Results

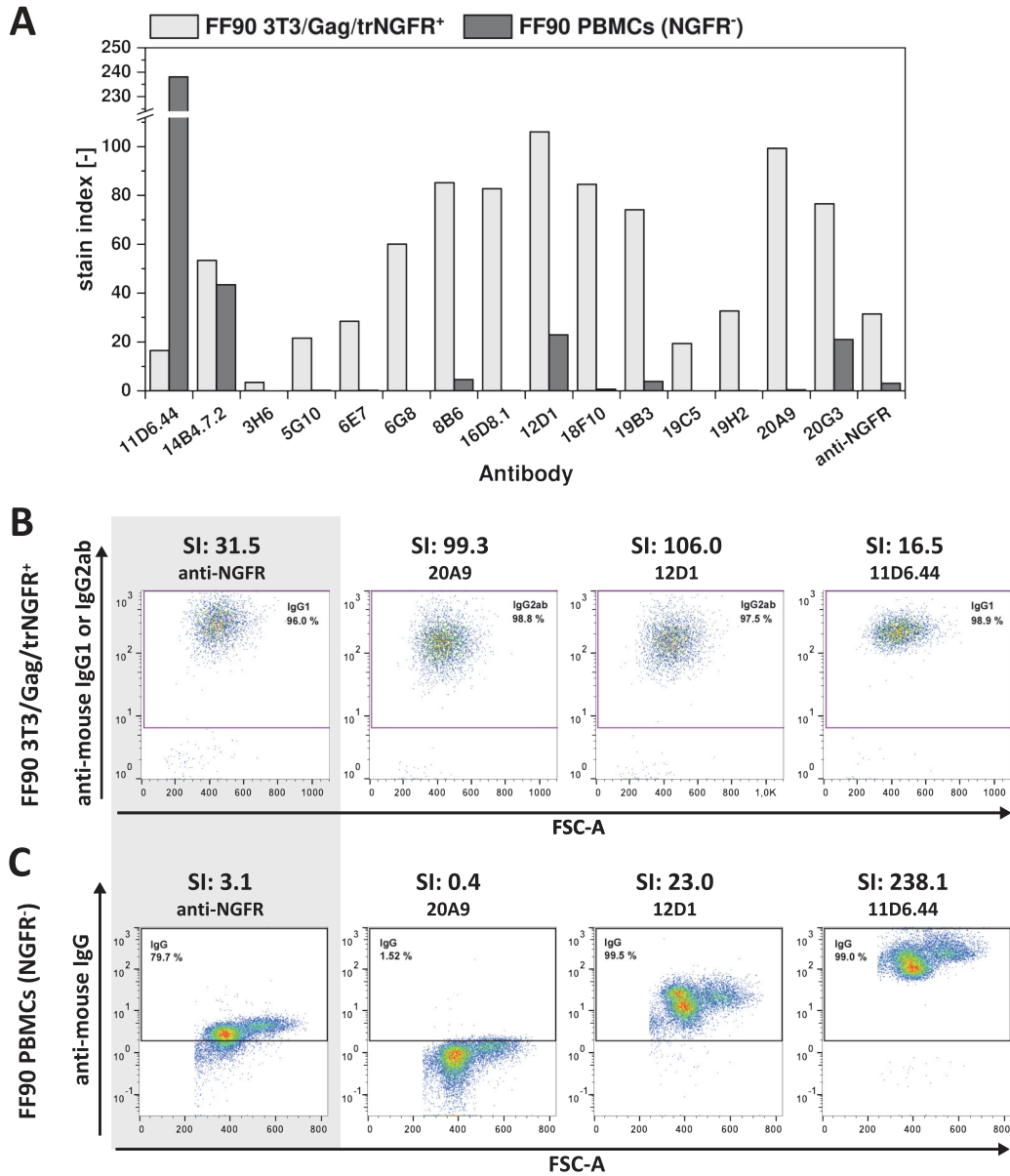


Figure 3.8. Specificity of hybridoma mAbs for FF90 NGFR. Human FF90 PBMCs were stained with either hybridoma supernatants or the commercial murine control antibody anti-NGFR mAb C40-1457. As positive control FF90 3T3/Gag/trNGFR cells were stained in parallel with hybridoma supernatants or the anti-NGFR mAb C40-1457. **(A)** Stain indices (SI) of murine antibodies used to stain FF90 3T3/Gag/trNGFR cells (light grey) and FF90 PBMCs (dark grey). SI were calculated as the difference between the mean fluorescent intensity (MFI) of the sample and the isotype control divided by 2-fold the standard deviation of the isotype control's MFI. **(B)** Exemplary anti-mouse IgG1 and anti-mouse IgG2ab vs. forward scatter area (FSC-A) plots of FF90 3T3/Gag/trNGFR control cells (trNGFR-positive). **(C)** Exemplary anti-mouse IgG vs. FSC-A plots of NGFR-negative FF90 PBMCs for four different SI values. The control antibody anti-NGFR mAb C40-1457 is highlighted in grey. Adapted from [Schatz et al. 2023b] (CC BY 4.0; <https://creativecommons.org/licenses/by/4.0/>).

3.3.4. The majority of generated hybridoma antibodies is also specific for FFPE 3T3/Gag/trNGFR cells

The ultimate aim of the immunization was to generate mAbs that recognize the FFPE target antigen. Samples and tissues preserved as FFPE blocks represent a huge source of material for research studies [Gaffney et al. 2018; Tucker et al. 2019]. To further test the hybridoma antibodies for applicability to FFPE samples, 3T3/Gag/trNGFR cells and PBMCs were alternatively fixed using formaldehyde and subsequently embedded in paraffin wax following the protocol for FFPE single cell preparation. After deparaffinization, heat-induced epitope retrieval was performed and the FFPE cells were used to test the 15 FF90 3T3/Gag/trNGFR-binding mAbs for their reactivity and specificity to FFPE NGFR.

Both hybridoma mAbs 11D6.44 and 14B4.7.2 from fusion MZ34 initially identified as FF90 3T3/-Gag/trNGFR binders were also able to recognize the alternatively fixed FFPE 3T3/Gag/trNGFR cells (Table 3.4). However, these two mAbs were not specific for FFPE NGFR as they bound to the NGFR-negative FFPE PBMCs. Of the 13 mAbs from fusion MZ35, 12 mAbs were identified as FFPE 3T3/Gag/trNGFR binders (92.3 % of the tested mAbs initially identified as reactive to FF90 3T3/Gag/trNGFR cells) and of the 12 identified FFPE binders, only three (25 %) mAbs bound to FFPE NGFR-negative PBMCs and therefore were unspecific for FFPE NGFR. Consequently, the remaining nine mAbs (75 %) were identified as FFPE NGFR-specific.

Table 3.4. Summary of the flow cytometric screening results of hybridoma cell cultures for FFPE NGFR reactivity and specificity. Fifteen hybridoma cultures identified as binders to FF90 3T3/Gag/trNGFR cells were screened for reactivity with FFPE 3T3/Gag/trNGFR cells and FFPE human PBMCs. Adapted from [Schatz et al. 2023b] (CC BY 4.0; <https://creativecommons.org/licenses/by/4.0/>).

ID	Immunization	Cells used for screening	Reactive mAbs/ tested mAbs	FFPE NGFR- specific mAbs
MZ34	3 x FF90 trNGFR-VLPs	FFPE	2/2 (100.0 %) ^a	
		3T3/Gag/trNGFR ⁺ FFPE PBMCs (NGFR ⁻)	2/2 (100.0 %) ^b	0/2 (0.0 %)
MZ35	4 x FF90 trNGFR-VLPs	FFPE	12/13 (92.3 %) ^a	
		3T3/Gag/trNGFR ⁺ FFPE PBMCs (NGFR ⁻)	3/12 (25.0 %) ^b	9/12 (75.0 %)

^a Number of positive individual hybridoma supernatants out of total number of tested hybridoma supernatants identified as FF90 3T3/Gag/trNGFR binders.

^b Number of NGFR-unspecific individual hybridoma supernatants out of total number of tested positive hybridoma supernatants identified as FFPE 3T3/Gag/trNGFR binders.

3. Results

The SIs of hybridoma supernatants used to stain FFPE 3T3/Gag/trNGFR cells were generally lower than the SIs of the FF90 3T3/Gag/trNGFR staining and ranged from 0.7 to 107.4 with the majority of SIs below 15 (Figure 3.9A). The antibody 19C5 exhibited a SI of 0.7 and was therefore classified as an FFPE non-binder. The other hybridoma antibodies had SIs > 1.0 and were rated as FFPE 3T3/Gag/trNGFR binders. However, the SI of antibody 3H6 was only 1.2. The anti-NGFR mAb C40-1457 labeled FFPE 3T3/Gag/trNGFR and revealed a SI of 48.4. Representative examples of antibodies binding to FFPE 3T3/Gag/trNGFR cells are shown in Figure 3.9B.

The SIs of NGFR-negative FFPE PBMC stainings ranged from 0 to 223.6 with the majority of SIs < 1. The SIs of hybridoma mAbs 8B6 and 20G3 were close to 1.0 exhibiting SIs of 1.1 and 0.9, respectively. The hybridoma mAbs 11D6.44 and 14B4.7.2 from fusion MZ34 as well as 8B6, 19B3 and 12D1 from fusion MZ35 showed SIs > 1.0 indicating non-specificity for FFPE NGFR. In contrast to the results obtained from the FF90 PBMCs labeling, the anti-NGFR mAb C40-1457 did not bind unspecifically to FFPE PBMCs. Figure 3.9C shows representative examples of anti-mouse IgG versus FSC-A dot plots of FFPE PBMCs at different SIs.

In summary, most hybridoma antibodies that recognized FF90 3T3/Gag/trNGFR cells specifically bound to FFPE 3T3/Gag/trNGFR cells, too. The two antibodies derived from fusion MZ34 were FFPE-reactive but not NGFR-specific. Nine antibodies – namely 3H6, 5G10, 6E7, 6G8, 16D8.1, 18F10, 19H2, 20A9 and 20G3 – derived from fusion MZ35 showed specificity for FFPE NGFR.

3. Results

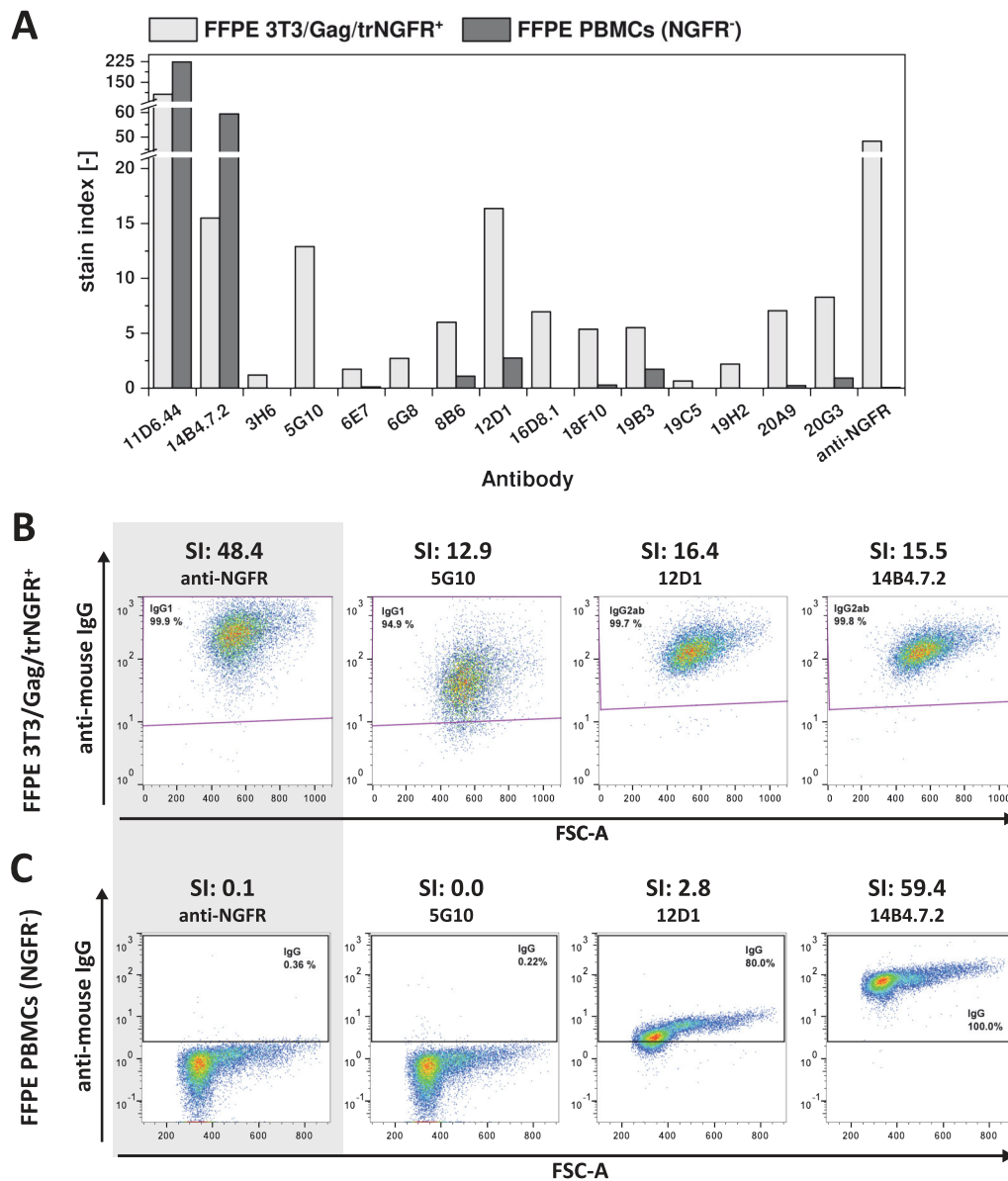


Figure 3.9. Reactivity and specificity of hybridoma mAbs for FFPE NGFR. FFPE 3T3/Gag/trNGFR cells were stained with hybridoma antibodies or the anti-NGFR mAb C40-1457 to identify hybridoma mAbs that recognize FFPE NGFR. In parallel, human FFPE PBMCs were stained with either hybridoma mAbs or the murine control antibody anti-NGFR mAb C40-1457 as well as the human anti-CD20 mAb to exclude CD20⁺ PBMCs from analysis. **(A)** Stain indices (SI) of murine antibodies used to stain FFPE 3T3/Gag/trNGFR cells (light grey) and FFPE PBMCs (dark grey). SI were calculated as the difference between the mean fluorescent intensity (MFI) of the sample and the isotype control divided by 2-fold the standard deviation of the isotype control MFI. **(B)** Exemplary anti-mouse IgG1+IgG2ab vs. FSC-A plots of FFPE 3T3/Gag/trNGFR cells. **(C)** Exemplary anti-mouse IgG vs. FSC-A plots of FFPE PBMCs for different SI values showing the anti-NGFR control antibody and the 5G10 hybridoma antibody as non-reactive mAbs (SI < 1), and the 12D1 and 14B4.7.2 hybridoma antibodies as reactive mAbs. The control antibody anti-NGFR mAb C40-1457 is highlighted in grey. Adapted from [Schatz et al. 2023b] (CC BY 4.0; <https://creativecommons.org/licenses/by/4.0/>).

4. Discussion

In this thesis, a novel approach to antigen preparation was developed allowing for the generation of FFPE-compatible mAbs using hybridoma technology. HIV-derived VLPs displaying trNGFR were produced in recombinant 293-F cell pools. The isolated trNGFR-VLPs were subjected to the novel simplified formaldehyde and 90 °C heat fixation (FF90) protocol developed in this thesis to generate FFPE-like trNGFR target antigen for immunization. In a flow cytometric screening setting, the capability of the FF90 trNGFR-VLPs to elicit antibodies specific for native, FF90 and FFPE trNGFR was evaluated.

At first, stable VLP producer cell pools were successfully established and Gag productivity was assessed in CFSNs. The stable 293-F/Mos1.Gag and 293-F/Mos1.Gag/trNGFR cell pools produced between 53 ng/mL to 180 ng/mL p24-Gag in CFSNs. Published data on the productivity of 293-F derivatives producing HIV-derived VLPs is usually obtained from transient expression of Gag proteins. Nevertheless, the measured p24-Gag concentrations of the stable cell pools were comparable to Gag concentrations reported for transient production [Cervera et al. 2013; Fuenmayor et al. 2018]. However, after isolation of VLPs from the CFSN employing ultracentrifugation, significant differences in VLP formation were observed between the 293-F/Mos1.Gag and the 293-F/Mos1.Gag/trNGFR cell pool. Approximately 10-fold more VLPs (535 ± 59 ng Gag) were isolated from 293-F/Mos1.Gag cultures, whereas only 55 ± 19 ng Gag-containing VLPs were produced by 293-F/Mos1.Gag/trNGFR cells. This difference in VLP productivity might be a result of the two-step generation of the 293-F/Mos1.Gag/trNGFR cell pool. The parental 293-F/Mos1.Gag cells were established first utilizing PB transposon vector components to stably introduce the *mos1.gag* CDS and a puromycin selection marker into the genome [Rosengarten et al. 2022b]. Secondly, the expression cassette for trNGFR and a hygromycin selection marker was stably introduced into the genomes of the polyclonal 293-F/Mos1.Gag cell pool utilizing the SB transposon system to avoid remobilization of the PB-based transposable element. Usually, establishment of more than one gene of interest using transposon vector systems is performed by co-transfection and simultaneous selection of all genes of interest at once [Berg et al. 2019; van Heuvel et al. 2021]. During the first weeks of establishing the stable 293-F/Mos1.Gag/trNGFR cell pool, the cells were selected using hygromycin alone. Puromycin was added to the cultures three weeks after transfection and since then both antibiotics were constantly applied during cultivation of the stable cell pool. The absence of puromycin selection in the early stages of cell pool establishment

4. Discussion

might have resulted in the enrichment of cell clones revealing a high trNGFR expression but lower Mos1.Gag expression levels. The stability of protein production of cell pools generated by PB-mediated gene transfer in the absence of selection was investigated recently. After an initial reduction by about 50 % of the initial protein concentration, the productivity of the investigated cell pools remained stable [Balasubramanian et al. 2015; Balasubramanian et al. 2016]. The authors reported an average reduction of productivity ranging between 10 % to 15 % per week during the first two months of cultivation. However, the investigated cell pools expressed only one protein encoded in a single transposon and the authors did not examine whether the cell pool regained its productivity after re-initialization of puromycin selection. Whether the lower VLP formation of the stable 293-F/Mos1.Gag/trNGFR cells compared to the parental 293-F/Mos1.Gag cells, was a result of a selection of poor Gag-expressing cells from the polyclonal parental cell pool or might have resulted from trNGFR expression interfering with efficient VLP formation remains elusive.

During the development of the stable 293-F-derived trNGFR-VLP producer cell pool, it was discovered that 293-F cells endogenously express the NGFR. Recently, Chen and colleagues reported the endogenous expression of the *ngfr* gene in 293T cells [Chen et al. 2020a]. Further investigation of additional HEK-293 derivatives by our group revealed that HEK-293, 293-F and 293T/17 cells expressed NGFR [Schatz et al. 2023a]. Using an NGFR-specific ELISA and a VLP capture assay, it was demonstrated that the full-length wild-type NGFR is not incorporated into VLPs produced by 293-F/Mos1.Gag cells. In contrast, trNGFR, with a truncated cytoplasmic tail of only 8 amino acids, is incorporated into VLPs as demonstrated in this thesis and published previously for HIV-derived viral vector particles [Jamali et al. 2019]. As NGFR is present in lipid rafts [Sharma et al. 2019], the sites of HIV budding, the failure to incorporate NGFR into VLPs most likely results from steric hindrance of the long cytoplasmic tail (155 amino acids) of wild-type NGFR. The trNGFR-VLPs described here incorporated on average 284 ± 24 trNGFR molecules per particle, which is within the range of 169 to 350 trNGFR molecules described for the lentiviral vector particles [Jamali et al. 2019].

The antigen format used for immunization is crucial for eliciting adequate antibody responses and should resemble the structure of the antigen in the application in which the generated mAb will be utilized [Ebersbach and Geisse 2012]. Therefore, the FF90 fixation procedure developed in this study aimed for the generation of FFPE-like antigens and consisted of formaldehyde fixation of the antigen and subsequent incubation at 90 °C. For the development of the FF90 procedure, the recombinant trNGFR expressed on the surface of human 293-F/Mos1.Gag/trNGFR cells was used as a model antigen. Changes in the immunoreactivity of the trNGFR after exposure to different reagents and conditions were monitored using two antibodies with different recognition capacities. The first anti-NGFR mAb is specific for an epitope present in native and acetone-

4. Discussion

or formaldehyde-fixed NGFR but not in FFPE NGFR. The second FFPE-compatible anti-NGFR mAb recognizes an epitope present in native, formaldehyde-fixed and FFPE NGFR. After FF90 treatment, only the FFPE-compatible mAb was able to bind to the 293-F/Mos1.Gag/trNGFR cells indicating that the target antigen changed its structure in an FFPE-like manner. The FF90 fixation was further evaluated by testing additional epitopes using FF90 human PBMCs and a panel of mAbs recognizing the CD markers CD3, CD4, CD8 and CD20. For each CD, a mAb recognizing only the native epitope but not the FFPE epitope and *vice versa* was used. Of the tested mAbs for native epitopes, only the anti-CD20 mAb was able to react with a subpopulation of the FF90 PBMCs. In contrast, two FFPE-compatible mAbs (anti-CD4 and the anti-CD20) were able to bind the respective FF90 CD4⁺ and CD20⁺ PBMC subpopulations. Although the FF90 fixation was not able to induce the appearance of all epitopes recognizable by the four tested FFPE-compatible mAbs, the results demonstrated that during the FF90 process the investigated membrane proteins at least partially acquired an antigen format similar to that obtained during the FFPE treatment. This assumption was further underlined by the binding profile of the majority of the generated hybridoma mAbs that recognized epitopes present on FF90 and FFPE 3T3/Gag/trNGFR cells but no native epitopes. Only a single mAb was identified in the first screening that was able to recognize an epitope present on native and FF90 3T3/Gag/trNGFR cells. As the FF90 procedure skips several steps present in the FFPE protocol including incubation in alcohol, paraffin embedding, clearing in xylene and heat-induced epitope retrieval, the missing immunoreactivity of the FFPE-compatible anti-CD3 and anti-CD8 mAbs might be attributed to the absence of modifications caused by the omitted steps.

The FF90 procedure was successfully applied to trNGFR-displaying VLPs. TEM analysis revealed that the FF90 trNGFR-VLPs maintained their spherical structure and the typical concentric ring of ordered immature Gag molecules below the VLP envelope [Wright et al. 2007; Martin et al. 2016]. The average diameter of FF90 VLPs determined by DLS measurement slightly increased to 179.5 ± 11.1 nm as compared to the diameter of 161.4 ± 13.5 nm of the native VLPs. The mean diameter of native VLPs was within the range typical for HIV-1-like particles (141 ± 35 nm; [Martin et al. 2016]). The low polydispersity index of 0.163 ± 0.021 of the FF90 VLP formulation indicated that the sample was monodisperse and no aggregation or disintegration of VLPs occurred during the FF90 fixation.

The FF90 trNGFR-VLPs were used to intravenously immunize mice to elicit an immune response directed against the fixed target antigen trNGFR. After three immunizations with 9.5 µg FF90 trNGFR-VLPs, serum IgG was analyzed and IgG antibodies binding to the FF90 3T3/Gag/trNGFR screening cells and to a smaller extend also to native cells were detected. Administration of additional 3.2 µg trNGFR-VLPs resulted in an increase of the response to FF90 and native cells.

Noteworthy, non-trNGFR-specific natural IgM antibodies present in the blood samples of non-immunized animals recognized the FF90 screening cells, but not native screening cells. Natural antibodies are present in the blood of non-immunized individuals at low titers, recognize bacterial and viral antigens and are often cross-reactive with a variety of antigens [Matter and Ochsenbein 2008]. As the membrane envelope of the trNGFR-VLPs originates from the human host cell membrane, it can be assumed that the natural IgM antibodies also recognize the FF90 trNGFR-VLPs. Natural IgM molecules are known to promote the delivery of viral particles to lymphatic organs and hence, improve adaptive immune responses [Boes et al. 1998; Boes 2000; Link et al. 2012; Panda and Ding 2015].

Despite the efficient generation of hybridoma cells, the frequency of FF90 3T3/Gag/trNGFR-reactive mAb-secreting hybridoma cultures identified in the initial screening was comparably low: Only 0.4 % of hybridoma cultures generated from the splenocytes of the mouse receiving three immunizations, and 3.6 % of the hybridoma cultures originating from the mouse receiving four immunizations were positive. This finding is in accordance with the results from Wang and colleagues who observed frequencies between 0.7 % and 89.6 % (median frequency of 2.3 %) of positive hybridoma cultures after 5 to 10 immunizations using a combination of 100 µg of soluble synthetic peptides and sodium dodecyl sulphate-polyacrylamide gel electrophoresis (SDS-PAGE)-purified proteins as immunogens [Wang et al. 2005]. However, since VLPs are generally more immunogenic than peptides and soluble proteins [Sailaja et al. 2007; McBurney et al. 2007; Khan et al. 2015], it is likely to assume that the FF90 treatment may have decreased the immunogenicity of the FF90 VLPs, resulting in the low percentage of reactive hybridoma cultures. Di Tommaso and colleagues investigated the influence of formaldehyde-treated bacterial proteins on antigen recognition by T cells *in vitro* [Di Tommaso et al. 1994]. The authors observed impaired T cell activation and antigen processing by B cells after formaldehyde treatment of the antigens. On the contrary, studies investigating the *in vivo* processing of native model antigens suggest that proteins that are more resistant to endo-lysosomal degradation by proteases – in other words antigen processing – are more immunogenic than less stable proteins [Delamarre et al. 2005; Delamarre et al. 2006]. Furthermore, proteins stabilized by aldehyde fixation (10 mM (0.03 %) paraformaldehyde and 2 mM glutaraldehyde) showed increased proteolytic resistance and immunogenicity [Delamarre et al. 2006]. Similar results were obtained by Hankaniemi and co-authors, who stabilized Coxsackievirus B1 VLPs in 0.01 % formalin solution and observed even increased immunogenicity of fixed VLPs compared to untreated VLPs [Hankaniemi et al. 2019a; Hankaniemi et al. 2019b]. Nevertheless, the concentrations of formaldehyde used in these studies were much lower than those used to prepare the FF90 VLPs. As a result, the proteins in FF90 VLPs may be considerably more cross-linked and therefore less susceptible to proteolytic degradation during antigen processing resulting in less efficient T cell activation and reduced B cell-mediated antibody responses.

23 of the 38 hybridoma cell clones (60.5 %) that initially produced FF90 3T3/Gag/trNGFR-reactive mAbs converted to non-producers after one or more passages. Wang and colleagues observed similar losses between two screens of up to 97 % for some antigens and screening methods [Wang et al. 2005]. These high percentages are most likely attributed to the instability of hybridoma cells and might be mitigated by repeated subcloning and enrichment of highly efficient producer cells in the hybridoma cell cultures [Kromenaker and Sreenc 1994; Bradbury et al. 2018].

Typically, soluble peptide or protein formulations are used for immunization. However, the use of soluble antigens often requires multiple immunizations and additional adjuvants. For example, Torigoe and colleagues immunized mice eight times with 200 µg of the extracellular domain of human leukocyte antigen mixed with Freund's adjuvant [Torigoe et al. 2012], and Suzuki and coauthors administered four times 100 µg synthetic peptides conjugated to keyhole limpet hemocyanin and mixed with alum adjuvant to isolate 12 hybridoma clones recognizing a CD44 variant [Suzuki et al. 2023]. For the isolation of FFPE-compatible mAbs directed against membrane proteins, denatured recombinant proteins were successfully utilized [O'Shannessy et al. 2011; Hatano et al. 2014; Hatano et al. 2019]. Good results were obtained by O'Shannessy *et al.* who administered three doses of 50 µg urea-denatured, reduced and alkylated recombinant protein to immunize mice and to isolate mAbs recognizing the folate receptor alpha, a glycoprotein with a complex three-dimensional structure [O'Shannessy et al. 2011]. In contrast to the studies described above, the FF90 VLP immunization required only four injections of up to 9.5 µg total protein and no additional adjuvants to generate 35 hybridoma clones initially producing FF90 3T3/Gag/trNGFR-reactive mAbs and resulted in the isolation of nine mAbs specific for FFPE NGFR. This might be attributed to the particulate structure of VLPs known to efficiently activate immune cells and stimulate humoral immune responses [Nooraei et al. 2021] and underlines the potential of FF90 VLPs as immunogens for the generation of FFPE-compatible mAbs despite the possible detrimental effect of formaldehyde fixation on immunogenicity. However, to what extent the FF90 treatment of the trNGFR-VLPs contributed to the elicitation of preferentially FFPE-compatible mAbs or might have affected the immunogenicity of VLPs is not yet clear, since in this thesis potential differences in mAb generation after immunization of mice with native trNGFR-VLPs were not examined.

The immunization of mice with four FF90 trNGFR-VLP injections led to the discovery of nine FFPE NGFR-specific mAbs, whereas immunization with only three injections elicited no FFPE NGFR-specific mAbs. As the number of hits in the initial FF90 3T3/Gag/trNGFR screening increased about 12-fold from 3 to 35 after administering an additional FF90 trNGFR-VLP boost, further optimization of the immunization scheme including additional boosts, higher amounts of VLPs or the addition of adjuvants may improve the immune response and enhance the percentage of

hybridomas that produce antigen-specific mAbs. The nine isolated mAbs recognized epitopes that were present on FF90 and FFPE cells but not detectable on native cells. To evaluate the applicability of the discovered mAbs for IHC, the mAbs should be further tested for reactivity and specificity in FFPE human tissue sections. In addition, conducting cross-blocking tests to map the epitopes recognized by the mAbs and sequencing of variable region cDNAs of the antibodies should reveal from how many different B cell clones the isolated reactive mAbs originated.

It is noteworthy that flow cytometric screening of hybridoma supernatants with FF90 cells recombinantly expressing the target antigen trNGFR represents a reliable method to identify mAb-secreting hybridomas capable of staining FFPE cells expressing the target antigen. This underlines that proteins subjected to the FF90 procedure acquired an FFPE-like antigen format. However, since the first screening was performed with FF90 3T3/Gag/trNGFR screening cells, hybridoma clones expressing antibodies that were exclusively reactive to FFPE 3T3/Gag/trNGFR cells but not to FF90 cells may have been missed. Nevertheless, in comparison to the FFPE procedure, the FF90 fixation protocol is easy-to-perform and requires less resources. FF90 cells for screening can be prepared in a few hours following a two-step protocol, whereas the FFPE procedure is considerable more complex and time-consuming as it includes formaldehyde fixation, dehydration, overnight paraffin wax embedding, dewaxing, rehydration and antigen retrieval.

In summary and as demonstrated in this thesis, the FF90 fixation is applicable for the preparation of enveloped HIV-derived VLPs decorated with the trNGFR cell surface antigen and facilitated the generation of mAbs specific for FFPE NGFR. It is feasible to assume that this simplified fixation method can also be utilized for VLPs derived from a range of different membrane-enveloped donor viruses employed for the display of surface antigens. This warrants and requires further studies. The FF90 VLP-based antigen delivery platform might be of particular interest for the development of FFPE-compatible mAbs for various membrane-anchored cell surface antigens that pose a challenge in other formulations and require conformationally authentic antigen structures. In addition, the FF90 fixation might be further utilized to modify soluble proteins for immunization and *in vitro* antibody screening, and thus should be a useful tool for future antibody discovery studies aiming at the isolation of FFPE-compatible mAbs.

5. Materials and Methods

5.1. Materials

5.1.1. List of chemicals and consumables

Table 5.1. Chemicals and consumables used in this thesis.

Component/Name	Vendor
Acella 100 sample carrier	anvajo, Germany
Ammonium persulphate (APS)	Carl Roth, Germany
AutoMACS [®] Running Buffer	Miltenyi Biotec, Germany
Azaserin	Sigma Aldrich, Germany
Bovine serum albumin (BSA), Fraction V	Carl Roth, Germany
Cell culture plates CELLSTAR [®] , 6-, 12-, 24-, 48- and 96 wells	Greiner Bio-One, Austria
Chemiluminescent substrate; SuperSignal [™] West Pico PLUS	Thermo Fisher Scientific, USA
Citrate	Carl Roth, Germany
DAPI staining solution	Miltenyi Biotec, Germany
DMEM, high glucose, pyruvate medium	Gibco/Thermo Fisher Scientific, USA
DMEM, high glucose	Biowest, France
Dynabeads Protein A immunoprecipitation kit	Thermo Fisher Scientific, USA
Ethylenediaminetetraacetic acid (EDTA)	VWR International, USA
ELISA HIV p24; QuickTiter [™] HIV Lentivirus Quantitation Kit	Cell Biolabs, USA
ELISA NGFR; RayBio [®] Human NGF R ELISA Kit	RayBiotech, USA
Erythrosine B	Carl Roth, Germany

5. Materials and Methods

Component/Name	Vendor
Ethanol denatured, 99.8 %	Carl Roth, Germany
FastDigest NotI	Thermo Fisher Scientific, USA
FastDigest Sall	Thermo Fisher Scientific, USA
FBS FetalClone I serum	Hyclone, USA
FcR Blocking Reagent, mouse	Miltenyi Biotec, Germany
FcR Blocking Reagent, human	Miltenyi Biotec, Germany
Fetal bovine serum, qualified, heat inactivated, Brazil (FBS)	Gibco/Thermo Fisher Scientific, USA
Formaldehyde solution; ROTI®Histofix 10 %	Carl Roth, Germany
FreeStyle™ 293 Expression medium	Thermo Fisher Scientific, USA
L-glutamine	Gibco/Thermo Fisher Scientific, USA
Glycine	Carl Roth, Germany
HEPES, 1 M in 0.8 % NaCl	Lonza, Switzerland
Hydrochloric acid	Carl Roth, Germany
Hygromycin B Gold	InvivoGen, France
Isopropanol, 99.5 %, for synthesis	Carl Roth, Germany
Laemmli buffer (4x ROTI®Load-1)	Carl Roth, Germany
MACSwell™ Imaging Frames, MACSwell Four	Miltenyi Biotec, Germany
Methanol, 99.9 %	Carl Roth, Germany
Microtiter plate, 96-well, F-well, BRANDplates®	Brand, Germany
Mouse IgG Bio kit	Roche Diagnostics, Germany
Opti-MEM™ I Reduced Serum Medium	Gibco/Thermo Fisher Scientific, USA
PageRuler™ Prestained Protein Ladder, 10 bis 180 kDa	Thermo Fisher Scientific, USA
Paraffin, for histology	Carl Roth, Germany
PEI MAX®, Transfection Grade Linear Polyethylenimine Hydrochloride (MW 40,000)	Polysciences, USA
Peripheral blood mononuclear cells (PBMCs)	DRK Blutspendedienst West, Hagen, Germany

5. Materials and Methods

Component/Name	Vendor
Phosphate buffered saline (PBS), 10x	Gibco/Thermo Fisher Scientific, USA
Phusion DNA Polymerase High-Fidelity PCR Kit	New England Biolabs, USA
Powdered milk, lowfat, blotting grade	Carl Roth, Germany
Puromycin	InvivoGen, France
PVDF membrane: ROTI®PVDF 0.45	Carl Roth, Germany
PVDF membrane syringe filters, 0.45 µm	Carl Roth, Germany
ROTIPHORESE®Gel 30 (37.5:1)	Carl Roth, Germany
ROTI®Histol	Carl Roth, Germany
ROTI®Nanoquant	Carl Roth, Germany
Shaker flasks with vent cap (125 mL, 250 mL, 500 mL)	Nalgene Nunc International, USA
Sodium chloride (NaCl)	Carl Roth, Germany
Sodium dodecyl sulphate (SDS)	Carl Roth, Germany
T4 DNA Ligase	New England Biolabs, USA
T25, T75 and T125 cell culture flasks	Carl Roth, Germany
TEMED, for electrophoresis	Carl Roth, Germany
TransIT®-LT1 transfection reagent	Mirus Bio, USA
D(+)-trehalose dihydrate, CELLPURE®	Carl Roth, Germany
Tris, PUFFERAN®	Carl Roth, Germany
Tris-HCl, PUFFERAN®	Carl Roth, Germany
Tween® 20	Carl Roth, Germany
Ultra Clear centrifuge tubes	Beckman Coulter, USA

5.1.2. List of antibodies

Table 5.3. Antibodies used for the detection of human antigens and viral proteins. Antibodies used for direct staining were conjugated to either allophycocyanin (APCy), fluorescein isothiocyanate (FITC) or phycoerythrin (PE). Unconjugated primary antibodies were used for indirect staining, VLP capture assays and Western blot-analysis, respectively. Abbreviations: horseradish peroxidase (HRP), nerve growth factor receptor (NGFR), immunoglobulin (Ig), research resource identifier (RRID).

Antigen	Clone	Conjugate	Ig species	RRID	Vendor
CD3, native	REA613	FITC	human	AB_2725966	Miltenyi Biotec, Germany
CD3, FFPE	REA1151	PE	human	AB_2725967	Miltenyi Biotec, Germany
CD4, native	REA623	PE	human	AB_2726036	Miltenyi Biotec, Germany
CD4, FFPE	REA1307	PE	human	AB_2921815	Miltenyi Biotec, Germany
CD8, native	REA734	FITC	human	AB_2659233	Miltenyi Biotec, Germany
CD8, FFPE	REA1024	PE	human	AB_2857415	Miltenyi Biotec, Germany
CD20, native	REA780	PE	human	AB_2656063	Miltenyi Biotec, Germany
CD20, FFPE	REA1087	FITC	human	AB_2857426	Miltenyi Biotec, Germany
CD45RA	REA562	APCy	human	AB_2726133	Miltenyi Biotec, Germany
CD271/NGFR, native	REA844	PE	human	AB_2725864	Miltenyi Biotec, Germany
CD271/NGFR, native	REA844	-	human	-	Miltenyi Biotec, Germany
CD271/NGFR, FFPE	C40-1457	PE	mouse	AB_396599	BD Biosciences, USA
CD271/NGFR, FFPE	C40-1457	-	mouse	AB_2152663	BD Biosciences, USA
CD271/NGFR, FFPE	REAL709	PE	human	AB_2819737	Miltenyi Biotec, Germany
HIV-Gag p17+p24+p55	polyclonal	-	rabbit	AB_1139524	Abcam, UK

isotype control antibodies

Antigen	Clone	Conjugate	Ig species	RRID	Vendor
isotype control	REA293	APCy	human	AB_27333447	Miltenyi Biotec, Germany
isotype control	REA293	FITC	human	AB_27333689	Miltenyi Biotec, Germany
isotype control	REA293	PE	human	AB_27333893	Miltenyi Biotec, Germany
isotype control	MOPC-21	PE	mouse	AB_396514	BD Biosciences, USA
isotype control	polyclonal	-	human	AB_2532958	Thermo Fisher Scientific, USA
isotype control	-	-	mouse	AB_10959891	Thermo Fisher Scientific, USA
<i>secondary antibodies</i>					
rabbit IgG	polyclonal	HRP	chicken	AB_2534661	Thermo Fisher Scientific, USA
mouse IgM	X-54	APCy	rat	AB_10829304	Miltenyi Biotec, Germany
mouse IgG1	X-56	APCy	rat	AB_2752118	Miltenyi Biotec, Germany
mouse IgG1	X-56	PE	rat	AB_2751742	Miltenyi Biotec, Germany
mouse IgG2ab	X-57	PE	rat	AB_2733867	Miltenyi Biotec, Germany

5.1.3. Equipment and software list

Table 5.5. List of equipment and software used in this thesis.

Description	Product	Vendor
Cell counter	fluidlab R-30	anvajo, Germany
Dynamic light scattering	Zetasizer nano ZS	Malvern Panalytical, UK
Electron microscope	JEM-2100Plus	JEOL, Germany
Flow cytometer	Cell Sorter S3e	Bio-Rad, USA
	MACSQuant [®] Analyzer 10	Miltenyi Biotec, Germany
Flow cytometric analysis	ProSort [™] software, v1.5	Bio-Rad, USA
	FlowJo [™] software, v10	BD Biosciences, USA
	MACSQuantify [™] software, v2.13.3	Miltenyi Biotec, Germany
Freezer (−80 °C)	HERAfreeze HFC-series 8740	Thermo Fisher Scientific, USA
Graphing and illustrating	Biorender	Biorender.com, USA
	Inkscape 1.2.2	inkscape Development Team, General Public License
	OriginPro software, version 2022b	OriginLab Corporation, USA
	Scribus software, version 1.4.8	Scribus Development Team, open source
IgG quantitation	Cedex Bio Analyzer	Roche Diagnostics, Germany
Incubator	Heracell [™] 150i	Thermo Fisher Scientific, USA
	Minitron	Infors HT, Switzerland
Microplate reader	Multiskan FC	Thermo Fisher Scientific, USA
	Infinite M1000Pro	Tecan, Switzerland
Microscope	VisiScope IT404	VWR, USA
Molecular cloning	SnapGene software	SnapGene, USA

5. Materials and Methods

Description	Product	Vendor
Protein electrophoresis	Mini-PROTEAN Tetra Vertical Electrophoresis Cell, Handcasting module, PowerPac™ Basic Power Supply	Bio-Rad, USA
PCR machine	Thermo cycler T100	Bio-Rad, USA
Protein transfer	Trans-Blot Turbo system	Bio-Rad, USA
Thermal mixer	TS basic	Cellmedia, Germany
Ultracentrifuge	Optima XE-90	Beckman Coulter, USA
VLP capture assay	Overhead shaker REAX2	Heidolph Instruments, Germany
	12-Tube Magnetic Separation Rack	New England Biolabs, USA
Western blot imaging	ChemiDoc	Bio-Rad, USA
	Image Lab™ software, version 5.2.1	Bio-Rad, USA

5.1.4. Compositions of buffers and solutions

Table 5.7. Compositions of buffers and solutions used in this thesis. If not otherwise stated, solutions and buffer ingredients were solved in demineralized water (dH₂O).

Buffer name	Composition
AutoMACS Running Buffer	ready-to-use, pH 7.2; contains PBS, BSA, EDTA and 0.09 % azide
Elution Buffer	ready-to-use, part of the Dynabead Protein A immunoprecipitation kit
FACS buffer	PBS, pH 7.2 to 7.4 supplemented with 2 mM EDTA and 0.5 % (w/v) BSA
TEC buffer	Tris-HCl, pH 9.0; EDTA; citrate (in-house recipe of Miltenyi Biotec, Germany; composition confidential)

Buffer name	Composition
Laemmli buffer	ready-to-use (4x ROTI®Load-1), contains SDS (approx. 8 % (w/v)), β -mercaptoethanol (approx. 20 % (v/v)), glycerol (approx. 40 % (v/v)) and bromophenol blue (approx. 0.015 % (w/v)). Phosphate buffered.
PBS	1:10 dilution of Gibco 10x PBS stock solution; pH 7.4
TBS-T washing buffer	2 mM Tris-HCl, 15 mM NaCl, 0.05 % (v/v) Tween-20; pH 7.4
Towbin blotting buffer	25 mM Tris, 190 mM glycine, 20 % (v/v) methanol
VLP storage solution	10 % (w/v) trehalose dissolved in PBS

5.2. Plasmids

In all expression constructs used in this study, the human cytomegalovirus promoter/enhancer (P_{CMV}) drives the expression of the proteins of interest, namely the group-specific antigen (Gag) proteins, a cytoplasmically truncated version of the nerve growth factor receptor (NGFR), the *Sleeping Beauty* (SB) and the *piggyBac* (PB) hyperactive transposases.

5.2.1. Design of the transposase expression vectors

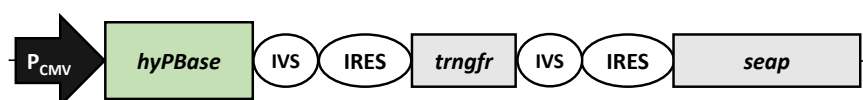
The pSB100x-trNGFR-SEAP construct is designed for the transient expression of the hyperactive SB transposase variant SB100x [Mátés et al. 2009], whereas the pHyPBase-trNGFR-SEAP construct encodes for the hyperactive *piggyBac* transposase (hyPBase) variant (GenBank Accession No. OL519599.1, [Yusa et al. 2011; Eggenschwiler et al. 2021]). As depicted in Figure 5.1A, the expression of the transposases is coupled to the expression of two reporter genes encoding the truncated human low affinity nerve growth factor receptor (trNGFR) [Yang et al. 1998; Castellino et al. 1999], and the secreted alkaline phosphatase (SEAP; GenBank Accession No. U89938, Clontech, USA), respectively, each separated by a synthetic intron (IVS) and an internal ribosomal entry site (IRES). The reporter genes enable the indirect detection of prolonged expression of the transposases after random stable integration of the transposase-encoding plasmids into the host cell genome. The transposase expression vectors pSB100x-trNGFR-SEAP and pHyPBase-trNGFR-SEAP were already present in our research group and their construction has been described previously [Berg et al. 2019; Berg et al. 2020; Rosengarten et al. 2022b].

A Transposase expression constructs

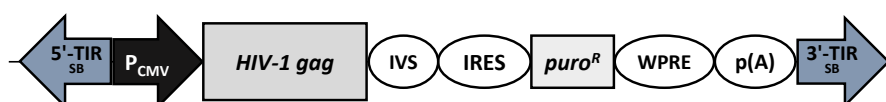
pSB100x-trNGFR-SEAP



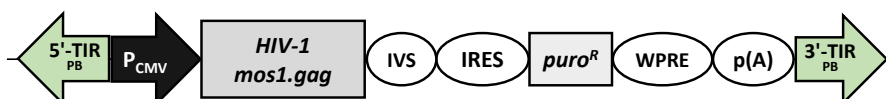
pHyPBBase-trNGFR-SEAP

**B Gag expression constructs**

pSB-gag-lpW



pPB-mos1.gag-lpW

**C Antigen expression construct**

pSB-cHS4-trNGFR-lhW

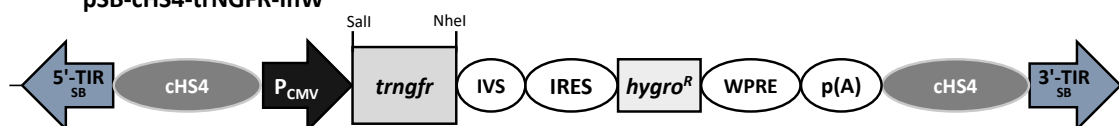


Figure 5.1. Schematic illustration of the transposon vector constructs. The cytomegalovirus promoter/enhancer (P_{CMV}) drives the expression in all three constructs. **(A)** The transposase expression vectors pSB100x-trNGFR-SEAP and pHyPBBase-trNGFR-SEAP are designed for the transient expression of the hyperactive *Sleeping Beauty* variant SB100x and the hyperactive *piggyBac* (hyPBBase) transposase, respectively. The expression of the transposases is coupled to the expression of the two reporter genes truncated nerve growth factor receptor (*trngfr*) and secreted alkaline phosphatase (*seap*), each separated by a synthetic intron (IVS) and an internal ribosomal entry site (IRES). **(B)** Two SB-specific terminal inverted repeats (TIRs) flank the transposable element of the Gag expression vector pSB-gag-lpW, whereas the transposable element of pPB-mos1.gag-lpW is flanked by PB-specific terminal inverted repeats (TIRs). The expression of the Gag proteins is coupled to a puromycin resistance gene (*puro^R*) as selection marker. The woodchuck hepatitis virus post transcriptional element (WPRE) and the bovine growth hormone polyadenylation signal (p(A)) terminate the expression cassettes. **(C)** In pSB-cHS4-trNGFR-lhW transposon donor vector the SB TIRs flank two copies of the core chicken beta-globin insulator sequences (cHS4). Here, the expression of the antigen of interest, trNGFR, is coupled to the hygromycin resistance gene (*hygro^R*) via a IVS and an IRES. The expression cassette ends with a WPRE and a p(A) signal. Adapted from [Schatz et al. 2023b] (CC BY 4.0; <https://creativecommons.org/licenses/by/4.0/>).

5.2.2. Design of the transposon donor vectors

The transposon donor vector plasmids were designed to provide the transposable elements flanked by transposase-specific TIRs. Each transposable element carries an expression cassette for a gene of interest and an additional selection marker.

5.2.2.1. *Sleeping Beauty* transposon donor vectors

The SB transposon donor plasmids pSB-IpW and pSB-cHS4-IhW were used as recipient vectors for the insertion of the genes of interest [Berg et al. 2019; Berg et al. 2020]. Plasmid maps of the recipient vectors are shown in Supplementary Figure S1 and Figure S2, respectively. The transposable elements of both plasmids are flanked by TIRs of the SB transposon originating from the Tc-like element (GenBank Accession No. L48685; [Ivics et al. 1997; Berg et al. 2019]). The multiple cloning site (MCS) is followed by an IVS, an attenuated IRES of encephalomyocarditis virus and a puromycin or hygromycin resistance gene derived from pIRESpuro3 and pIREShyg3 (Clontech Laboratories, USA), respectively. The woodchuck hepatitis virus posttranscriptional element (WPRE; nucleotides 1093–1684; GenBank Accession No. J04514) and the bovine growth hormone polyadenylation signal (p(A)) terminate the expression cassettes. In the pSB-cHS4-IhW transposon donor vector, a chicken β -globin (cHS4) insulator element (GenBank accession no. U78775) was added upstream of the P_{CMV} and downstream of the p(A) signal respectively, to protect transgene expression after transposition from gene silencing [Sharma et al. 2012].

Design of the Gag expression vector The Gag expression vector pSB-gag-IpW depicted in Figure 5.1B was generated in our research group by insertion of the human codon-optimized sequence of *gag* coding for the human immunodeficiency virus (HIV)-1 Gag precursor polyprotein (p55-Gag) of isolate NY5 (Uniprot accession no. P12493) into the pSB-IpW recipient vector.

Molecular cloning of the trNGFR expression vector The trNGFR expression vector pSB-cHS4-trNGFR-IhW depicted in Figure 5.1C encodes for the trNGFR antigen. The pSB-cHS4-IhW recipient vector was linearized using the FastDigest NheI and Sall restriction enzymes (Thermo Fisher Scientific, USA). The *trNGFR* coding sequence (CDS) flanked by NotI and Sall restriction sites was generated from pSB100x-trNGFR-SEAP by polymerase chain reaction (PCR) using the primer pair NheI-trNGFR forward (5'-atatgctagcacCATGGGGCAGGTGCCAC-3', Eurofins Genomics, Germany) and Sall-trNGFR reverse (5'-atatgtcgaCCTAGAGGATCCCCCTGTTCCAC-3', Eurofins Genomics, Germany). Lowercase letters indicate primer overhangs harboring the restriction sites, stuffer and Kozak sequences (the latter only in the forward primer). The PCR was initiated using the Phusion HF DNA polymerase (New England Biolabs, USA), 100 ng template DNA and 0.5 μ M of forward and reverse primers, respectively. Initial denaturation was carried

out at 98 °C for 30 s, followed by 30 cycles of denaturation for 20 s at 98 °C, annealing for 10 s at primer-specific temperatures and elongation at 72 °C for 15 s/kb, as well as a final elongation step for 5 min at 72 °C. The amplicon was digested with FastDigest NheI and Sall and ligated into the opened recipient vector using T4 DNA Ligase (New England Biolabs, USA). The generated pSB-cHS4-trNGFR-IhW transposon donor vector was analyzed utilizing restriction enzyme digest and the DNA sequence of the trNGFR CDS was confirmed by Sanger sequencing (Microsynth Seqlab, Germany).

5.2.2.2. *PiggyBac* transposon donor vector

The PB transposon donor plasmid pPB-mos1.gag-IpW consists of the transposable element flanked by PB TIRs (Figure 5.1B) and was generated by [Rosengarten et al. 2022b]. The TIRs originate from plasmid PB-CAG-DDdCas9VP192-T2A-GFP-IRES-Neo, which was a gift from Timo Otonkoski (Addgene plasmid No. 102885; RRID: Addgene_102885; [Weltner et al. 2018]). The transposable element of pPB-mos1.gag-IpW contains the P_{CMV} that drives the expression of the HIV *mosaic gag* (*mos1.gag*) CDS followed by an IVS, an IRES and a puromycin resistance gene derived from pIRESpuro3 (Clontech Laboratories, USA). The DNA sequence of *mos1.gag* consists of synthetically shuffled Gag sequences originating from different HIV variants [Fischer et al. 2007] and was taken from US patent no.10,369,214 [Langedijk et al. 2019]. The sequence was synthesized and codon optimized for the expression in human and Chinese hamster ovary cells (Genscript, USA). The WPRE (nucleotides 1093–1684; GenBank accession no. J04514) and the bovine growth hormone polyadenylation signal (p(A)) terminate the expression cassette.

5.3. Cell culture

5.3.1. Cell lines, media and culture conditions

Adherent murine NIH/3T3 fibroblasts (ATCC Cat.No. CRL-1658, RRID: CVCL_0594) and recombinant cells derived from NIH-3T3 cells were cultivated in T75 cell culture flasks (Carl Roth, Germany) and 12 mL Dulbecco's modified Eagle high glucose, pyruvate medium (DMEM; Gibco/Thermo Fisher Scientific, USA) supplemented with 4 mM L-glutamine and 10 % fetal bovine serum (FBS). Cell cultures were maintained at 37 °C in a humidified atmosphere at 5 % CO₂ in an incubator (Heracell™ 150i, Thermo Fisher Scientific, USA). For passaging, adherent cells were detached using 1 mM ethylenediaminetetraacetic acid (EDTA) in phosphate buffered saline (PBS; Gibco/Thermo Fisher Scientific, USA).

The mouse myeloma cell line Sp2/0-Ag14 (ATCC Cat.No. CRL-8287, RRID: CVCL_2199) was cultivated in T125 cell culture flasks and 25 mL Sp2/0 culture medium consisting of

DMEM (BioWest, France) supplemented with 10% FBS (Hyclone, USA), 2 mM L-glutamine (Gibco/Thermo Fisher Scientific, USA) and 20 mM HEPES (Lonza, Switzerland). Cells were maintained at 37 °C in a humidified atmosphere at 9% CO₂.

Human FreeStyle™ 293-F suspension cells (RRID: CVCL_D603, Thermo Fisher Scientific, USA) and recombinant cells derived from 293-F cells were cultivated in serum-free FreeStyle™ 293 Expression medium (Thermo Fisher Scientific, USA) at 37 °C, 8% CO₂ and 137 rpm in a shaker incubator (Minitron, Infors HT, Switzerland) with an orbit of 5 cm. The cultivation was routinely carried out in 125 mL disposable shaker flasks with vent caps (Nalgene Nunc International, USA) and 20 mL FreeStyle™ 293 Expression medium. Cell cultures were passaged every 3 to 4 days at viable cell densities (VCDs) between 0.3×10^6 and 2.0×10^6 viable cells/mL.

VCDs and viabilities were assessed using either a cell counter and the acella 100 sample carriers (anvajo, Germany) or by counting the staining cells stained with 0.1% (w/v) erythrosine B solution in an improved Neubauer counting chamber (Carl Roth, Germany).

5.3.2. Establishment of stable recombinant cells

Stable recombinant cells were generated using PB and SB transposon vector gene transfer.

5.3.2.1. Generation of the NGFR screening cell line

For the generation of the 3T3/Gag/trNGFR screening cell line, the human *trngfr* expression cassette was introduced into the 3T3/Gag cell pool already present in our research group. The 3T3/Gag cell pool was established by co-transfection of NIH-3T3 cells with the SB transposase expression construct and the pSB-gag-lpW Gag expression vector.

One day prior to transfection, 1.0×10^5 3T3/Gag cells per well were seeded in a 6-well cell culture plate (Greiner Bio-One, Austria). On the following day, cells were transfected using the and TransIT®-LT1 transfection reagent (Mirus Bio, USA) and 2.50 µg total plasmid DNA diluted in Opti-MEM™ I reduced serum medium (Gibco/Thermo Fisher Scientific, USA). For the generation of the NGFR screening cell pool, cells were co-transfected with 2.25 µg of transposon donor vector pSB-trNGFR-lhW and 0.25 µg of the SB transposase expression construct (pSB100x-trNGFR-SEAP). Three days post transfection, transfected cells were subjected to increasing concentrations of hygromycin (InvivoGen, France) starting at a concentration of 50 µg/mL. At the end of the increasingly stringent selection, the 3T3/Gag/trNGFR cell pool was cultivated at 400 µg/mL hygromycin.

The NGFR screening cell line was generated by cloning of 3T3/Gag/trNGFR cells already pre-selected at 400 µg/mL hygromycin. Cells were stained using anti-NGFR antibodies as described in Chapter 5.5.1 and the top 15 % of trNGFR-expressing cells were collected using the Se3 cell sorter (Bio-Rad, USA). Sorted cells were plated in 96-well cell culture plates using limiting dilution to generate single cell clones. Clones were expanded using DMEM containing 400 µL/mL hygromycin. The clone H6 showing the highest trNGFR expression was selected as the NGFR screening cell line (Figure S3).

5.3.2.2. Generation of 293-F VLP producer cell pools

The stable virus-like particle (VLP) producer cell pool 293-F/Mos1.Gag was generated by Rosengarten *et al.* using PB transposon vectors encoding for the hyPBBase and for Mos1.Gag proteins, respectively [Rosengarten *et al.* 2022b]. In brief, 40 µg of pPB-mos1.gag-lpW and 10 µg of pHyPBBase-trNGFR-SEAP were incubated with 150 µg polyethylenimine (PEI) transfection reagent (PEI:DNA mass ratio of 3:1; linear PEI, MW 40,000; Polysciences Inc., USA) for 15 min at room temperature. Next, 30×10^6 viable 293-F cells were harvested and resuspended in 6 mL FreeStyle expression medium, transfected with the PEI:DNA transfection mixture and incubated at 37 °C, 8 % CO₂ and 135 rpm. Additional 9 mL medium were added after three hours. On the following day, cells were diluted to a VCD of 1.0×10^6 viable cells/mL. Four days after transfection, cells were subjected to increasing concentrations of puromycin starting at a concentration of 2 µg/mL puromycin until the final concentration of 15 µg/mL. After initial selection, the stable 293-F/Mos1.Gag cell pool was routinely cultivated at 10 µg/mL puromycin.

The stable trNGFR-VLP producer cell pool 293-F/Mos1.Gag/trNGFR was generated utilizing SB vector-mediated transposon. For this purpose, 16.0 µg of pSB-trNGFR-lhW and 2.5 µg of pSB100x-trNGFR-SEAP DNA was incubated with 110 µg PEI transfection reagent for 5 min at room temperature. As described above, 30×10^6 viable cells/mL from the 293-F/Mos1.Gag cell pool were co-transfected with the PEI:DNA transfection mixture containing the SB transposase expression construct and the SB transposon donor vector encoding for the trNGFR. Three days post transfection, stable 293-F/Mos1.Gag/trNGFR cells were selected using 50 µg/mL hygromycin. The hygromycin concentrations were constantly elevated for three weeks to a final concentration of 200 µg/mL hygromycin. For further cultivation, 10 µg/mL puromycin was constantly applied in addition to hygromycin.

5.3.3. VLP production, concentration and storage

293-F VLP producer cells were seeded at 0.5×10^6 viable cells/mL in 125 mL, 250 mL or 500 mL shaker flasks containing 20 mL, 40 mL or 100 mL serum-free FreeStyle™ 293 expression

medium, respectively, and expanded for three days. To harvest VLPs from cell cultures revealing a viability higher than 90%, the supernatant was separated from the cells using low-speed centrifugation at 300 rcf for 5 min. The clarified supernatant was filtered using 0.45 µm polyvinylidene fluoride (PVDF) membrane syringe filters (Carl Roth, Germany) to remove residual cells and cell debris. The cell-free supernatant (CFSN) was either stored at –20 °C or subjected to ultracentrifugation for VLP isolation and concentration.

For VLP concentration, CFSN was centrifuged at 112 700 rcf at 4 °C for 1.5 h using the Optima XE-90 ultracentrifuge (Beckman Coulter, USA), the SW28 swing-out rotor (Beckman Coulter, USA) and Ultra Clear centrifuge tubes (Beckman Coulter, USA). The supernatant was discarded and the VLP pellet was air-dried for approximately 20 min and resuspended using 60 µL of VLP storage solution (Table 5.8, [Lynch et al. 2012]) per 10 mL CFSN and stored at –80 °C until further analysis.

5.4. Fixation of cells and VLPs

5.4.1. Formaldehyde, ethanol and heat treatment of single cells

Cells were harvested from cell cultures, washed with PBS and fixed using 4% formaldehyde solution (Carl Roth, Germany) for 1 h. Formaldehyde-fixed cells were pelleted by centrifugation at 300 rcf for 5 min and washed three times in PBS.

Formaldehyde-fixed 293-F/Mos1.Gag/trNGFR cells were incubated in increasing concentrations of ethanol. Cells were initially incubated in 2 mL 48% ethanol for 20 min. Additional 2 mL 99.8% ethanol (Carl Roth, Germany) was added so that the ethanol concentration was approximately 70%. Cells were incubated in 70% ethanol for another 20 min. For the final 20 min incubation in 90% ethanol, additional 15 mL 99.8% ethanol was added to the cell suspension. The resulting formaldehyde- and ethanol-fixed cells were pelleted by centrifugation at 600 rcf for 5 min, washed and stored in PBS at 4 °C.

Formaldehyde-fixed cells suspended in PBS were subjected to heat fixation at 70 °C, 80 °C, 90 °C and 100 °C for 1 h, respectively. After cooldown, the cells were stored at 4 °C.

5.4.2. Formaldehyde-fixed paraffin-embedded single cell preparation

Formaldehyde-fixed paraffin-embedded (FFPE) single cells were prepared following an internal, confidential standard operating procedure (SOP) of Miltenyi Biotec, Germany. The protocol mimics the steps performed during FFPE tissue embedding. Cells were fixed using 4% paraformaldehyde solution followed by a stepwise dehydration in an ascending ethanol series, clearing in ROTI®Histol,

a xylene substitute, and embedding in paraffin at 60 °C. After paraffin embedding, cells were deparaffinized, rehydrated using descending ethanol concentrations and heat-induced antigen retrieval was performed using TEC buffer (Table 5.8). FFPE single cells were stored at 4 °C in AutoMACS Running Buffer (Miltenyi BioTec, Germany).

5.4.3. Preparation of formaldehyde-fixed and 90 °C-fixed VLPs

VLPs were produced and concentrated as described in Chapter 5.3.3. For the preparation of trNGFR-VLPs for immunization, concentrated VLP samples were pooled and contained up to 2 µg Gag proteins. VLPs were fixed in 2 mL 4% formaldehyde solution for 1 h. The reaction was stopped by adding 150 mM glycine. After fixation, VLP samples were immediately diluted in 35 mL PBS resulting in a formaldehyde concentration of approximately 0.2% and the VLPs were separated from the solution using ultracentrifugation (112 700 rcf, 4 °C, 1.5 h). The VLP pellet was resuspended in PBS, heated to 90 °C for 1 h, sterile-filtered using 0.45 µm PVDF syringe filters (Carl Roth, Germany) and stored at –80 °C. VLPs undergoing this procedure were termed formaldehyde- and 90 °C-fixed (FF90) VLPs.

5.5. Characterization of cells and VLPs

5.5.1. Flow cytometric analysis of cells

Up to 1×10^6 cells were washed in PBS and resuspended in 100 µL FACS buffer (Table 5.8) containing fluorophore-conjugated monoclonal antibodies (mAbs) directed against the target antigen (Table 5.4) and incubated in the dark at 4 °C for 10 min. Human peripheral blood mononuclear cells (PBMCs) from anonymous healthy donors (DRK Blutspendedienst West, Hagen, Germany) were incubated with additional human Fc receptor (FcR) blocking reagent (Miltenyi Biotec, Germany). As a control, cells were immunolabeled with matching isotype control antibodies. Cells were washed by adding 1 mL PBS and pelleted at 300 rcf for 5 min. Cells were resuspended in 1 mL FACS buffer and measured using either S3e Cell Sorter (Bio-Rad, USA) or MACSQuant Analyzer 10 flow cytometer (Miltenyi Biotec, Germany).

Flow cytometric analysis was performed using either the MACSQuantify or FlowJo software (Table 5.6). Debris and doublets were excluded from analysis in a forward scatter area (FSC-A) versus side scatter area (SSC-A) plot followed by single cell selection in a FSC-A versus forward scatter height (FSC-H) or forward scatter width (FSC-W) plot. Fluorescent signals mediated by the binding of the fluorophore-conjugated mAbs to the cells were investigated in the corresponding fluorescence channels.

Stain index

The stain index (SI) describes the ratio of the separation between the cell population labeled with the antigen-specific antibodies and the cell population incubated with isotype control antibodies divided by two times the standard deviation (SD) of the isotype control. The mean fluorescent intensities (MFI) and the SDs were calculated using the FlowJo software (Table 5.6).

Stain indices were calculated as follows [Maecker et al. 2004]:

$$SI = \frac{MFI_{sample} - MFI_{iso}}{2 \times SD_{iso}} \quad (\text{Equation 5.1})$$

with	SI	stain index
	MFI	mean fluorescent intensity
	iso	isotype control
	SD	standard deviation

5.5.2. Protein quantitation

5.5.2.1. Total protein quantitation

The amount of total protein in VLP samples for injection was quantified using a modified Bradford assay (ROTI[®]Nanoquant; Carl Roth, Germany). 400 µg/mL bovine serum albumin (BSA; Carl Roth, Germany) were solved in PBS to prepare the bovine serum albumin (BSA) stock solution. For the calibration series ranging from 1.0 µg/mL to 100.0 µg/mL, the BSA stock solution was subsequently diluted in H₂O. The ROTI[®]Nanoquant reagent (Carl Roth, Germany) was used according to the manufacturer's instructions. The assay was performed in 96 well plates (Brand, Germany). The optical density of the standard dilutions and the samples was measured at 590 nm and 450 nm using the Infinite M1000Pro microplate reader (Tecan, Switzerland).

5.5.2.2. Enzyme-linked immunosorbent assays

CFSN and VLP samples were analyzed for their Gag and NGFR concentrations using enzyme-linked immunosorbent assays (ELISAs) and the microplate reader Multiskan FC (Thermo Fisher Scientific, USA). Samples were analyzed as analytical duplicates.

The p55-Gag proteins were detected employing the HIV-1 p24 capsid ELISA (Cell Biolabs, USA). With the exception of modifying the p24-Gag standard dilution series to a concentration range of 0.39 ng/mL to 25.00 ng/mL, the p24 capsid ELISA was performed following the manufacturer's instructions. Particle numbers were calculated utilizing Equation 5.2, by assuming that there is an average of 3500 p55-Gag molecules per immature VLP [Lavado-García et al. 2021] and the

5. Materials and Methods

number of detected p24-Gag molecules is equal to the number of p55-Gag molecules, as p24-Gag is a subunit of the p55-Gag precursor proteins. The molecular weight of p24-Gag was estimated as 24 000 Da. This equates to 7.17×10^9 VLPs per 1 μg detected p24-Gag.

$$m_{p24} = \frac{n_{Gag} \times M}{N_A} \times F \quad (\text{Equation 5.2})$$

with	m_{p24}	total amount of p24-Gag of 1 VLP	[ng]
	n_{Gag}	number of molecules of 1 VLP	[-]
	M	molecular weight of p24-Gag	[Da or g/mol]
	N_A	Avogadro constant	[1/mol]
	F	conversion factor of 10^9	[ng/g]

NGFR concentrations in CFSN and VLP samples were measured using the human NGFR ELISA kit according to the manufacturer's instructions (RayBiotech, USA). The number of trNGFR molecules per VLP was calculated as described in Equation 5.3. The molecular weight of trNGFR was calculated using the ProtParam Tool (RRID: SCR_018087) based on the amino acid sequence and was determined to be approximately 29 500 Da.

$$n_{trNGFR} = \frac{N_A \times m_{trNGFR} \times n_{VLP}}{M \times F} \quad (\text{Equation 5.3})$$

with	n_{trNGFR}	number of trNGFR molecules per VLP	[-]
	m_{trNGFR}	total amount of trNGFR per 1 μg p24-Gag	[ng]
	N_A	Avogadro constant	[1/mol]
	n_{VLP}	number of VLPs per 1 μg p24-Gag	[-]
	M	molecular weight of trNGFR	[Da or g/mol]
	F	conversion factor of 10^9	[ng/g]

5.5.3. VLP capture assay

The VLP capture assay consists of two major steps: (i) Immunoprecipitation of VLPs using surface antigen-specific antibodies and (ii) detection of the Gag viral core protein using Western blotting. The VLP capture assay was performed according to the protocol published by [\[Rosengarten et al. 2022a\]](#). Protein A-conjugated magnetic beads (50 μL per sample; Dynabeads Protein A immunoprecipitation kit; Thermo Fisher Scientific, USA) were incubated rotating with either 10 μg antigen-specific antibodies or matching isotype control antibodies (Table 5.4) for 1 h at room temperature. The beads were thoroughly washed to remove unbound antibodies. Next, the

antibody-coated beads were incubated with VLPs for 3 h under rotation. The VLP input into the capture assay was up to 25 ng of Gag proteins. After incubation, the beads were again washed extensively to remove unbound VLPs. For preparation of denatured protein samples, beads were incubated with a mixture containing 22.5 μ L Elution Buffer and 7.5 μ L 4x Laemmli buffer (Table 5.8) for 5 min at 95 °C. Beads were separated from denatured proteins in a magnetic field and 15 μ L of each sample were subjected to sodium dodecyl sulphate-polyacrylamide gel electrophoresis (SDS-PAGE) and subsequent Western blot analysis.

5.5.4. Western blotting

Denatured protein samples were separated employing SDS-PAGE (Protocol B.1, Appendix). Separated proteins were transferred to a PVDF membrane in Towbin blotting buffer using the Trans-Blot Turbo system (Bio-Rad, USA) as described in detail in protocol B.2 in the appendix. After blotting, the membrane was blocked for 1 h using 2% (w/v) powdered milk dissolved in TBS-T washing buffer (Table 5.8). For detection of p55-Gag, the membrane was incubated with anti-HIV-Gag p17 p24 p55 polyclonal primary antibodies (1:2000 in TBS-T, Table 5.4) overnight at 4 °C. Unbound antibodies were washed away using TBS-T buffer. Subsequently, the membrane was incubated with polyclonal anti-rabbit immunoglobulin (Ig)G-horseradish peroxidase (HRP) conjugates (Table 5.4) diluted 1:5000 in TBS-T for 2 h at room temperature. Labelled proteins were visualized using chemiluminescence detection (SuperSignal™ West Pico PLUS chemiluminescent substrate, Thermo Fisher Scientific, USA; ChemiDoc imaging system, Bio-Rad, USA).

5.5.5. Dynamic light scattering measurement

VLP samples were diluted using filtered PBS (PVDF membrane filters, 0.45 μ m; Carl Roth, Germany). Particle size distribution was measured using the Zetasizer nano ZS (Malvern Panalytical, UK) and quartz glass cuvettes with an optical path length of 10 mm and 4 mm width. For each measurement 100 μ L sample was used and backscatter was detected at 173°. The number of runs for each sample was 15 with a duration of 10 s and „protein analysis“ was selected as a model (solvent: water, refractive index of 1.330, viscosity of 0.8872 mPa s; material: protein, refractive index of 1.450).

5.5.6. Transmission electron microscopic imaging

VLPs were visualized using transmission electron microscopy (TEM) and the uranyl acetate negative staining method. The preparation and imaging of the TEM VLP samples was performed by the Imaging Facility Service staff at CECAD, Germany. In brief, VLP samples in PBS or VLP storage solution were mixed with paraformaldehyde (final concentration: 1%) and a volume of 5 μ L was transferred to copper grids. After incubation at RT for 20 min, the grid was washed extensively

with PBS and incubated with 1 % (v/v) glutaraldehyde in PBS. Afterwards, samples were washed extensively with H₂O. Samples were stained with 1 % (w/v) uranyl acetate solution for 4 min at RT in the dark. After air-drying, the samples were visualized using the 200 kV JEM-2100Plus Electron Microscope (JEOL, Germany).

5.5.7. Statistics

The independent two-sample *t*-test was used to calculate p-values and to determine if there is a mean difference between two samples. P-values of less than 0.05 were considered as statistically significant. In addition, it was determined whether the two samples have equal variance using the two-sample test for variance. In case the variance between the two samples differed at the 0.05 level, the Welch's correction for *t*-tests was used. Statistics were calculated using OriginPro software (OriginLab Corporation, USA; Table 5.6)

5.6. Generation and screening of antibodies

5.6.1. Immunization of mice

Two female 8 weeks old BALB/cAnNCrl mice (RRID: IMSR_CRL:547; Charles River, Germany) were immunized intravenously (i.v.) with sterile-filtered FF90 trNGFR-VLPs in PBS (9.5 µg of total protein) on day 0, 14 and 28, respectively. Blood samples were taken two days after the last injection and analyzed for reactive antibodies as described in Chapter 5.6.3. The first mouse was sacrificed and the spleen was removed for hybridoma cell generation. The second mouse was immunized with a fourth dose of FF90 trNGFR-VLPs (3.2 µg of total protein) on day 56. Two days later blood samples were analyzed. The second mouse was sacrificed on day 59 and the spleen was removed for hybridoma cell generation. The immunization schedule is summarized in Figure 3.6. Experiments involving animal handling were approved by the Governmental Review Committee on Animal Care in North Rhine-Westphalia, Germany and performed according to guidelines and regulations (Landesamt für Natur, Umwelt and Verbraucherschutz NRW, Approval number 84-02.05.40.17.081, dated 6th of September, 2017).

5.6.2. Generation of hybridoma cells

The generation of hybridoma cells was performed following an internal, confidential SOP of Miltenyi Biotec, Germany. In brief, murine Sp2/0 myeloma cells were prepared and cultured as described in Chapter 5.3.1. Myeloma cells were fused with splenocytes isolated from the murine spleen using polyethylene glycol. Generated hybridoma cells were diluted in hypoxanthine- and azaserine-containing selection medium and plated in flat bottom 96-well cell culture plates (Greiner Bio-One,

Austria). Cultures were fed with growth medium containing 20 % FBS and 0.1 mM hypoxanthine 5 d after fusion. Cultures showing one or more clusters of cells were investigated for antigen-specific antibody expression. Positive cultures harboring a single cell cluster were expanded in increasing concentrations of hypoxanthin-free subcloning medium. From reactive cultures showing more than one cell cluster, single cells were isolated using limiting dilution techniques to establish monoclonal cell cultures.

5.6.3. Flow cytometric screening

Blood plasma samples and hybridoma supernatants were screened for antibodies binding to the 3T3/Gag/trNGFR screening cell line. Fixed cells for screening were prepared as described in Chapter 5.4.2, whereas native cells were harvested from cell cultures on the day of testing. For screening, native and fixed 3T3/Gag/trNGFR cells were mixed and blocked using mouse FcR blocking reagent (Miltenyi BioTec, Germany) for 10 min at room temperature prior to incubation with antibodies.

Blood samples were centrifuged at 1000 rcf for 10 min and 25 μ L to 35 μ L of serum supernatant were incubated with a mixture of 2×10^5 native cells and 3×10^5 FF90 3T3/Gag/trNGFR cells for 20 min at room temperature. The serum was tested for murine IgM and IgG antibodies binding to 3T3/Gag/trNGFR cells using phycoerythrin (PE)-conjugated anti-mouse IgG1 and IgG2ab secondary antibodies as well as allophycocyanin (APCy)-conjugated anti-mouse IgM antibodies (Table 5.4). Secondary antibodies and 3T3/Gag/trNGFR cells were incubated for 15 min at room temperature.

Cell culture supernatants were harvested from hybridoma cultures and 85 μ L supernatant was incubated with a mixture of 2×10^4 native and 2×10^4 fixed cells for 20 min at room temperature. Unbound antibodies were removed by two washing steps with FACS buffer. For secondary staining, cells were incubated with PE-conjugated anti-mouse IgG1 and APCy-conjugated anti-mouse IgG2ab antibodies (Table 5.4) for 15 min at room temperature. After washing, cells were resuspended in 50 μ L FACS buffer and measured using the MACSQuant Analyzer 10 flow cytometer (Miltenyi Biotec, Germany). Cells incubated with either DMEM or 15 ng of anti-NGFR mAb C40-1457 and secondary antibody conjugates were used as controls.

Flow cytometric analysis was performed using the MACSQuantify software. A representative gating strategy and analysis is shown in Figure 5.2. Debris and doublets were excluded from analysis and native and fixed cells were discriminated in a VioBlue versus FSC-A plot. Fixed cells, that is FF90 and FFPE cells, showed autofluorescence at 450/50 nm (VioBlue channel), and thus could be discriminated from native cells. Fluorescence mediated by binding of the PE-

5. Materials and Methods

or APCy-conjugated anti-mouse IgG1 and IgG2ab secondary antibodies was investigated in the respective fluorophore versus FSC-A plots.

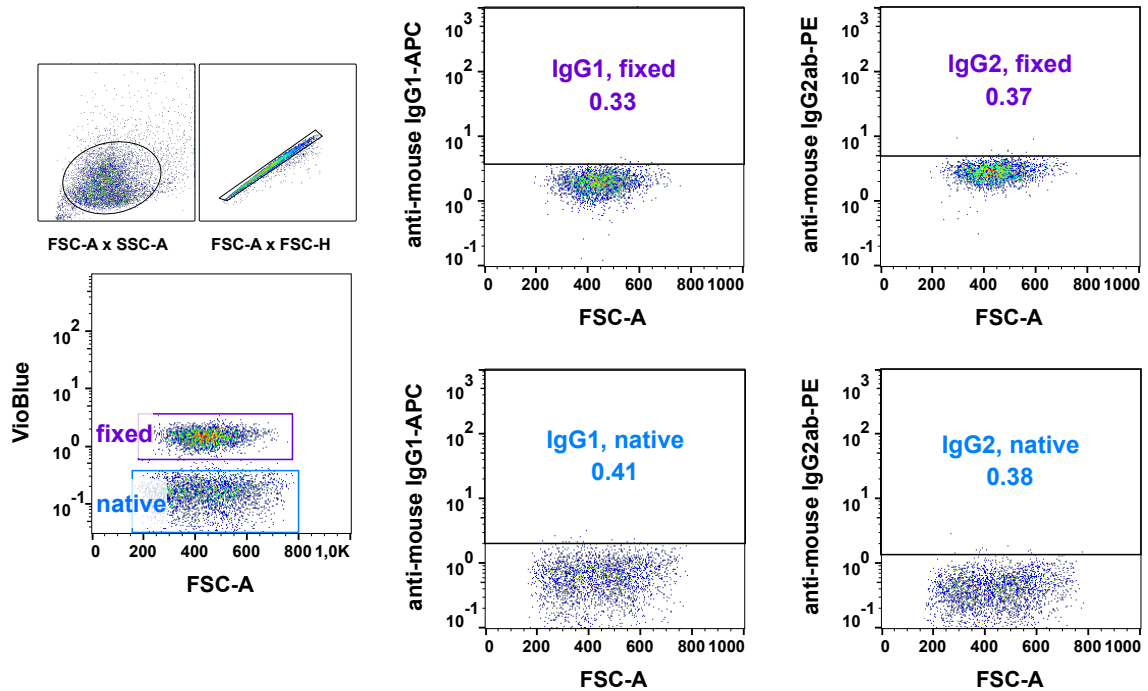


Figure 5.2. Representative example of the gating strategy for flow cytometric screening of hybridoma supernatants. The example shows the control staining using only secondary antibodies. A mixture of native and FF90 3T3/Gag/trNGFR cells was gated in a forward scatter area (FSC-A) versus SSC-A plot to exclude debris followed by doublet exclusion in a FSC-A versus forward scatter height (FSC-H) plot. Autofluorescence of fixed cells at 450/50 nm enabled the discrimination from native cells in the VioBlue versus FSC-A plot. Mouse IgG1 and IgG2ab antibodies binding to native and fixed cells were detected using APCy- and PE-conjugated anti-mouse IgG1 and IgG2ab secondary antibodies.

6. References

- Abd El-Aleem, S. A., Saber, E. A., Aziz, N. M., El-Sherif, H., Abdelraof, A. M., Djouhri, L.** (2022). “Follicular dendritic cells”. *Journal of Cellular Physiology* 237.4, pp. 2019–2033. DOI: 10.1002/jcp.30662.
- Aichele, P., Zinke, J., Grode, L., Schwendener, R. A., Kaufmann, S. H. E., Seiler, P.** (2003). “Macrophages of the splenic marginal zone are essential for trapping of blood-borne particulate antigen but dispensable for induction of specific T cell responses”. *The Journal of Immunology* 171.3, pp. 1148–1155. DOI: 10.4049/jimmunol.171.3.1148.
- Alfadhli, A., Still, A., Barklis, E.** (2009). “Analysis of Human Immunodeficiency Virus Type 1 Matrix Binding to Membranes and Nucleic Acids”. *Journal of Virology* 83.23, pp. 12196–12203. DOI: 10.1128/jvi.01197-09.
- Alfadhli, A., McNett, H., Tsagli, S., Bächinger, H. P., Peyton, D. H., Barklis, E.** (2011). “HIV-1 matrix protein binding to RNA”. *Journal of Molecular Biology* 410.4, pp. 653–666. DOI: 10.1016/j.jmb.2011.04.063.
- Asgarov, K., Balland, J., Tirole, C., Bouard, A., Mougey, V., Ramos, D., Barroso, A., Zangiaccomi, V., Jary, M., Kim, S., Gonzalez-Pajuelo, M., Royer, B., Haard, H. de, Clark, A., Wijdenes, J., Borg, C.** (2017). “A new anti-mesothelin antibody targets selectively the membrane-associated form”. *mAbs* 9.3, pp. 567–577. DOI: 10.1080/19420862.2017.1288770.
- Babcook, J. S., Leslie, K. B., Olsen, O. A., Salmon, R. A., Schrader, J. W.** (1996). “A novel strategy for generating monoclonal antibodies from single, isolated lymphocytes producing antibodies of defined specificities”. *Proceedings of the National Academy of Sciences of the United States of America* 93.15, pp. 7843–7848. DOI: 10.1073/pnas.93.15.7843.
- Bachmann, M. F., Rohrer, U. H., Kündig, T. M., Bürki, K., Hengartner, H., Zinkernagel, R. M.** (1993). “The influence of antigen organization on B cell responsiveness”. *Science* 262.5138, pp. 1448–1451. DOI: 10.1126/science.8248784.
- Bachmann, M. F., Jennings, G. T.** (2010). “Vaccine delivery: a matter of size, geometry, kinetics and molecular patterns”. *Nature reviews. Immunology* 10.11, pp. 787–796. DOI: 10.1038/nri2868.
- Balasubramanian, S., Matasci, M., Kadlecova, Z., Baldi, L., Hacker, D. L., Wurm, F. M.** (2015). “Rapid recombinant protein production from piggyBac transposon-mediated stable CHO cell pools”. *Journal of Biotechnology* 200, pp. 61–69. DOI: 10.1016/j.jbiotec.2015.03.001.

- Balasubramanian, S., Rajendra, Y., Baldi, L., Hacker, D. L., Wurm, F. M.** (2016). "Comparison of three transposons for the generation of highly productive recombinant CHO cell pools and cell lines". *Biotechnology and Bioengineering* 113.6, pp. 1234–1243. DOI: 10.1002/bit.25888.
- Barbas, C. F., Kang, A. S., Lerner, R. A., Benkovic, S. J.** (1991). "Assembly of combinatorial antibody libraries on phage surfaces: the gene III site". *Proceedings of the National Academy of Sciences of the United States of America* 88.18, pp. 7978–7982. DOI: 10.1073/pnas.88.18.7978.
- Barinova, K. V., Khomyakova, E. V., Kuravsky, M. L., Schmalhausen, E. V., Muronetz, V. I.** (2017). "Denaturing action of adjuvant affects specificity of polyclonal antibodies". *Biochemical and Biophysical Research Communications* 482.4, pp. 1265–1270. DOI: 10.1016/j.bbrc.2016.12.026.
- Batista, F. D., Iber, D., Neuberger, M. S.** (2001). "B cells acquire antigen from target cells after synapse formation". *Nature* 411.6836, pp. 489–494. DOI: 10.1038/35078099.
- Baumgärtel, V., Ivanchenko, S., Dupont, A., Sergeev, M., Wiseman, P. W., Kräusslich, H. G., Bräuchle, C., Müller, B., Lamb, D. C.** (2011). "Live-cell visualization of dynamics of HIV budding site interactions with an ESCRT component". *Nature Cell Biology* 13.4, pp. 469–476. DOI: 10.1038/ncb2215.
- Beausejour, Y., Tremblay, M. J.** (2004). "Interaction between the Cytoplasmic Domain of ICAM-1 and Pr55Gag Leads to Acquisition of Host ICAM-1 by Human Immunodeficiency Virus Type 1". *Journal of Virology* 78.21, pp. 11916–11925. DOI: 10.1128/jvi.78.21.11916-11925.2004.
- Berg, K., Schäfer, V. N., Bartnicki, N., Eggenschwiler, R., Cantz, T., Stitz, J.** (2019). "Rapid establishment of stable retroviral packaging cells and recombinant susceptible target cell lines employing novel transposon vectors derived from Sleeping Beauty". *Virology* 531, pp. 40–47. DOI: 10.1016/j.virol.2019.02.014.
- Berg, K., Schäfer, V. N., Tschorn, N., Stitz, J.** (2020). "Advanced Establishment of Stable Recombinant Human Suspension Cell Lines Using Genotype-Phenotype Coupling Transposon Vectors". *Methods in Molecular Biology (Clifton, N.J.)* 2070, pp. 351–361. DOI: 10.1007/978-1-4939-9853-1_20.
- Bezbaruah, R., Chavda, V. P., Nongrang, L., Alom, S., Deka, K., Kalita, T., Ali, F., Bhattacharjee, B., Vora, L.** (2022). "Nanoparticle-Based Delivery Systems for Vaccines". *Vaccines* 10.11. DOI: 10.3390/vaccines10111946.
- Biorender.com** (2023). *BioRender Templates*. URL: <https://app.biorender.com/biorender-templates> (visited on 04/01/2023).
- Boes, M.** (2000). "Role of natural and immune IgM antibodies in immune responses". *Molecular Immunology* 37.18, pp. 1141–1149. DOI: 10.1016/s0161-5890(01)00025-6.
- Boes, M., Esau, C., Fischer, M. B., Schmidt, T., Carroll, M., Chen, J.** (1998). "Enhanced B-1 cell development, but impaired IgG antibody responses in mice deficient in secreted IgM". *Journal of Immunology* 160.10, pp. 4776–4787.

- Boix-Besora, A., Lorenzo, E., Lavado-García, J., Gòdia, F., Cervera, L.** (2022). “Optimization, Production, Purification and Characterization of HIV-1 GAG-Based Virus-like Particles Functionalized with SARS-CoV-2”. *Vaccines* 10.2. DOI: 10.3390/vaccines10020250.
- Bradbury, A. R. M., Trinklein, N. D., Thie, H., Wilkinson, I. C., Tandon, A. K., Anderson, S., Bladen, C. L., Jones, B., Aldred, S. F., Bestagno, M., Burrone, O., Maynard, J., Ferrara, F., Trimmer, J. S., Görnemann, J., Glanville, J., Wolf, P., Frenzel, A., Wong, J., Koh, X. Y., Eng, H.-Y., Lane, D., Lefranc, M.-P., Clark, M., Dübel, S.** (2018). “When monoclonal antibodies are not monospecific: Hybridomas frequently express additional functional variable regions”. *mAbs* 10.4, pp. 539–546. DOI: 10.1080/19420862.2018.1445456.
- Breitling, F., Dübel, S., Seehaus, T., Klewinghaus, I., Little, M.** (1991). “A surface expression vector for antibody screening”. *Gene* 104.2, pp. 147–153. DOI: 10.1016/0378-1119(91)90244-6.
- Brodie, C., Oshiba, A., Renz, H., Bradley, K., Gelfand, E. W.** (1996). “Nerve growth-factor and anti-CD40 provide opposite signals for the production of IgE in interleukin-4-treated lymphocytes”. *European Journal of Immunology* 26.1, pp. 171–178. DOI: 10.1002/eji.1830260127.
- Buonaguro, L., Tornesello, M. L., Tagliamonte, M., Gallo, R. C., Wang, L. X., Kamin-Lewis, R., Abdelwahab, S., Lewis, G. K., Buonaguro, F. M.** (2006). “Baculovirus-derived human immunodeficiency virus type 1 virus-like particles activate dendritic cells and induce ex vivo T-cell responses”. *Journal of Virology* 80.18, pp. 9134–9143. DOI: 10.1128/jvi.00050-06.
- Burakova, Y., Madera, R., McVey, S., Schlup, J. R., Shi, J.** (2018). “Adjuvants for Animal Vaccines”. *Viral Immunology* 31.1, pp. 11–22. DOI: 10.1089/vim.2017.0049.
- Carrasco, Y. R., Batista, F. D.** (2007). “B cells acquire particulate antigen in a macrophage-rich area at the boundary between the follicle and the subcapsular sinus of the lymph node”. *Immunity* 27.1, pp. 160–171. DOI: 10.1016/j.immuni.2007.06.007.
- Castellino, S. M., Kurtzberg, J., Smith, C.** (1999). “Retroviral vector-mediated gene transfer into umbilical cord blood-derived megakaryocyte and platelet progenitors”. *Biology of Blood and Marrow Transplantation* 5.4, pp. 215–221. DOI: 10.1053/bbmt.1999.v5.pm10465101.
- Cervera, L., Gòdia, F., Tarrés-Freixas, F., Aguilar-Gurrieri, C., Carrillo, J., Blanco, J., Gutiérrez-Granados, S.** (2019). “Production of HIV-1-based virus-like particles for vaccination: achievements and limits”. *Applied Microbiology and Biotechnology* 103.18, pp. 7367–7384. DOI: 10.1007/s00253-019-10038-3.
- Cervera, L., Gutiérrez-Granados, S., Martínez, M., Blanco, J., Gòdia, F., Segura, M. M.** (2013). “Generation of HIV-1 Gag VLPs by transient transfection of HEK 293 suspension cell cultures using an optimized animal-derived component free medium”. *Journal of Biotechnology* 166.4, pp. 152–165. DOI: 10.1016/j.jbiotec.2013.05.001.
- Chen, L., Zhang, H., Zhang, L., Li, W., Fan, F., Wu, X., Wu, X., Lin, J.** (2020a). “Cas9 Protein Triggers Differential Expression of Inherent Genes Especially NGFR Expression in 293T Cells”. *Cellular and Molecular Bioengineering* 13.1, pp. 61–72. DOI: 10.1007/s12195-019-00606-y.

- Chen, S., Xu, J., Liu, M., Rao, A. L., Zandi, R., Gill, S. S., Mohideen, U.** (2020b). "Investigation of HIV-1 Gag binding with RNAs and lipids using Atomic Force Microscopy". *PloS One* 15.2, e0228036. DOI: 10.1371/journal.pone.0228036.
- Chen, Z., Wholey, W.-Y., Hassani Najafabadi, A., Moon, J. J., Grigorova, I., Chackerian, B., Cheng, W.** (2020c). "Self-Antigens Displayed on Liposomal Nanoparticles above a Threshold of Epitope Density Elicit Class-Switched Autoreactive Antibodies Independent of T Cell Help". *The Journal of Immunology* 204.2, pp. 335–347. DOI: 10.4049/jimmunol.1801677.
- Christodouloupoulos, I., Cannon, P. M.** (2001). "Sequences in the cytoplasmic tail of the gibbon ape leukemia virus envelope protein that prevent its incorporation into lentivirus vectors". *Journal of Virology* 75.9, pp. 4129–4138. DOI: 10.1128/JVI.75.9.4129-4138.2001.
- Chua, A. J. S., Vituret, C., Tan, M. L. C., Gonzalez, G., Boulanger, P., Ng, M.-L., Hong, S.-S.** (2013). "A novel platform for virus-like particle-display of flaviviral envelope domain III: induction of Dengue and West Nile virus neutralizing antibodies". *Virology Journal* 10. DOI: 10.1186/1743-422X-10-129.
- Datta, S. A., Heinrich, F., Raghunandan, S., Krueger, S., Curtis, J. E., Rein, A., Nanda, H.** (2011). "HIV-1 Gag extension: Conformational changes require simultaneous interaction with membrane and nucleic acid". *Journal of Molecular Biology* 406.2, pp. 205–214. DOI: 10.1016/j.jmb.2010.11.051.
- Delamarre, L., Couture, R., Mellman, I., Trombetta, E. S.** (2006). "Enhancing immunogenicity by limiting susceptibility to lysosomal proteolysis". *The Journal of Experimental Medicine* 203.9, pp. 2049–2055. DOI: 10.1084/jem.20052442.
- Delamarre, L., Pack, M., Chang, H., Mellman, I., Trombetta, E. S.** (2005). "Differential lysosomal proteolysis in antigen-presenting cells determines antigen fate". *Science* 307.5715, pp. 1630–1634. DOI: 10.1126/science.1108003.
- Deml, L., Speth, C., Dierich, M. P., Wolf, H., Wagner, R.** (2005). "Recombinant HIV-1 Pr55gag virus-like particles: potent stimulators of innate and acquired immune responses". *Molecular Immunology* 42.2, pp. 259–277. DOI: 10.1016/j.molimm.2004.06.028.
- Deo, V. K., Kato, T., Park, E. Y.** (2016). "Virus-Like Particles Displaying Recombinant Short-Chain Fragment Region and Interleukin 2 for Targeting Colon Cancer Tumors and Attracting Macrophages". *Journal of Pharmaceutical Sciences* 105.5, pp. 1614–1622. DOI: 10.1016/j.xphs.2016.02.011.
- Deo, V. K., Yui, M., Alam, J., Yamazaki, M., Kato, T., Park, E. Y.** (2014). "A model for targeting colon carcinoma cells using single-chain variable fragments anchored on virus-like particles via glycosyl phosphatidylinositol anchor". *Pharmaceutical Research* 31.8, pp. 2166–2177. DOI: 10.1007/s11095-014-1316-4.
- Di Tommaso, A., Magistris, M. T. de, Bugnoli, M., Marsili, I., Rappuoli, R., Abrignani, S.** (1994). "Formaldehyde treatment of proteins can constrain presentation to T cells by limiting

- antigen processing”. *Infection and Immunity* 62.5, pp. 1830–1834. DOI: 10.1128/iai.62.5.1830-1834.1994.
- Dodd, R. B., Wilkinson, T., Schofield, D. J.** (2018). “Therapeutic Monoclonal Antibodies to Complex Membrane Protein Targets: Antigen Generation and Antibody Discovery Strategies”. *BioDrugs* 32.4, pp. 339–355. DOI: 10.1007/s40259-018-0289-y.
- Ebersbach, H., Geisse, S.** (2012). “Antigen generation and display in therapeutic antibody drug discovery – a neglected but critical player”. *Biotechnology Journal* 7.12, pp. 1433–1443. DOI: 10.1002/biot.201200066.
- Eggenschwiler, R., Gschwendtberger, T., Felski, C., Jahn, C., Langer, F., Sternecker, J., Hermann, A., Lühmann, J., Steinemann, D., Haase, A., Martin, U., Petri, S., Cantz, T.** (2021). “A selectable all-in-one CRISPR prime editing piggyBac transposon allows for highly efficient gene editing in human cell lines”. *Scientific Reports* 11.1. DOI: 10.1038/s41598-021-01689-2.
- Favard, C., Chojnacki, J., Merida, P., Yandrapalli, N., Mak, J., Eggeling, C., Muriaux, D.** (2019). “HIV-1 Gag specifically restricts PI(4,5)P₂ and cholesterol mobility in living cells creating a nanodomain platform for virus assembly”. *Science Advances* 5.10. DOI: 10.1126/sciadv.aaw8651.
- Fischer, W., Perkins, S., Theiler, J., Bhattacharya, T., Yusim, K., Funkhouser, R., Kuiken, C., Haynes, B., Letvin, N. L., Walker, B. D., Hahn, B. H., Korber, B. T.** (2007). “Polyvalent vaccines for optimal coverage of potential T-cell epitopes in global HIV-1 variants”. *Nature Medicine* 13.1, pp. 100–106. DOI: 10.1038/nm1461.
- Fontana, D., Garay, E., Cervera, L., Kratje, R., Prieto, C., Gòdia, F.** (2021). “Chimeric VLPs Based on HIV-1 Gag and a Fusion Rabies Glycoprotein Induce Specific Antibodies against Rabies and Foot-and-Mouth Disease Virus”. *Vaccines* 9.3. DOI: 10.3390/vaccines9030251.
- Fox, C. B., Kramer, R. M., Barnes, V. L., Dowling, Q. M., Vedvick, T. S.** (2013). “Working together: interactions between vaccine antigens and adjuvants”. *Therapeutic Advances in Vaccines* 1.1, pp. 7–20. DOI: 10.1177/2051013613480144.
- Fuenmayor, J., Gòdia, F., Cervera, L.** (2017). “Production of virus-like particles for vaccines”. *New Biotechnology* 39.Pt B, pp. 174–180. DOI: 10.1016/j.nbt.2017.07.010.
- Fuenmayor, J., Cervera, L., Gutiérrez-Granados, S., Gòdia, F.** (2018). “Transient gene expression optimization and expression vector comparison to improve HIV-1 VLP production in HEK293 cell lines”. *Applied Microbiology and Biotechnology* 102.1, pp. 165–174. DOI: 10.1007/s00253-017-8605-x.
- Fujii, K., Morita, S., Mochizuki, M., Shibuya-Takahashi, R., Fujimori, H., Yamaguchi, K., Abe, J., Yamazaki, T., Imai, T., Sugamura, K., Yasuda, J., Satoh, K., Sato, I., Saito-Koyama, R., Fujishima, F., Sasano, H., Kato, Y., Matsuura, K., Asada, Y., Tamai, K.** (2022). “Establishment of a monoclonal antibody against glycosylated CD271 specific for cancer cells in immunohistochemistry”. *Cancer Science* 113.8, pp. 2878–2887. DOI: 10.1111/cas.15340.

6. References

- Gaa, R., Menang-Ndi, E., Pratapa, S., Nguyen, C., Kumar, S., Doerner, A.** (2021). “Versatile and rapid microfluidics-assisted antibody discovery”. *mAbs* 13.1, p. 1978130. DOI: 10.1080/19420862.2021.1978130.
- Gaffney, E. F., Riegman, P. H., Grizzle, W. E., Watson, P. H.** (2018). “Factors that drive the increasing use of FFPE tissue in basic and translational cancer research”. *Biotechnic & Histochemistry* 93.5, pp. 373–386. DOI: 10.1080/10520295.2018.1446101.
- Gaines, C. R., Tkacik, E., Rivera-Oven, A., Somani, P., Achimovich, A., Alabi, T., Zhu, A., Getachew, N., Yang, A. L., McDonough, M., Hawkins, T., Spadaro, Z., Summers, M. F.** (2018). “HIV-1 Matrix Protein Interactions with tRNA: Implications for Membrane Targeting”. *Journal of Molecular Biology* 430.14, pp. 2113–2127. DOI: 10.1016/j.jmb.2018.04.042.
- Gao, Y., Huang, X., Zhu, Y., Lv, Z.** (2018). “A brief review of monoclonal antibody technology and its representative applications in immunoassays”. *Journal of Immunoassay & Immunochemistry* 39.4, pp. 351–364. DOI: 10.1080/15321819.2018.1515775.
- Gentile, M., Adrian, T., Scheidler, A., Ewald, M., Dianzani, F., Pauli, G., Gelderblom, H. R.** (1994). “Determination of the size of HIV using adenovirus type 2 as an internal length marker”. *Journal of Virological Methods* 48.1, pp. 43–52. DOI: 10.1016/0166-0934(94)90087-6.
- Gonelli, C. A., King, H. A. D., Mackenzie, C., Sonza, S., Center, R. J., Purcell, D. F. J.** (2021). “Immunogenicity of HIV-1-Based Virus-Like Particles with Increased Incorporation and Stability of Membrane-Bound Env”. *Vaccines* 9.3. DOI: 10.3390/vaccines9030239.
- Gram, H., Marconi, L. A., Barbas, C. F., Collet, T. A., Lerner, R. A., Kang, A. S.** (1992). “In vitro selection and affinity maturation of antibodies from a naive combinatorial immunoglobulin library”. *Proceedings of the National Academy of Sciences of the United States of America* 89.8, pp. 3576–3580. DOI: 10.1073/pnas.89.8.3576.
- Greenfield, E. A.** (2022). “Immunizing Animals”. *Cold Spring Harbor Protocols* 2022.7, Pdb.top100180. DOI: 10.1101/pdb.top100180.
- Hammarstedt, M., Garoff, H.** (2004). “Passive and Active Inclusion of Host Proteins in Human Immunodeficiency Virus Type 1 Gag Particles during Budding at the Plasma Membrane”. *Journal of Virology* 78.11, pp. 5686–5697. DOI: 10.1128/jvi.78.11.5686-5697.2004.
- Hammarstedt, M., Wallengren, K., Pedersen, K. W., Roos, N., Garoff, H.** (2000). “Minimal exclusion of plasma membrane proteins during retroviral envelope formation”. *Proceedings of the National Academy of Sciences of the United States of America* 97.13, pp. 7527–7532. DOI: 10.1073/pnas.120051597.
- Hankaniemi, M. M., Stone, V. M., Andrejeff, T., Heinimäki, S., Sioofy-Khojine, A.-B., Marjomäki, V., Hyöty, H., Blazevic, V., Flodström-Tullberg, M., Hytönen, V. P., Laitinen, O. H.** (2019a). “Formalin treatment increases the stability and immunogenicity of coxsackievirus B1 VLP vaccine”. *Antiviral Research* 171, p. 104595. DOI: 10.1016/j.antiviral.2019.104595.

- Hankaniemi, M. M., Stone, V. M., Sioofy-Khojine, A.-B., Heinimäki, S., Marjomäki, V., Hyöty, H., Blazevic, V., Laitinen, O. H., Flodström-Tullberg, M., Hytönen, V. P.** (2019b). “A comparative study of the effect of UV and formalin inactivation on the stability and immunogenicity of a Coxsackievirus B1 vaccine”. *Vaccine* 37.40, pp. 5962–5971. DOI: 10.1016/j.vaccine.2019.08.037.
- Harper, D. M., Franco, E. L., Wheeler, C. M., Moscicki, A.-B., Romanowski, B., Roteli-Martins, C. M., Jenkins, D., Schuid, A., Costa Clemens, S. A., Dubin, G.** (2006). “Sustained efficacy up to 4.5 years of a bivalent L1 virus-like particle vaccine against human papillomavirus types 16 and 18: follow-up from a randomised control trial”. *Lancet (London, England)* 367.9518, pp. 1247–1255. DOI: 10.1016/S0140-6736(06)68439-0.
- Hatano, R., Yamada, T., Madokoro, H., Otsuka, H., Komiya, E., Itoh, T., Narita, Y., Iwata, S., Yamazaki, H., Matsuoka, S., Dang, N. H., Ohnuma, K., Morimoto, C.** (2019). “Development of novel monoclonal antibodies with specific binding affinity for denatured human CD26 in formalin-fixed paraffin-embedded and decalcified specimens”. *PLoS One* 14.6, e0218330. DOI: 10.1371/journal.pone.0218330.
- Hatano, R., Yamada, T., Matsuoka, S., Iwata, S., Yamazaki, H., Komiya, E., Okamoto, T., Dang, N. H., Ohnuma, K., Morimoto, C.** (2014). “Establishment of monoclonal anti-human CD26 antibodies suitable for immunostaining of formalin-fixed tissue”. *Diagnostic Pathology* 9, p. 30. DOI: 10.1186/1746-1596-9-30.
- Haverkamp, A.-K., Bosch, B. J., Spitzbarth, I., Lehmecker, A., Te, N., Bensaid, A., Segalés, J., Baumgärtner, W.** (2019). “Detection of MERS-CoV antigen on formalin-fixed paraffin-embedded nasal tissue of alpacas by immunohistochemistry using human monoclonal antibodies directed against different epitopes of the spike protein”. *Veterinary Immunology and Immunopathology* 218, p. 109939. DOI: 10.1016/j.vetimm.2019.109939.
- Heath, W. R., Kato, Y., Steiner, T. M., Caminschi, I.** (2019). “Antigen presentation by dendritic cells for B cell activation”. *Current Opinion in Immunology* 58, pp. 44–52. DOI: 10.1016/j.coi.2019.04.003.
- Henriksson, P., Pfeiffer, T., Zentgraf, H., Alke, A., Bosch, V.** (1999). “Incorporation of wild-type and C-terminally truncated human epidermal growth factor receptor into human immunodeficiency virus-like particles: insight into the processes governing glycoprotein incorporation into retroviral particles”. *Journal of Virology* 73.11, pp. 9294–9302. DOI: 10.1128/jvi.73.11.9294-9302.1999.
- Hogue, I. B., Grover, J. R., Soheilian, F., Nagashima, K., Ono, A.** (2011). “Gag Induces the Coalescence of Clustered Lipid Rafts and Tetraspanin-Enriched Microdomains at HIV-1 Assembly Sites on the Plasma Membrane”. *Journal of Virology* 85.19, pp. 9749–9766. DOI: 10.1128/jvi.00743-11.

- Hsing, L. C., Rudensky, A. Y.** (2005). "The lysosomal cysteine proteases in MHC class II antigen presentation". *Immunological Reviews* 207, pp. 229–241. DOI: 10.1111/j.0105-2896.2005.00310.x.
- Hu, W., Yu, Q., Hu, N., Byrd, D., Amet, T., Shikuma, C., Shiramizu, B., Halperin, J. A., Qin, X.** (2010). "A high-affinity inhibitor of human CD59 enhances complement-mediated virolysis of HIV-1: implications for treatment of HIV-1/AIDS". *Journal of Immunology* 184.1, pp. 359–368. DOI: 10.4049/jimmunol.0902278.
- Ikomi, F., Hanna, G. K., Schmid-Schönbein, G. W.** (1999). "Size- and surface-dependent uptake of colloid particles into the lymphatic system". *Lymphology* 32.3, pp. 90–102.
- Ivics, Z., Hackett, P. B., Plasterk, R. H., Izsvák, Z.** (1997). "Molecular Reconstruction of Sleeping Beauty, a Tc1-like Transposon from Fish, and Its Transposition in Human Cells". *Cell* 91.4, pp. 501–510. DOI: 10.1016/S0092-8674(00)80436-5.
- Jalaguier, P., Cantin, R., Maaroufi, H., Tremblay, M. J.** (2015). "Selective Acquisition of Host-Derived ICAM-1 by HIV-1 Is a Matrix-Dependent Process". *Journal of Virology* 89.1, pp. 323–336. DOI: 10.1128/jvi.02701-14.
- Jamali, A., Kapitza, L., Schaser, T., Johnston, I. C. D., Buchholz, C. J., Hartmann, J.** (2019). "Highly Efficient and Selective CAR-Gene Transfer Using CD4- and CD8-Targeted Lentiviral Vectors". *Molecular Therapy: Methods & Clinical Development* 13, pp. 371–379. DOI: 10.1016/j.omtm.2019.03.003.
- Jegerlehner, A., Storni, T., Lipowsky, G., Schmid, M., Pumpens, P., Bachmann, M. F.** (2002). "Regulation of IgG antibody responses by epitope density and CD21-mediated costimulation". *European Journal of Immunology* 32.11, pp. 3305–3314. DOI: 10.1002/1521-4141(200211)32:11<3305::AID-IMMU3305>3.0.CO;2-J.
- Jones, M. L., Alfaleh, M. A., Kumble, S., Zhang, S., Osborne, G. W., Yeh, M., Arora, N., Hou, J. J. C., Howard, C. B., Chin, D. Y., Mahler, S. M.** (2016). "Targeting membrane proteins for antibody discovery using phage display". *Scientific Reports* 6, p. 26240. DOI: 10.1038/srep26240.
- Jong, J. M. H. de, Schuurhuis, D. H., Ioan-Facsinay, A., Welling, M. M., Camps, M. G. M., van der Voort, E. I. H., Huizinga, T. W. J., Ossendorp, F., Verbeek, J. S., Toes, R. E. M.** (2006). "Dendritic cells, but not macrophages or B cells, activate major histocompatibility complex class II-restricted CD4+ T cells upon immune-complex uptake *in vivo*". *Immunology* 119.4, pp. 499–506. DOI: 10.1111/j.1365-2567.2006.02464.x.
- Junt, T., Moseman, E. A., Iannaccone, M., Massberg, S., Lang, P. A., Boes, M., Fink, K., Henrickson, S. E., Shayakhmetov, D. M., Di Paolo, N. C., van Rooijen, N., Mempel, T. R., Whelan, S. P., Andrian, U. H. von** (2007). "Subcapsular sinus macrophages in lymph nodes clear lymph-borne viruses and present them to antiviral B cells". *Nature* 450, pp. 110–114. DOI: 10.1038/nature06287.

- Kaczmarczyk, S. J., Sitaraman, K., Young, H. A., Hughes, S. H., Chatterjee, D. K.** (2011). "Protein delivery using engineered virus-like particles". *Proceedings of the National Academy of Sciences of the United States of America* 108.41, pp. 16998–17003. DOI: 10.1073/pnas.1101874108.
- Karsten, U., Papsdorf, G., Roloff, G., Stolley, P., Abel, H., Walther, I., Weiss, H.** (1985). "Monoclonal anti-cytokeratin antibody from a hybridoma clone generated by electrofusion". *European Journal of Cancer & Clinical Oncology* 21.6, pp. 733–740. DOI: 10.1016/0277-5379(85)90271-8.
- Khan, F., Porter, M., Schwenk, R., DeBot, M., Saudan, P., Dutta, S.** (2015). "Head-to-Head Comparison of Soluble vs. Q β VLP Circumsporozoite Protein Vaccines Reveals Selective Enhancement of NANP Repeat Responses". *PloS One* 10.11, e0142035. DOI: 10.1371/journal.pone.0142035.
- Kleindienst, P., Brocker, T.** (2005). "Concerted antigen presentation by dendritic cells and B cells is necessary for optimal CD4 T-cell immunity *in vivo*". *Immunology* 115.4, pp. 556–564. DOI: 10.1111/j.1365-2567.2005.02196.x.
- Knopp, Y., Geis, F. K., Heckl, D., Horn, S., Neumann, T., Kuehle, J., Meyer, J., Fehse, B., Baum, C., Morgan, M., Meyer, J., Schambach, A., Galla, M.** (2018). "Transient Retrovirus-Based CRISPR/Cas9 All-in-One Particles for Efficient, Targeted Gene Knockout". *Molecular Therapy: Nucleic Acids* 13, pp. 256–274. DOI: 10.1016/j.omtn.2018.09.006.
- Knudsen, B. S., Zhao, P., Resau, J., Cottingham, S., Gherardi, E., Xu, E., Berghuis, B., Daugherty, J., Grabinski, T., Toro, J., Giambernardi, T., Skinner, R. S., Gross, M., Hudson, E., Kort, E., Lengyel, E., Ventura, A., West, R. A., Xie, Q., Hay, R., Vande Woude, G., Cao, B.** (2009). "A novel multipurpose monoclonal antibody for evaluating human c-Met expression in preclinical and clinical settings". *Applied Immunohistochemistry & Molecular Morphology* 17.1, pp. 57–67. DOI: 10.1097/PAI.0b013e3181816ae2.
- Köhler, G., Milstein, C.** (1975). "Continuous cultures of fused cells secreting antibody of predefined specificity". *Nature* 256, pp. 495–497. DOI: 10.1038/256495a0.
- Krementsov, D. N., Rassam, P., Margeat, E., Roy, N. H., Schneider-Schaulies, J., Milhiet, P. E., Thali, M.** (2010). "HIV-1 assembly differentially alters dynamics and partitioning of tetraspanins and raft components". *Traffic* 11.11, pp. 1401–1414. DOI: 10.1111/j.1600-0854.2010.01111.x.
- Kromenaker, S. J., Srienc, F.** (1994). "Stability of producer hybridoma cell lines after cell sorting: a case study". *Biotechnology Progress* 10.3, pp. 299–307. DOI: 10.1021/bp00027a010.
- Kueng, H. J., Leb, V. M., Haiderer, D., Raposo, G., They, C., Derdak, S. V., Schmetterer, K. G., Neunkirchner, A., Sillaber, C., Seed, B., Pickl, W. F.** (2007). "General Strategy for Decoration of Enveloped Viruses with Functionally Active Lipid-Modified Cytokines". *Journal of Virology* 81.16, pp. 8666–8676. DOI: 10.1128/jvi.00682-07.

- Kurokawa, A., Yamamoto, Y.** (2022). “Development of monoclonal antibodies specific to Marek disease virus-EcoRI-Q (Meq) for the immunohistochemical diagnosis of Marek disease using formalin-fixed, paraffin-embedded samples”. *Journal of Veterinary Diagnostic Investigation* 34.3, pp. 458–464. DOI: 10.1177/10406387221080444.
- Langedijk, J. P. M., van Manen, D., Vellinga, J., Wegmann, F., Callendret, B. C. S., Krarup, A., Stitz, J.** (2019). “Synthetic human immunodeficiency virus (HIV) envelope antigen, vectors, and compositions thereof”. U.S. Patent 10,369,214-B2, 6 August, 2019. (Visited on 03/07/2023).
- Laustsen, A. H., Greiff, V., Karatt-Vellatt, A., Muyldermans, S., Jenkins, T. P.** (2021). “Animal Immunization, in Vitro Display Technologies, and Machine Learning for Antibody Discovery”. *Trends in Biotechnology* 39.12, pp. 1263–1273. DOI: 10.1016/j.tibtech.2021.03.003.
- Lavado-García, J., Jorge, I., Boix-Besora, A., Vázquez, J., Gòdia, F., Cervera, L.** (2021). “Characterization of HIV-1 virus-like particles and determination of Gag stoichiometry for different production platforms”. *Biotechnology and Bioengineering* 118.7, pp. 2660–2675. DOI: 10.1002/bit.27786.
- Lee, W., Suresh, M.** (2022). “Vaccine adjuvants to engage the cross-presentation pathway”. *Frontiers in Immunology* 13, p. 940047. DOI: 10.3389/fimmu.2022.940047.
- Lee, Y., Lee, Y.-T., Ko, E.-J., Kim, K.-H., Hwang, H. S., Park, S., Kwon, Y.-M., Kang, S. M.** (2017). “Soluble F proteins exacerbate pulmonary histopathology after vaccination upon respiratory syncytial virus challenge but not when presented on virus-like particles”. *Human Vaccines & Immunotherapeutics* 13.11, pp. 2594–2605. DOI: 10.1080/21645515.2017.1362514.
- Legler, D. F., Doucey, M.-A., Schneider, P., Chapatte, L., Bender, F. C., Bron, C.** (2005). “Differential insertion of GPI-anchored GFPs into lipid rafts of live cells”. *The FASEB Journal* 19.1, pp. 73–75. DOI: 10.1096/fj.03-1338fje.
- Lehmann, A., Wixted, J. H. F., Shapovalov, M. V., Roder, H., Dunbrack, R. L., Robinson, M. K.** (2015). “Stability engineering of anti-EGFR scFv antibodies by rational design of a lambda-to-kappa swap of the VL framework using a structure-guided approach”. *mAbs* 7.6, pp. 1058–1071. DOI: 10.1080/19420862.2015.1088618.
- Levental, I., Lingwood, D., Grzybek, M., Coskun, U., Simons, K.** (2010). “Palmitoylation regulates raft affinity for the majority of integral raft proteins”. *Proceedings of the National Academy of Sciences of the United States of America* 107.51, pp. 22050–22054. DOI: 10.1073/pnas.1016184107.
- Li, H., Dou, J., Ding, L., Spearman, P.** (2007). “Myristoylation Is Required for Human Immunodeficiency Virus Type 1 Gag-Gag Multimerization in Mammalian Cells”. *Journal of Virology* 81.23, pp. 12899–12910. DOI: 10.1128/jvi.01280-07.
- Lillehoj, H., Sasai, K., Matsuda, H.** (1994). “Development and Characterization of Chicken-Chicken B Cell Hybridomas Secreting Monoclonal Antibodies that Detect Sporozoite and

- Merozoite Antigens of *Eimeria*". *Poultry Science* 73.11, pp. 1685–1693. DOI: 10.3382/ps.0731685. URL: <https://www.sciencedirect.com/science/article/pii/S0032579119521095>.
- Lin, J.-R., Izar, B., Wang, S., Yapp, C., Mei, S., Shah, P. M., Santagata, S., Sorger, P. K.** (2018). "Highly multiplexed immunofluorescence imaging of human tissues and tumors using t-CyCIF and conventional optical microscopes". *eLife* 7. DOI: 10.7554/eLife.31657.
- Link, A., Zabel, F., Schnetzler, Y., Titz, A., Brombacher, F., Bachmann, M. F.** (2012). "Innate immunity mediates follicular transport of particulate but not soluble protein antigen". *Journal of Immunology* 188.8, pp. 3724–3733. DOI: 10.4049/jimmunol.1103312.
- Link, N., Aubel, C., Kelm, J. M., Marty, R. R., Greber, D., Djonov, V., Bourhis, J., Weber, W., Fussenegger, M.** (2006). "Therapeutic protein transduction of mammalian cells and mice by nucleic acid-free lentiviral nanoparticles". *Nucleic Acids Research* 34.2, e16. DOI: 10.1093/nar/gnj014.
- Lorent, J. H., Levental, I.** (2015). "Structural determinants of protein partitioning into ordered membrane domains and lipid rafts". *Chemistry and Physics of Lipids* 192, pp. 23–32. DOI: 10.1016/j.chemphyslip.2015.07.022. URL: <http://www.sciencedirect.com/science/article/pii/S000930841530027X>.
- Lu, B., Javidi-Parsijani, P., Makani, V., Mehraein-Ghomi, F., Sarhan, W. M., Sun, D., Yoo, K. W., Atala, Z. P., Lyu, P., Atala, A.** (2019). "Delivering SaCas9 mRNA by lentivirus-like bionanoparticles for transient expression and efficient genome editing". *Nucleic Acids Research* 47.8, e44. DOI: 10.1093/nar/gkz093.
- Lynch, A., Meyers, A. E., Williamson, A.-L., Rybicki, E. P.** (2012). "Stability studies of HIV-1 Pr55gag virus-like particles made in insect cells after storage in various formulation media". *Virology Journal* 9, p. 210. DOI: 10.1186/1743-422X-9-210.
- Ma, H., Ó'Fágáin, C., O'Kennedy, R.** (2020). "Antibody stability: A key to performance - Analysis, influences and improvement". *Biochimie* 177, pp. 213–225. DOI: 10.1016/j.biochi.2020.08.019.
- Maecker, H. T., Frey, T., Nomura, L. E., Trotter, J.** (2004). "Selecting fluorochrome conjugates for maximum sensitivity". *Cytometry. Part A* 62A.2, pp. 169–173. DOI: 10.1002/cyto.a.20092.
- Manolova, V., Flace, A., Bauer, M., Schwarz, K., Saudan, P., Bachmann, M. F.** (2008). "Nanoparticles target distinct dendritic cell populations according to their size". *European Journal of Immunology* 38.5, pp. 1404–1413. DOI: 10.1002/eji.200737984.
- Martin, J. L., Cao, S., Maldonado, J. O., Zhang, W., Mansky, L. M.** (2016). "Distinct Particle Morphologies Revealed through Comparative Parallel Analyses of Retrovirus-Like Particles". *Journal of Virology* 90.18, pp. 8074–8084. DOI: 10.1128/jvi.00666-16.
- Mátés, L., Chuah, M. K. L., Belay, E., Jerchow, B., Manoj, N., Acosta-Sanchez, A., Grzela, D. P., Schmitt, A., Becker, K., Matrai, J., Ma, L., Samara-Kuko, E., Gysemans, C., Pryputniewicz, D., Miskey, C., Fletcher, B., VandenDriessche, T., Ivics, Z., Izsvák, Z.** (2009). "Molecular

6. References

- evolution of a novel hyperactive Sleeping Beauty transposase enables robust stable gene transfer in vertebrates". *Nature Genetics* 41.6, pp. 753–761. DOI: 10.1038/ng.343.
- Matter, M. S., Ochsenbein, A. F.** (2008). "Natural antibodies target virus-antibody complexes to organized lymphoid tissue". *Autoimmunity Reviews* 7.6, pp. 480–486. DOI: 10.1016/j.autrev.2008.03.018.
- McBurney, S. P., Young, K. R., Ross, T. M.** (2007). "Membrane embedded HIV-1 envelope on the surface of a virus-like particle elicits broader immune responses than soluble envelopes". *Virology* 358.2, pp. 334–346. DOI: 10.1016/j.virol.2006.08.032.
- McCafferty, J., Griffiths, A. D., Winter, G., Chiswell, D. J.** (1990). "Phage antibodies: filamentous phage displaying antibody variable domains". *Nature* 348.6301, pp. 552–554. DOI: 10.1038/348552a0.
- McConnell, A. D., Do, M., Neben, T. Y., Spasojevic, V., MacLaren, J., Chen, A. P., Altobelli, L., Macomber, J. L., Berkebile, A. D., Horlick, R. A., Bowers, P. M., King, D. J.** (2012). "High affinity humanized antibodies without making hybridomas; immunization paired with mammalian cell display and *in vitro* somatic hypermutation". *PloS One* 7.11, e49458. DOI: 10.1371/journal.pone.0049458.
- Miltenyi Biotec** (undated). *CD271 (LNGFR) Antibody, anti-human, REAfinity™*. URL: <https://www.miltenyibiotec.com/DE-en/products/cd271-Ingfr-antibody-anti-human-reafinity-rea844.html#conjugate=pe:size=30-tests-in-60-ul> (visited on 03/02/2023).
- Montefiori, D. C., Cornell, R. J., Zhou, J. Y., Zhou, J. T., Hirsch, V. M., Johnson, P. R.** (1994). "Complement control proteins, CD46, CD55, and CD59, as common surface constituents of human and simian immunodeficiency viruses and possible targets for vaccine protection". *Virology* 205.1, pp. 82–92. DOI: 10.1006/viro.1994.1622.
- Morgan, B., Thorpe, L. W., Marchetti, D., Perez-Polo, J. R.** (1989). "Expression of nerve growth factor receptors by human peripheral blood mononuclear cells". *Journal of Neuroscience Research* 23, pp. 41–45. DOI: 10.1002/jnr.490230106.
- Mücksch, F., Laketa, V., Müller, B., Schultz, C., Kräusslich, H.-G.** (2017). "Synchronized HIV assembly by tunable PIP2 changes reveals PIP2 requirement for stable Gag anchoring". *eLife* 6. DOI: 10.7554/eLife.25287.
- Murray, P. S., Li, Z., Wang, J., Tang, C. L., Honig, B., Murray, D.** (2005). "Retroviral matrix domains share electrostatic homology: Models for membrane binding function throughout the viral life cycle". *Structure* 13.10, pp. 1521–1531. DOI: 10.1016/j.str.2005.07.010.
- Nagano, K., Tsutsumi, Y.** (2021). "Phage Display Technology as a Powerful Platform for Antibody Drug Discovery". *Viruses* 13. DOI: 10.3390/v13020178.
- Nooraei, S., Bahrololum, H., Hoseini, Z. S., Katalani, C., Hajizade, A., Easton, A. J., Ahmadian, G.** (2021). "Virus-like particles: preparation, immunogenicity and their roles as nanovaccines

- and drug nanocarriers". *Journal of Nanobiotechnology* 19.1, p. 59. DOI: 10.1186/s12951-021-00806-7.
- O'Shannessy, D. J., Somers, E. B., Albone, E., Cheng, X., Park, Y. C., Tomkowicz, B. E., Hamuro, Y., Kohl, T. O., Forsyth, T. M., Smale, R., Fu, Y.-S., Nicolaidis, N. C.** (2011). "Characterization of the human folate receptor alpha via novel antibody-based probes". *Oncotarget* 2, pp. 1227–1243. DOI: 10.18632/oncotarget.412.
- Ochsenbein, A. F., Zinkernagel, R. M.** (2000). "Natural antibodies and complement link innate and acquired immunity". *Immunology Today* 21.12, pp. 624–630. DOI: 10.1016/s0167-5699(00)01754-0.
- Panda, S., Ding, J. L.** (2015). "Natural antibodies bridge innate and adaptive immunity". *Journal of Immunology* 194.1, pp. 13–20. DOI: 10.4049/jimmunol.1400844.
- Parray, H. A., Shukla, S., Samal, S., Shrivastava, T., Ahmed, S., Sharma, C., Kumar, R.** (2020). "Hybridoma technology a versatile method for isolation of monoclonal antibodies, its applicability across species, limitations, advancement and future perspectives". *International Immunopharmacology* 85, p. 106639. DOI: 10.1016/j.intimp.2020.106639.
- Pedrioli, A., Oxenius, A.** (2021). "Single B cell technologies for monoclonal antibody discovery". *Trends in Immunology* 42.12, pp. 1143–1158. DOI: 10.1016/j.it.2021.10.008.
- Perry, S. T., Keogh, E., Morton, M., Koudstaal, W., Pascual, G.** (2019). "Single-cell Screening Method for the Selection and Recovery of Antibodies with Desired Specificities from Enriched Human Memory B Cell Populations". *Journal of Visualized Experiments* 150. DOI: 10.3791/59809.
- Personal communication** (2021). *List of anti-NGFR mAbs tested for FFPE tissue reactivity: The anti-NGFR mAb REA844 (Miltenyi Biotec, Germany) is not reactive with NGFR in FFPE tissue samples.* Johnston, Ian C. D. (Miltenyi Biotec Germany).
- Pitoiset, F., Vazquez, T., Levacher, B., Nehar-Belaid, D., Dérian, N., Vigneron, J., Klatzmann, D., Bertrand, B.** (2017). "Retrovirus-Based Virus-Like Particle Immunogenicity and Its Modulation by Toll-Like Receptor Activation". *Journal of Virology* 91.21, pp. 1–14. DOI: 10.1128/JVI.
- Qin, D., Wu, J., Vora, K. A., Ravetch, J. V., Szakal, A. K., Manser, T., Tew, J. G.** (2000). "Fc gamma receptor IIB on follicular dendritic cells regulates the B cell recall response". *Journal of Immunology* 164.12, pp. 6268–6275. DOI: 10.4049/jimmunol.164.12.6268.
- Ramos-Vara, J. A., Miller, M. A.** (2014). "When tissue antigens and antibodies get along: revisiting the technical aspects of immunohistochemistry—the red, brown, and blue technique". *Veterinary Pathology* 51.1, pp. 42–87. DOI: 10.1177/0300985813505879.
- Rief, N., Waschow, C., Nastainczyk, W., Montenarh, M., Götz, C.** (1998). "Production and characterization of a rabbit monoclonal antibody against human CDC25C phosphatase". *Hybridoma* 17.4, pp. 389–394. DOI: 10.1089/hyb.1998.17.389.

- Roche, P. A., Furuta, K.** (2015). “The ins and outs of MHC class II-mediated antigen processing and presentation”. *Nature Reviews Immunology* 15, pp. 203–216. DOI: 10.1038/nri3818.
- Rosengarten, J. F., Schatz, S., Stitz, J.** (2022a). “Detection of Neutralization-sensitive Epitopes in Antigens Displayed on Virus-Like Particle (VLP)-Based Vaccines Using a Capture Assay”. *Journal of Visualized Experiments* 180. DOI: 10.3791/63137.
- Rosengarten, J. F., Schatz, S., Wolf, T., Barbe, S., Stitz, J.** (2022b). “Components of a HIV-1 vaccine mediate virus-like particle (VLP)-formation and display of envelope proteins exposing broadly neutralizing epitopes”. *Virology* 568, pp. 41–48. DOI: 10.1016/j.virol.2022.01.008.
- Rulli, S. J., Hibbert, C. S., Mirro, J., Pederson, T., Biswal, S., Rein, A.** (2007). “Selective and Nonselective Packaging of Cellular RNAs in Retrovirus Particles”. *Journal of Virology* 81.12, pp. 6623–6631. DOI: 10.1128/jvi.02833-06.
- Saad, J. S., Loeliger, E., Luncsford, P., Liriano, M., Tai, J., Kim, A., Miller, J., Joshi, A., Freed, E. O., Summers, M. F.** (2007). “Point Mutations in the HIV-1 Matrix Protein Turn Off the Myristyl Switch”. *Journal of Molecular Biology* 366.2, pp. 574–585. DOI: 10.1016/j.jmb.2006.11.068.
- Sailaja, G., Skountzou, I., Quan, F.-S., Compans, R. W., Kang, S.-M.** (2007). “Human immunodeficiency virus-like particles activate multiple types of immune cells”. *Virology* 362.2, pp. 331–341. DOI: 10.1016/j.virol.2006.12.014.
- Schatz, S., van Dijk, F. H., Dubiel, A. E., Cantz, T., Eggenschwiler, R., Stitz, J.** (2023a). “Generation of Human 293-F Suspension NGFR Knockout Cells Using CRISPR/Cas9 Coupled to Fluorescent Protein Expression”. *Genotype Phenotype Coupling: Methods and Protocols*. Ed. by S. Zielonka, S. Krah. New York, NY: Springer US, pp. 361–371. DOI: 10.1007/978-1-0716-3279-6_20.
- Schatz, S., Willnow, L., Winkels, M., Rosengarten, J. F., Theek, B., Johnston, I. C. D., Stitz, J.** (2023b). “Generation of Antibodies Selectively Recognizing Epitopes in a Formaldehyde-Fixed Cell-Surface Antigen Using Virus-Like Particle Display and Hybridoma Technology”. *Antibodies* 12.3, p. 57. DOI: 10.3390/antib12030057.
- Schneider, I. C., Hartmann, J., Braun, G., Stitz, J., Klamp, T., Bihi, M., Sahin, U., Buchholz, C. J.** (2018). “Displaying Tetra-Membrane Spanning Claudins on Enveloped Virus-Like Particles for Cancer Immunotherapy”. *Biotechnology Journal* 13.3, e1700345. DOI: 10.1002/biot.201700345.
- Schnierle, B. S., Stitz, J., Bosch, V., Nocken, F., Merget-Millitzer, H., Engelstädter, M., Kurth, R., Groner, B., Cichutek, K.** (1997). “Pseudotyping of murine leukemia virus with the envelope glycoproteins of HIV generates a retroviral vector with specificity of infection for CD4-expressing cells”. *Proceedings of the National Academy of Sciences of the United States of America* 94.16, pp. 8640–8645. DOI: 10.1073/pnas.94.16.8640.
- Segura, M. M., Garnier, A., Di Falco, M. R., Whissell, G., Meneses-Acosta, A., Arcand, N., Kamen, A.** (2008). “Identification of Host Proteins Associated with Retroviral Vector Particles by

6. References

- Proteomic Analysis of Highly Purified Vector Preparations”. *Journal of Virology* 82.3, pp. 1107–1117. DOI: 10.1128/jvi.01909-07.
- Sharma, D., Barhwal, K. K., Biswal, S. N., Srivastava, A. K., Bhardwaj, P., Kumar, A., Chaurasia, O. P., Hota, S. K.** (2019). “Hypoxia-mediated alteration in cholesterol oxidation and raft dynamics regulates BDNF signalling and neurodegeneration in hippocampus”. *Journal of Neurochemistry* 148.2, pp. 238–251. DOI: 10.1111/jnc.14609.
- Sharma, N., Hollensen, A. K., Bak, R. O., Staunstrup, N. H., Schröder, L. D., Mikkelsen, J. G.** (2012). “The impact of cHS4 insulators on DNA transposon vector mobilization and silencing in retinal pigment epithelium cells”. *PloS One* 7.10, e48421. DOI: 10.1371/journal.pone.0048421.
- Shulman, M., Wilde, C. D., Köhler, G.** (1978). “A better cell line for making hybridomas secreting specific antibodies”. *Nature* 276.5685, pp. 269–270. DOI: 10.1038/276269a0.
- Sixt, M., Kanazawa, N., Selg, M., Samson, T., Roos, G., Reinhardt, D. P., Pabst, R., Lutz, M. B., Sorokin, L.** (2005). “The conduit system transports soluble antigens from the afferent lymph to resident dendritic cells in the T cell area of the lymph node”. *Immunity* 22.1, pp. 19–29. DOI: 10.1016/j.immuni.2004.11.013.
- Sorouri, M., Fitzsimmons, S. P., Aydanian, A. G., Bennett, S., Shapiro, M. A.** (2014). “Diversity of the Antibody Response to Tetanus Toxoid: Comparison of Hybridoma Library to Phage Display Library”. *PloS One* 9.9, e106699. DOI: 10.1371/journal.pone.0106699.
- Spieker-Polet, H., Sethupathi, P., Yam, P. C., Knight, K. L.** (1995). “Rabbit monoclonal antibodies: generating a fusion partner to produce rabbit-rabbit hybridomas”. *Proceedings of the National Academy of Sciences of the United States of America* 92.20, pp. 9348–9352. DOI: 10.1073/pnas.92.20.9348.
- Starkie, D. O., Compson, J. E., Rapecki, S., Lightwood, D. J.** (2016). “Generation of Recombinant Monoclonal Antibodies from Immunised Mice and Rabbits via Flow Cytometry and Sorting of Antigen-Specific IgG+ Memory B Cells”. *PloS One* 11.3. DOI: 10.1371/journal.pone.0152282.
- Stitz, J., Buchholz, C. J., Engelstädter, M., Uckert, W., Bloemer, U., Schmitt, I., Cichutek, K.** (2000). “Lentiviral Vectors Pseudotyped with Envelope Glycoproteins Derived from Gibbon Ape Leukemia Virus and Murine Leukemia Virus 10A1”. *Virology* 273.1, pp. 16–20. DOI: 10.1006/viro.2000.0394. URL: <https://www.sciencedirect.com/science/article/pii/S0042682200903945>.
- Suzuki, H., Tanaka, T., Goto, N., Kaneko, M. K., Kato, Y.** (2023). “Development of a Novel Anti-CD44 Variant 4 Monoclonal Antibody C44Mab-108 for Immunohistochemistry”. *Current Issues in Molecular Biology* 45.3, pp. 1875–1888. DOI: 10.3390/cimb45030121.
- Thavarajah, R., Mudimbaimannar, V. K., Elizabeth, J., Rao, U. K., Ranganathan, K.** (2012). “Chemical and physical basics of routine formaldehyde fixation”. *Journal of Oral and Maxillofacial Pathology* 16.3, pp. 400–405. DOI: 10.4103/0973-029X.102496.

- Thornhill, D., Olety, B., Ono, A.** (2019). “Relationships between MA-RNA Binding in Cells and Suppression of HIV-1 Gag Mislocalization to Intracellular Membranes”. *Journal of Virology* 93.23. DOI: 10.1128/JVI.00756-19.
- Torigoe, T., Asanuma, H., Nakazawa, E., Tamura, Y., Hirohashi, Y., Yamamoto, E., Kanaseki, T., Hasegawa, T., Sato, N.** (2012). “Establishment of a monoclonal anti-pan HLA class I antibody suitable for immunostaining of formalin-fixed tissue: unusually high frequency of down-regulation in breast cancer tissues”. *Pathology International* 62.5, pp. 303–308. DOI: 10.1111/j.1440-1827.2012.02789.x.
- Trier, N. H., Hansen, P. R., Houen, G.** (2012). “Production and characterization of peptide antibodies”. *Methods (San Diego, Calif.)* 56.2, pp. 136–144. DOI: 10.1016/j.ymeth.2011.12.001.
- Tucker, T. C., Durbin, E. B., McDowell, J. K., Huang, B.** (2019). “Unlocking the potential of population-based cancer registries”. *Cancer* 125.21, pp. 3729–3737. DOI: 10.1002/cncr.32355.
- Tuekprakhon, A., Puiprom, O., Sasaki, T., Michiels, J., Bartholomeeusen, K., Nakayama, E. E., Meno, M. K., Phadungsombat, J., Huits, R., Ariën, K. K., Luplertlop, N., Shioda, T., Leangwutiwong, P.** (2018). “Broad-spectrum monoclonal antibodies against chikungunya virus structural proteins: Promising candidates for antibody-based rapid diagnostic test development”. *PloS One* 13.12, e0208851. DOI: 10.1371/journal.pone.0208851.
- Valenzuela, P., Medina, A., Rutter, W. J., Ammerer, G., Hall, B. D.** (1982). “Synthesis and assembly of hepatitis B virus surface antigen particles in yeast”. *Nature* 298.5872, pp. 347–350. DOI: 10.1038/298347a0.
- Valldorf, B., Hinz, S. C., Russo, G., Pekar, L., Mohr, L., Klemm, J., Doerner, A., Krah, S., Hust, M., Zielonka, S.** (2022). “Antibody display technologies: selecting the cream of the crop”. *Biological Chemistry* 403.5-6, pp. 455–477. DOI: 10.1515/hsz-2020-0377.
- van Heuvel, Y., Berg, K., Hirsch, T., Winn, K., Modlich, U., Stitz, J.** (2021). “Establishment of a novel stable human suspension packaging cell line producing ecotropic retroviral MLV(PVC-211) vectors efficiently transducing murine hematopoietic stem and progenitor cells”. *Journal of Virological Methods* 297, p. 114243. DOI: 10.1016/j.jviromet.2021.114243.
- Votteler, J., Sundquist, W. I.** (2013). “Virus budding and the ESCRT pathway”. *Cell Host and Microbe* 14, pp. 232–241. DOI: 10.1016/j.chom.2013.08.012.
- Walsh, G.** (2018). “Biopharmaceutical benchmarks 2018”. *Nature Biotechnology* 36.12, pp. 1136–1145. DOI: 10.1038/nbt.4305.
- Walsh, G., Walsh, E.** (2022). “Biopharmaceutical benchmarks 2022”. *Nature Biotechnology* 40.12, pp. 1722–1760. DOI: 10.1038/s41587-022-01582-x.
- Wang, X., Cho, B., Suzuki, K., Xu, Y., Green, J. A., An, J., Cyster, J. G.** (2011). “Follicular dendritic cells help establish follicle identity and promote B cell retention in germinal centers”. *The Journal of Experimental Medicine* 208.12, pp. 2497–2510. DOI: 10.1084/jem.20111449.

- Wang, X., Campoli, M., Cho, H. S., Ogino, T., Bandoh, N., Shen, J., Hur, S. Y., Kageshita, T., Ferrone, S.** (2005). "A method to generate antigen-specific mAb capable of staining formalin-fixed, paraffin-embedded tissue sections". *Journal of Immunological Methods* 299.1-2, pp. 139–151. DOI: 10.1016/j.jim.2005.02.006.
- Weiss, E. R., Göttlinger, H.** (2011). "The role of cellular factors in promoting HIV budding". *Journal of Molecular Biology* 410.4, pp. 525–533. DOI: 10.1016/j.jmb.2011.04.055.
- Wellner, A., McMahon, C., Gilman, M. S. A., Clements, J. R., Clark, S., Nguyen, K. M., Ho, M. H., Hu, V. J., Shin, J.-E., Feldman, J., Hauser, B. M., Caradonna, T. M., Wingler, L. M., Schmidt, A. G., Marks, D. S., Abraham, J., Kruse, A. C., Liu, C. C.** (2021). "Rapid generation of potent antibodies by autonomous hypermutation in yeast". *Nature Chemical Biology* 17.10, pp. 1057–1064. DOI: 10.1038/s41589-021-00832-4.
- Weltner, J., Balboa, D., Katayama, S., Bespalov, M., Krjutškov, K., Jouhilahti, E.-M., Trokovic, R., Kere, J., Otonkoski, T.** (2018). "Human pluripotent reprogramming with CRISPR activators". *Nature Communications* 9. DOI: 10.1038/s41467-018-05067-x.
- Werner, M., Chott, A., Fabiano, A., Battifora, H.** (2000). "Effect of formalin tissue fixation and processing on immunohistochemistry". *The American Journal of Surgical Pathology* 24.7, pp. 1016–1019. DOI: 10.1097/00000478-200007000-00014.
- Wright, E. R., Schooler, J. B., Ding, H. J., Kieffer, C., Fillmore, C., Sundquist, W. I., Jensen, G. J.** (2007). "Electron cryotomography of immature HIV-1 virions reveals the structure of the CA and SP1 Gag shells". *The EMBO Journal* 26.8, pp. 2218–2226. DOI: 10.1038/sj.emboj.7601664.
- Wu, M., Ke, Q., Bi, J., Li, X., Huang, S., Liu, Z., Ge, L.** (2022). "Substantially Improved Electrofusion Efficiency of Hybridoma Cells: Based on the Combination of Nanosecond and Microsecond Pulses". *Bioengineering (Basel, Switzerland)* 9.9. DOI: 10.3390/bioengineering9090450.
- Yang, A. G., Zhang, X., Torti, F., Chen, S. Y.** (1998). "Anti-HIV type 1 activity of wild-type and functional defective RANTES intrakine in primary human lymphocytes". *Human Gene Therapy* 9.14, pp. 2005–2018. DOI: 10.1089/hum.1998.9.14-2005.
- Yurtsever, D., Lorent, J. H.** (2020). "Structural Modifications Controlling Membrane Raft Partitioning and Curvature in Human and Viral Proteins". *The Journal of Physical Chemistry B* 124.35, pp. 7574–7585. DOI: 10.1021/acs.jpcc.0c03435.
- Yusa, K., Zhou, L., Li, M. A., Bradley, A., Craig, N. L.** (2011). "A hyperactive piggyBac transposase for mammalian applications". *Proceedings of the National Academy of Sciences of the United States of America* 108.4, pp. 1531–1536. DOI: 10.1073/pnas.1008322108.
- Zaroff, S., Tan, G.** (2019). "Hybridoma technology: the preferred method for monoclonal antibody generation for in vivo applications". *BioTechniques* 67.3, pp. 90–92. DOI: 10.2144/btn-2019-0054.

6. References

- Zhang, S., Cubas, R., Li, M., Chen, C., Yao, Q.** (2009). "Virus-like particle vaccine activates conventional B2 cells and promotes B cell differentiation to IgG2a producing plasma cells". *Molecular Immunology* 46.10, pp. 1988–2001. DOI: 10.1016/j.molimm.2009.03.008.
- Zhu, P., Liu, J., Bess, J., Chertova, E., Lifson, J. D., Grisé, H., Ofek, G. A., Taylor, K. A., Roux, K. H.** (2006). "Distribution and three-dimensional structure of AIDS virus envelope spikes". *Nature* 441.7095, pp. 847–852. DOI: 10.1038/nature04817.

List of Figures

2.1. Overview on different monoclonal antibody (mAb) discovery technologies	5
2.2. Schematic illustration of antibody formats.	6
2.3. Illustration of the key steps involved in the elicitation of antigen-specific antibodies.	9
2.4. Schematic illustration of the HIV-1 Gag precursor polyprotein.	13
2.5. Simplified structures of a mature HIV-1 virion and a HI-like particle (VLP).	14
3.1. Flow cytometric results of cell surface expression of NGFR.	19
3.2. Indirect detection of NGFR displayed on VLPs.	21
3.3. Flow cytometric results of NGFR staining of 293-F/Mos1.Gag/trNGFR cells after fixation.	23
3.4. Flow cytometric results of native and FF90 PBMCs stained with different CD marker antibodies recognizing either native or FFPE epitopes.	25
3.5. Morphology of VLPs before and after fixation.	26
3.6. Immunization schedule	28
3.7. Flow cytometric results of murine IgG antibodies present in blood plasma.	29
3.8. Specificity of hybridoma mAbs for FF90 NGFR.	32
3.9. Reactivity and specificity of hybridoma mAbs for FFPE NGFR.	35
5.1. Schematic illustration of the transposon vector constructs.	50
5.2. Representative example of the gating strategy for flow cytometric screening of hybridoma supernatants.	62
S1. Schematic of the pSB-IpW transposon donor plasmid	85
S2. Schematic of the pSB-cHS4-IhW transposon donor plasmid.	86
S3. Flow cytometric analysis of trNGFR expression of 3T3/Gag/trNGFR cells.	87
S4. Flow cytometric analysis of murine blood IgM antibodies reactive with 3T3/Gag/-trNGFR cells.	88
S5. Flow cytometric results of the positive hybridoma supernatants MZ34-5H11 and MZ34-11D6 identified in the first screening.	89
S6. Flow cytometric results of the positive hybridoma supernatants MZ34-14B4 and MZ35-1E2 identified in the first screening.	90

List of Figures

S7. Flow cytometric results of the positive hybridoma supernatants MZ35-3H6 and MZ35-4B6 identified in the first screening.	90
S8. Flow cytometric results of the positive hybridoma supernatants MZ35-4F8 and MZ35-4F9 identified in the first screening.	91
S9. Flow cytometric results of the positive hybridoma supernatants MZ35-5G10 and MZ35-5H10 identified in the first screening.	91
S10. Flow cytometric results of the positive hybridoma supernatants MZ35-6D12 and MZ35-6E7 identified in the first screening.	92
S11. Flow cytometric results of the positive hybridoma supernatants MZ35-6G8 and MZ35-8B6 identified in the first screening.	92
S12. Flow cytometric results of the positive hybridoma supernatants MZ35-9F5 and MZ35-10F11 identified in the first screening.	93
S13. Flow cytometric results of the positive hybridoma supernatants MZ35-11F6 and MZ35-12D1 identified in the first screening.	93
S14. Flow cytometric results of the positive hybridoma supernatants MZ35-13F7 and MZ35-14F2 identified in the first screening.	94
S15. Flow cytometric results of the positive hybridoma supernatants MZ35-16D8 and MZ35-17A1 identified in the first screening.	94
S16. Flow cytometric results of the positive hybridoma supernatants MZ35-17G10 and MZ35-18A1 identified in the first screening.	95
S17. Flow cytometric results of the positive hybridoma supernatants MZ35-18D9 and MZ35-18D10 identified in the first screening.	95
S18. Flow cytometric results of the positive hybridoma supernatants MZ35-18E12 and MZ35-18F10 identified in the first screening.	96
S19. Flow cytometric results of the positive hybridoma supernatants MZ35-18H9 and MZ35-19B3 identified in the first screening.	96
S20. Flow cytometric results of the positive hybridoma supernatants MZ35-19C5 and MZ35-19H2 identified in the first screening.	97
S21. Flow cytometric results of the positive hybridoma supernatants MZ35-20A9 and MZ35-20A10 identified in the first screening.	97
S22. Flow cytometric results of the positive hybridoma supernatants MZ35-20F6 and MZ35-20G3 identified in the first screening.	98
S23. Flow cytometric results of the positive hybridoma supernatant MZ35-20G10 identified in the first screening.	98

List of Tables

3.1. Gag content of VLP samples produced by 293-F/Mos1.Gag and 293-F/Mos1.Gag/trNGFR cell pools	20
3.2. NGFR content of cell-free supernatant samples harvested from 293-F, 293-F/Mos1.Gag and 293-F/Mos1.Gag/trNGFR cell cultures	20
3.3. Summary of the flow cytometric screening results of hybridoma cell cultures for FF90 NGFR reactivity and specificity.	30
3.4. Summary of the flow cytometric screening results of hybridoma cell cultures for FFPE NGFR reactivity and specificity.	33
5.1. Chemicals and consumables used in this thesis.	42
5.3. Antibodies used for the detection of human antigens and viral proteins	45
5.5. List of equipment and software used in this thesis.	47
5.7. Composition of buffers and solutions	48
S1. MFIs and SIs of NGFR expression of 293-F-derived cells.	87

Appendix

A. Supplementary data

A.1. Plasmid maps

Created with SnapGene®

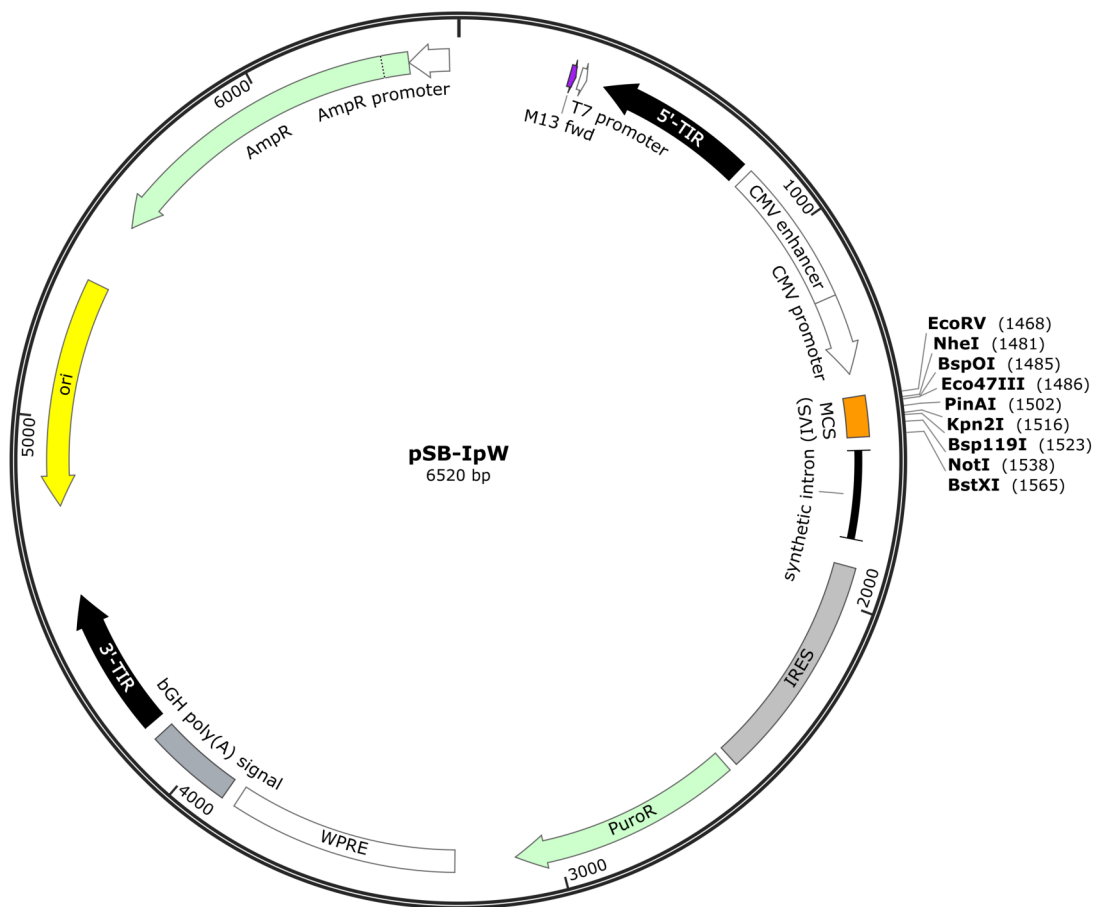


Figure S1. Schematic of the pSB-IpW transposon donor plasmid [Berg et al. 2019; Berg et al. 2020].

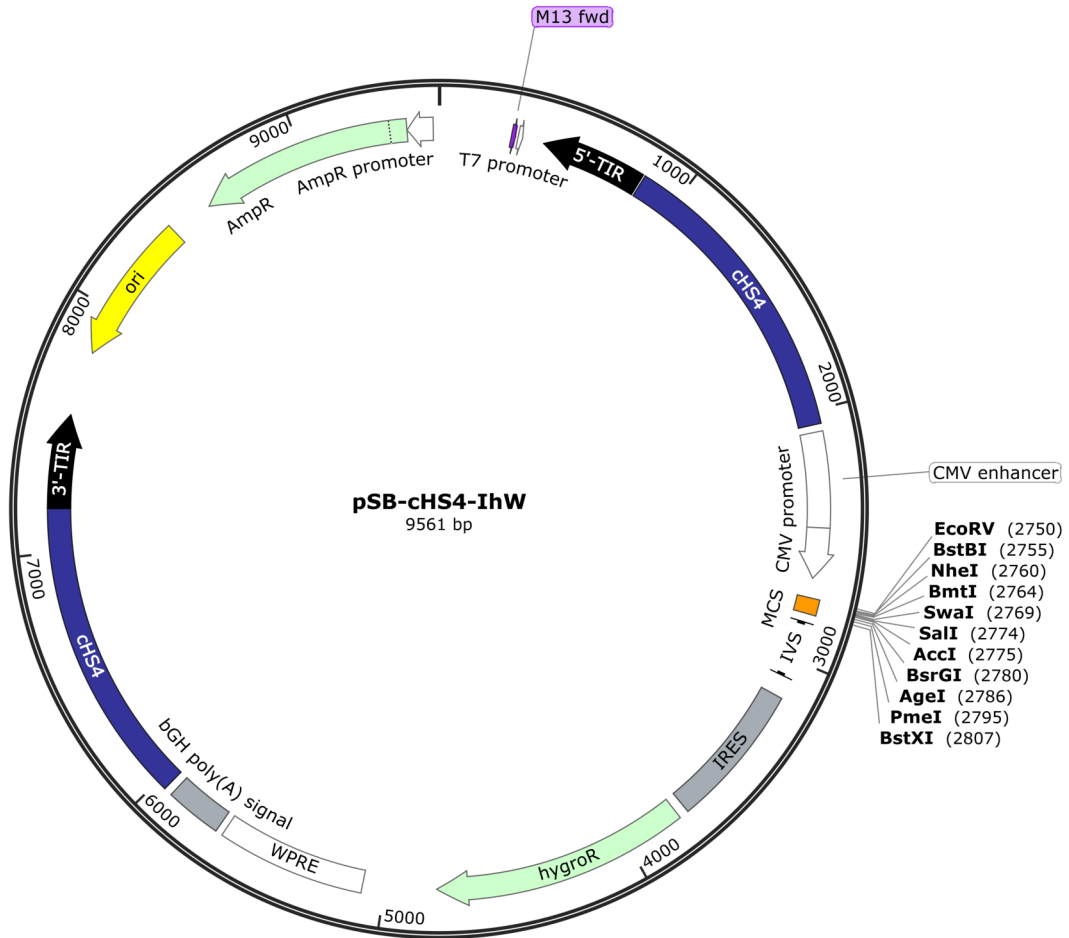


Figure S2. Schematic of the pSB-cHS4-IhW transposon donor plasmid.

A.2. NGFR staining of recombinant cells

Table S1. Mean fluorescent intensities (MFIs), standard deviations (SD) and stain indices (SIs) of 293-F-derived cells stained with anti-NGFR REA844 monoclonal antibodies and matching isotype control antibodies conjugated to phycoerythrin (PE). MFI and SD were calculated using the FlowJo software. SIs were calculated as the difference between the MFIs of the anti-NGFR-labeled cells and the MFI of the isotype controls divided by 2-fold the SD of MFIs of the isotype controls.

Cells	isotype control		anti-NGFR		stain index
	MFI	SD	MFI	SD	
293-F	6.7	3.4	70.0	71.0	9.4
293-F/Mos1.Gag	3.1	1.6	34.3	36.0	9.9
293-F/Mos1.Gag/trNGFR	3.0	2.3	289.0	123.0	63.0

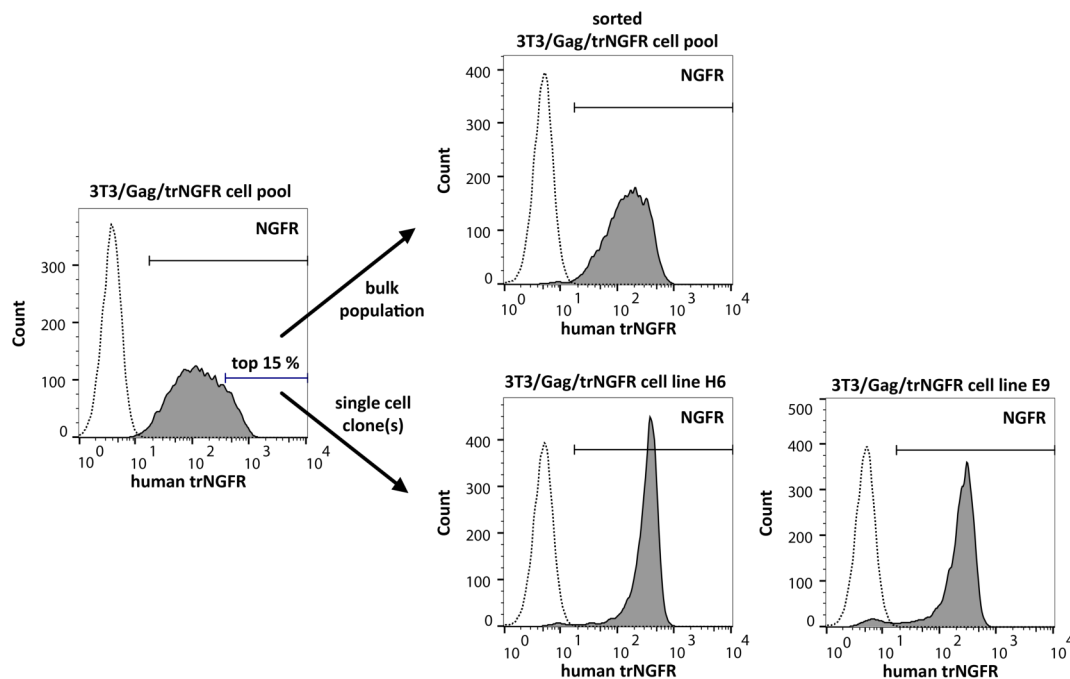


Figure S3. Flow cytometric analysis of trNGFR expression of 3T3/Gag/trNGFR cells. The 3T3/Gag/trNGFR cell pool selected at 400 $\mu\text{g}/\text{mL}$ hygromycin was labeled with PE-conjugated anti-NGFR mAb REA844. The top 15% of trNGFR-expressing cells were isolated employing cell sorting. Sorted cells were either cultivated as bulk population or diluted to obtain single cells and to establish the clonal cell lines H6 and E9. The clone H6 was chosen as NGFR screening cell line for screening of hybridoma antibodies.

A.3. IgM antibodies in blood samples

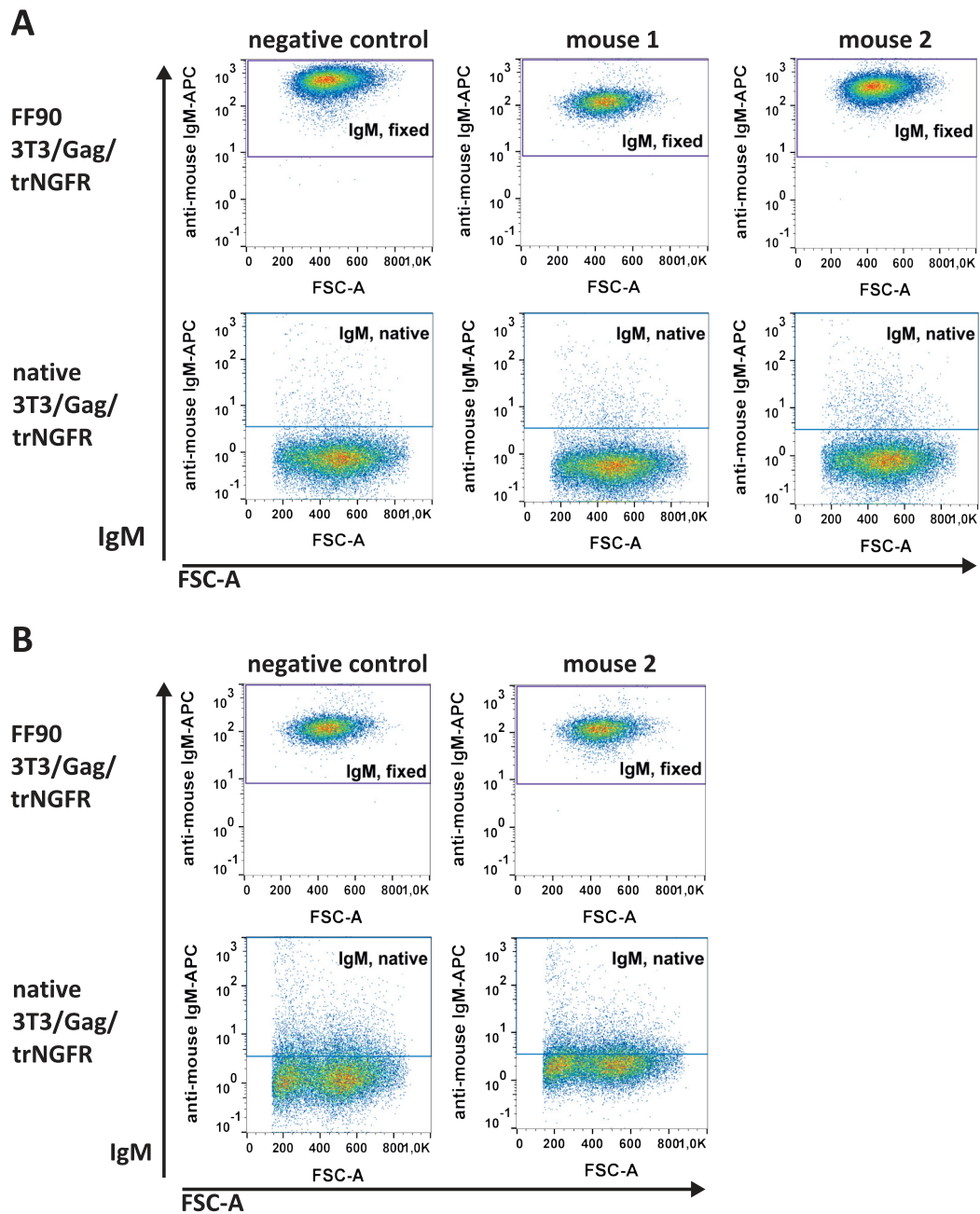


Figure S4. Flow cytometric analysis of murine blood IgM antibodies reactive with 3T3/Gag/trNGFR cells. Murine IgM antibodies were labelled with APC-conjugated anti-mouse IgM antibodies. **A** Blood plasma samples drawn from mice two days after three immunizations with FF90 trNGFR-VLPs (mouse 1 and mouse 2) and from the negative control mouse not immunized with the VLP immunogen. The screening cells were incubated with 35 μ L of plasma. **B** Plasma samples drawn from mouse 2 two days after receiving a fourth dose of FF90 trNGFR-VLPs and from a negative control mouse not immunized with the VLP immunogen. The screening cells were incubated with 25 μ L of plasma.

A.4. Results of positive hybridoma supernatants identified in the first screening

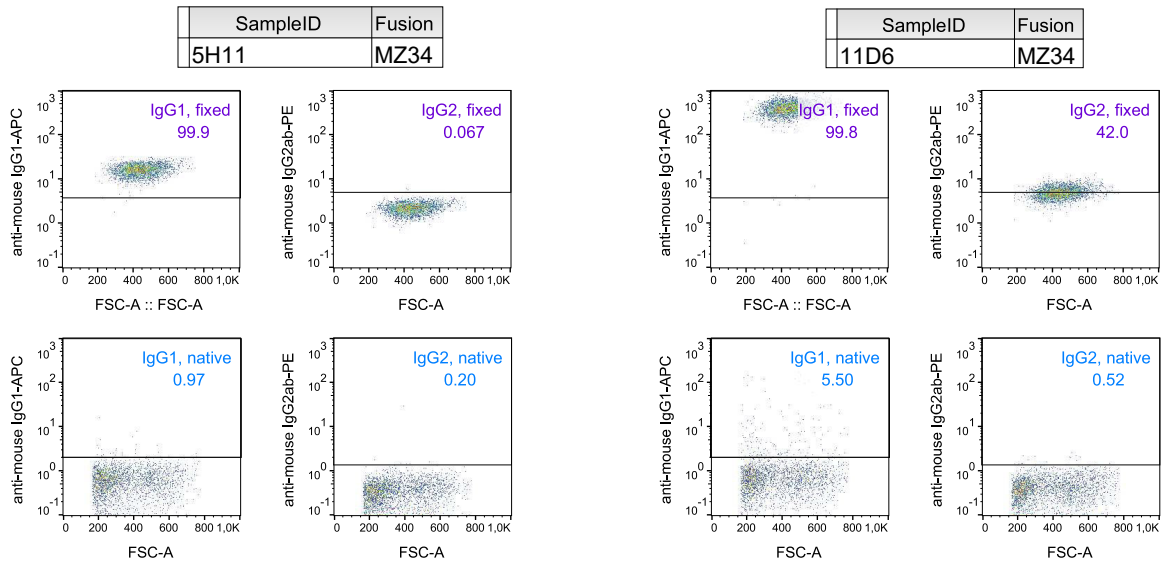


Figure S5. Flow cytometric results of the positive hybridoma supernatants 5H11 and 11D6 from fusion MZ34 identified in the first screening using native and FF90-fixed 3T3/Gag/trNGFR cells. The anti-mouse IgG1 vs. forward scatter area (FSC-A) plot as well as the anti-mouse IgG2ab vs. FSC-A plot of FF90 3T3/Gag/trNGFR cells are shown in the upper panels (purple), whereas the dot plots for native 3T3/Gag/trNGFR cells are in the lower panels (blue).

A. Supplementary data

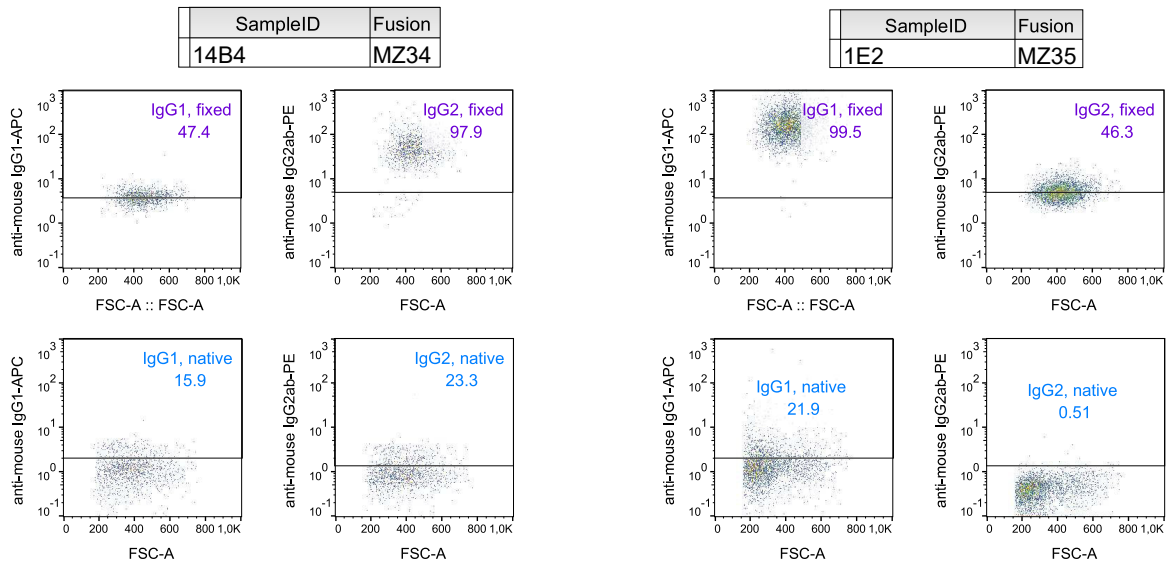


Figure S6. Flow cytometric results of the positive hybridoma supernatants 14B4 from fusion MZ34 and 1E2 from fusion MZ35 identified in the first screening using native and FF90-fixed 3T3/Gag/trNGFR cells. The anti-mouse IgG1 vs. forward scatter area (FSC-A) plot as well as the anti-mouse IgG2ab vs. FSC-A plot of FF90 3T3/Gag/trNGFR cells are shown in the upper panels (purple), whereas the dot plots for native 3T3/Gag/trNGFR cells are in the lower panels (blue).

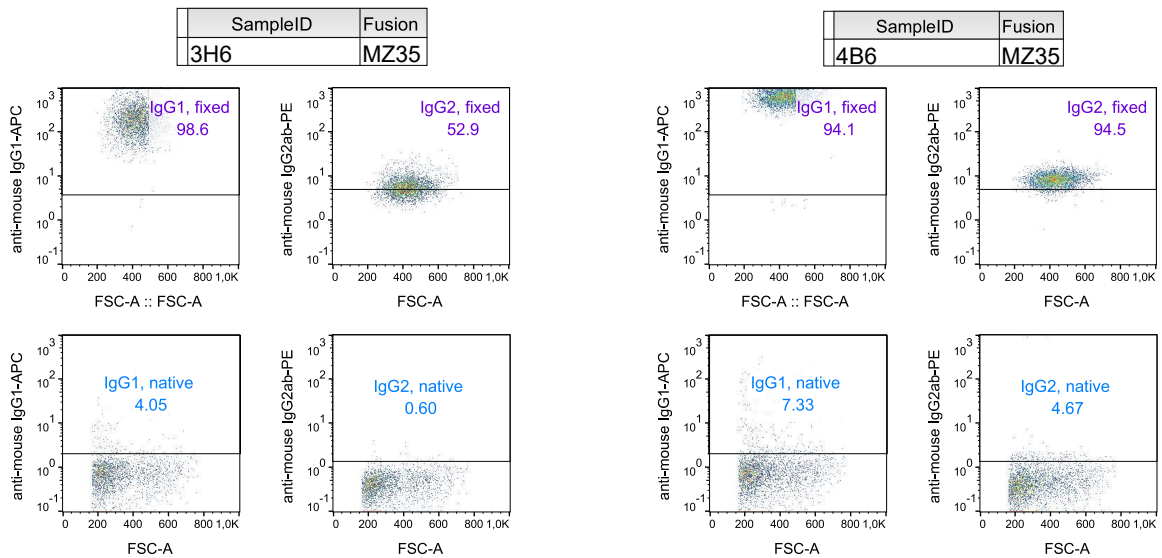


Figure S7. Flow cytometric results of the positive hybridoma supernatants 3H6 and 4B6 from fusion MZ35 identified in the first screening using native and FF90-fixed 3T3/Gag/trNGFR cells. The anti-mouse IgG1 vs. forward scatter area (FSC-A) plot as well as the anti-mouse IgG2ab vs. FSC-A plot of FF90 3T3/Gag/trNGFR cells are shown in the upper panels (purple), whereas the dot plots for native 3T3/Gag/trNGFR cells are in the lower panels (blue).

A. Supplementary data

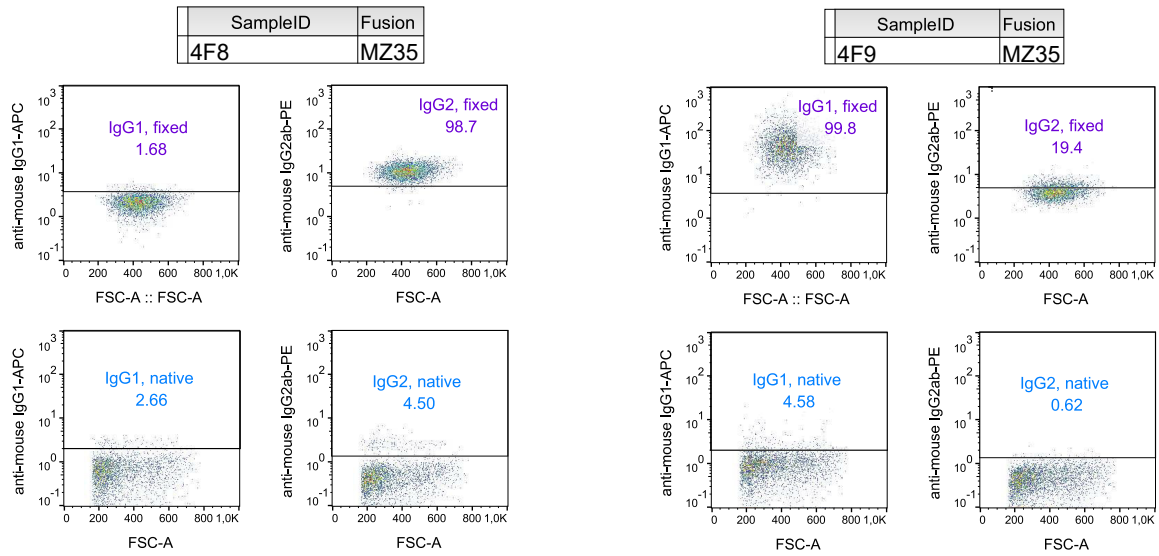


Figure S8. Flow cytometric results of the positive hybridoma supernatants 4F8 and 4F9 from fusion MZ35 identified in the first screening using native and FF90-fixed 3T3/Gag/trNGFR cells. The anti-mouse IgG1 vs. forward scatter area (FSC-A) plot as well as the anti-mouse IgG2ab vs. FSC-A plot of FF90 3T3/Gag/trNGFR cells are shown in the upper panels (purple), whereas the dot plots for native 3T3/Gag/trNGFR cells are in the lower panels (blue).

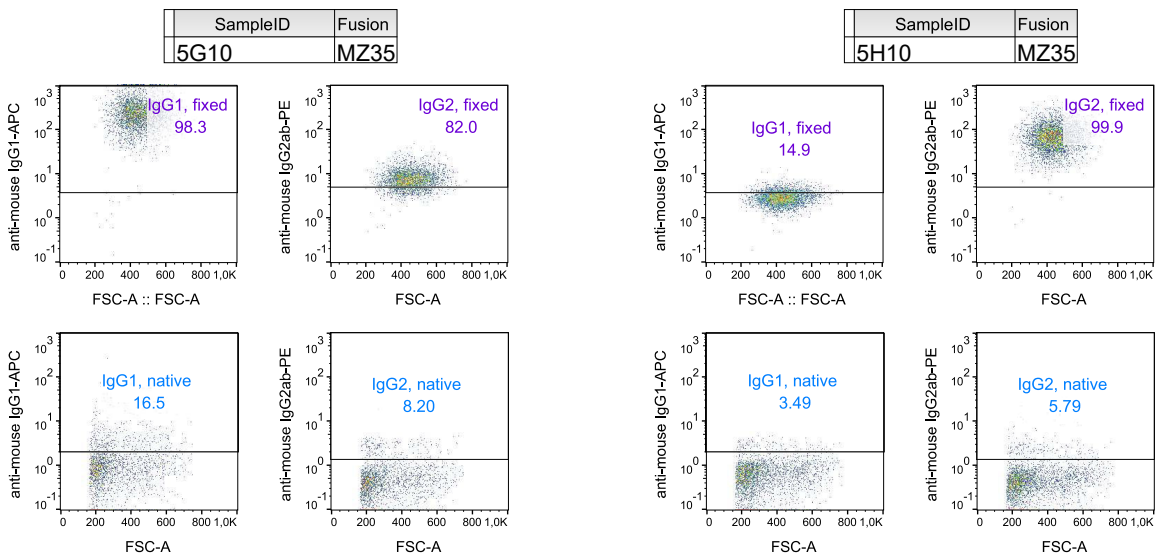


Figure S9. Flow cytometric results of the positive hybridoma supernatants 5G10 and 5H10 from fusion MZ35 identified in the first screening using native and FF90-fixed 3T3/Gag/trNGFR cells. The anti-mouse IgG1 vs. forward scatter area (FSC-A) plot as well as the anti-mouse IgG2ab vs. FSC-A plot of FF90 3T3/Gag/trNGFR cells are shown in the upper panels (purple), whereas the dot plots for native 3T3/Gag/trNGFR cells are in the lower panels (blue).

A. Supplementary data

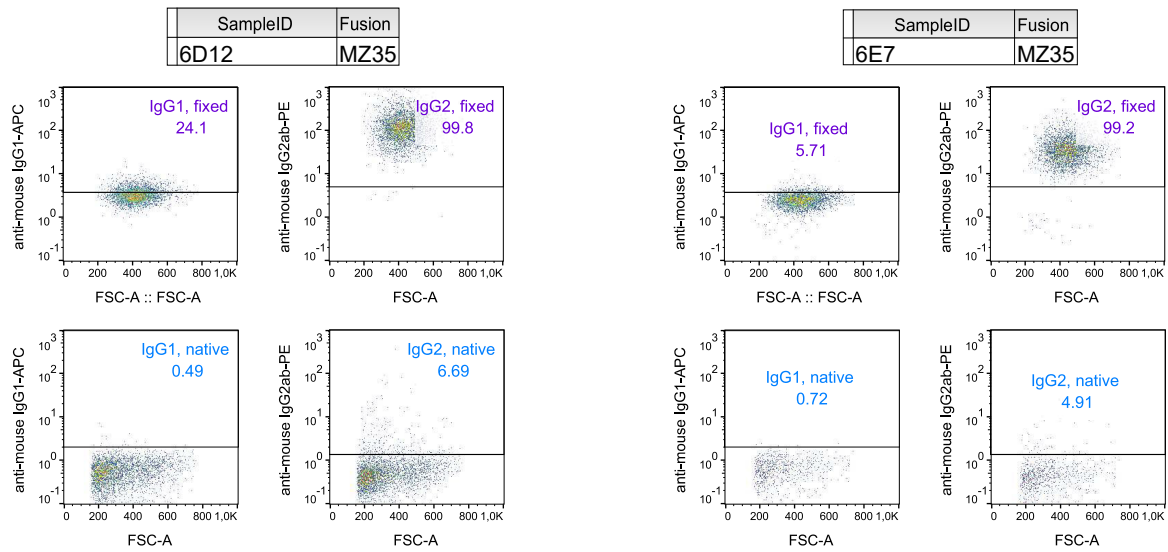


Figure S10. Flow cytometric results of the positive hybridoma supernatants 6D12 and 6E7 from fusion MZ35 identified in the first screening using native and FF90-fixed 3T3/Gag/trNGFR cells. The anti-mouse IgG1 vs. forward scatter area (FSC-A) plot as well as the anti-mouse IgG2ab vs. FSC-A plot of FF90 3T3/Gag/trNGFR cells are shown in the upper panels (purple), whereas the dot plots for native 3T3/Gag/trNGFR cells are in the lower panels (blue).

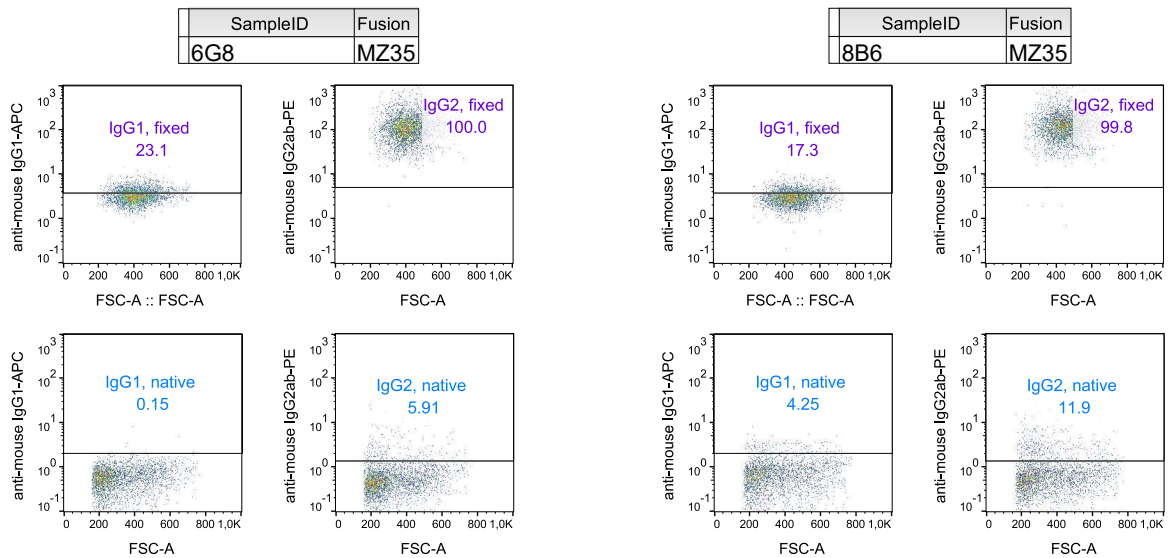


Figure S11. Flow cytometric results of the positive hybridoma supernatants 6G8 and 8B6 from fusion MZ35 identified in the first screening using native and FF90-fixed 3T3/Gag/trNGFR cells. The anti-mouse IgG1 vs. forward scatter area (FSC-A) plot as well as the anti-mouse IgG2ab vs. FSC-A plot of FF90 3T3/Gag/trNGFR cells are shown in the upper panels (purple), whereas the dot plots for native 3T3/Gag/trNGFR cells are in the lower panels (blue).

A. Supplementary data

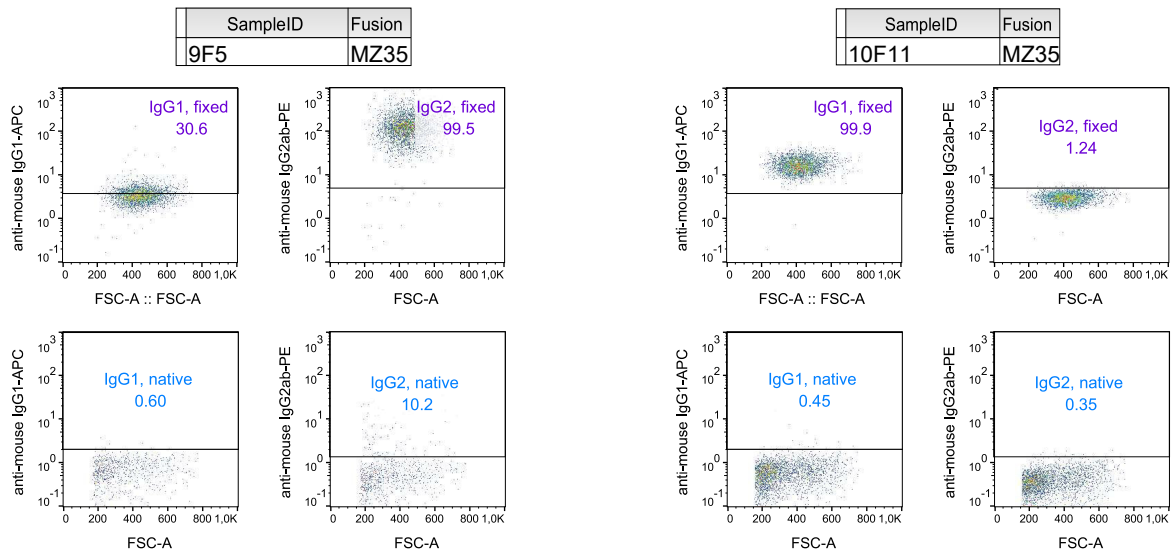


Figure S12. Flow cytometric results of the positive hybridoma supernatants 9F5 and 10F11 from fusion MZ35 identified in the first screening using native and FF90-fixed 3T3/Gag/trNGFR cells. The anti-mouse IgG1 vs. forward scatter area (FSC-A) plot as well as the anti-mouse IgG2ab vs. FSC-A plot of FF90 3T3/Gag/trNGFR cells are shown in the upper panels (purple), whereas the dot plots for native 3T3/Gag/trNGFR cells are in the lower panels (blue).

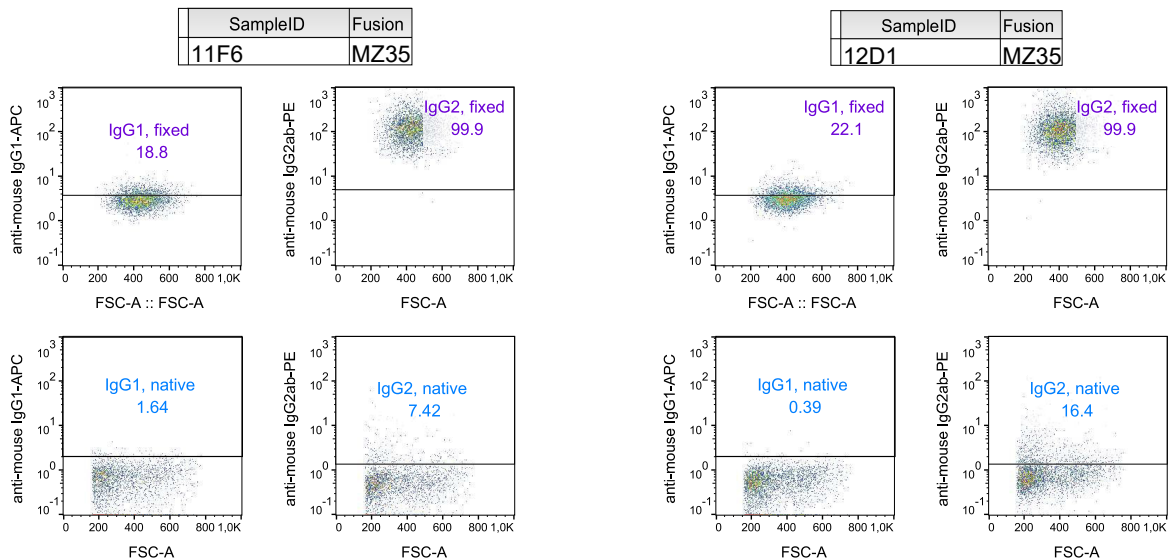


Figure S13. Flow cytometric results of the positive hybridoma supernatants 11F6 and 12D1 from fusion MZ35 identified in the first screening using native and FF90-fixed 3T3/Gag/trNGFR cells. The anti-mouse IgG1 vs. forward scatter area (FSC-A) plot as well as the anti-mouse IgG2ab vs. FSC-A plot of FF90 3T3/Gag/trNGFR cells are shown in the upper panels (purple), whereas the dot plots for native 3T3/Gag/trNGFR cells are in the lower panels (blue).

A. Supplementary data

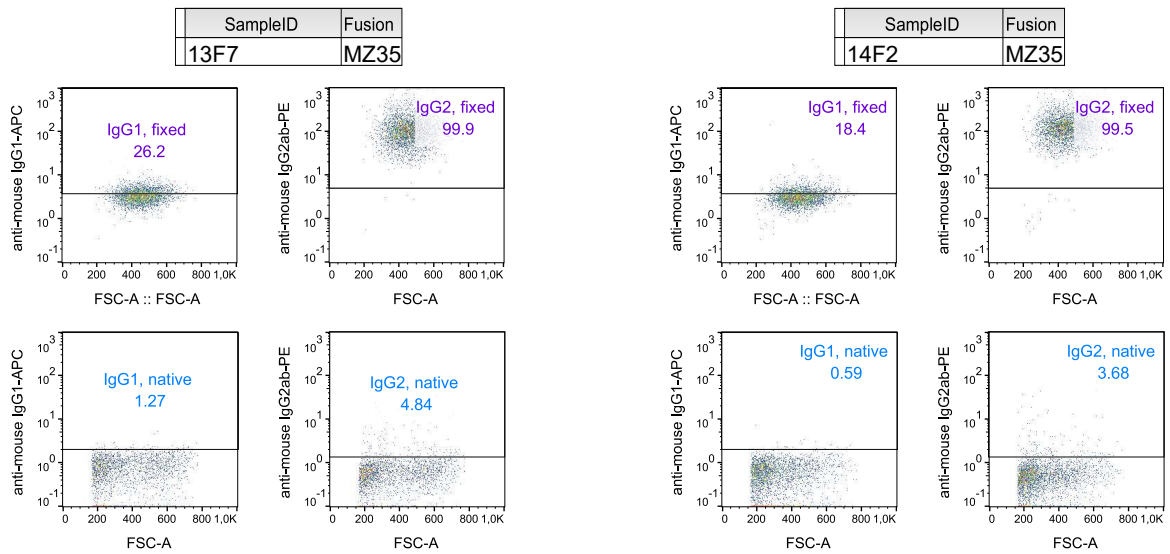


Figure S14. Flow cytometric results of the positive hybridoma supernatants 13F7 and 14F2 from fusion MZ35 identified in the first screening using native and FF90-fixed 3T3/Gag/trNGFR cells. The anti-mouse IgG1 vs. forward scatter area (FSC-A) plot as well as the anti-mouse IgG2ab vs. FSC-A plot of FF90 3T3/Gag/trNGFR cells are shown in the upper panels (purple), whereas the dot plots for native 3T3/Gag/trNGFR cells are in the lower panels (blue).

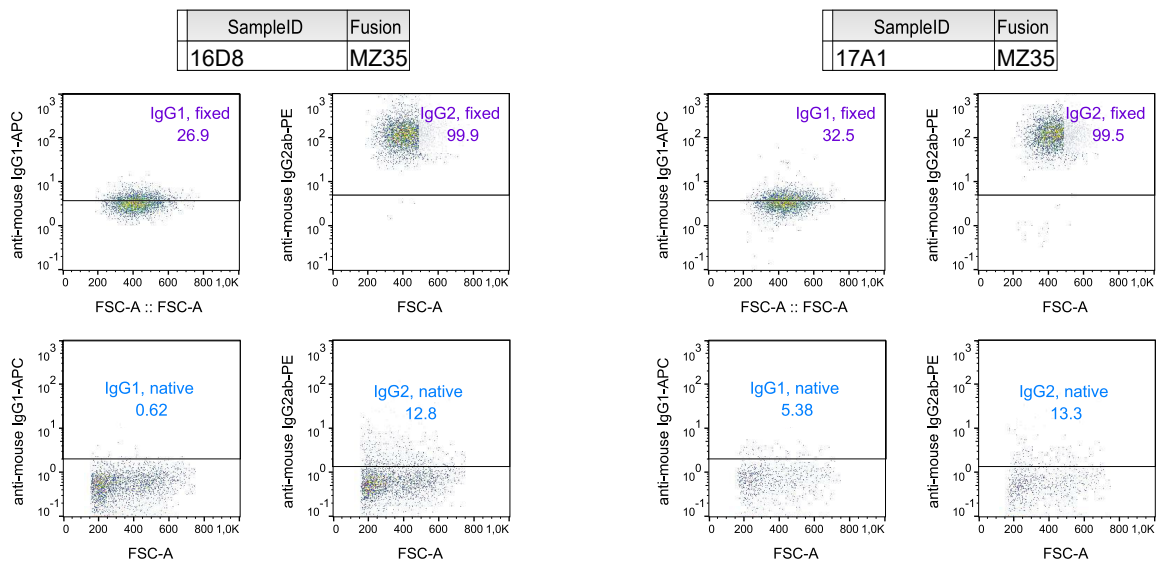


Figure S15. Flow cytometric results of the positive hybridoma supernatants 16D8 and 17A1 from fusion MZ35 identified in the first screening using native and FF90-fixed 3T3/Gag/trNGFR cells. The anti-mouse IgG1 vs. forward scatter area (FSC-A) plot as well as the anti-mouse IgG2ab vs. FSC-A plot of FF90 3T3/Gag/trNGFR cells are shown in the upper panels (purple), whereas the dot plots for native 3T3/Gag/trNGFR cells are in the lower panels (blue).

A. Supplementary data

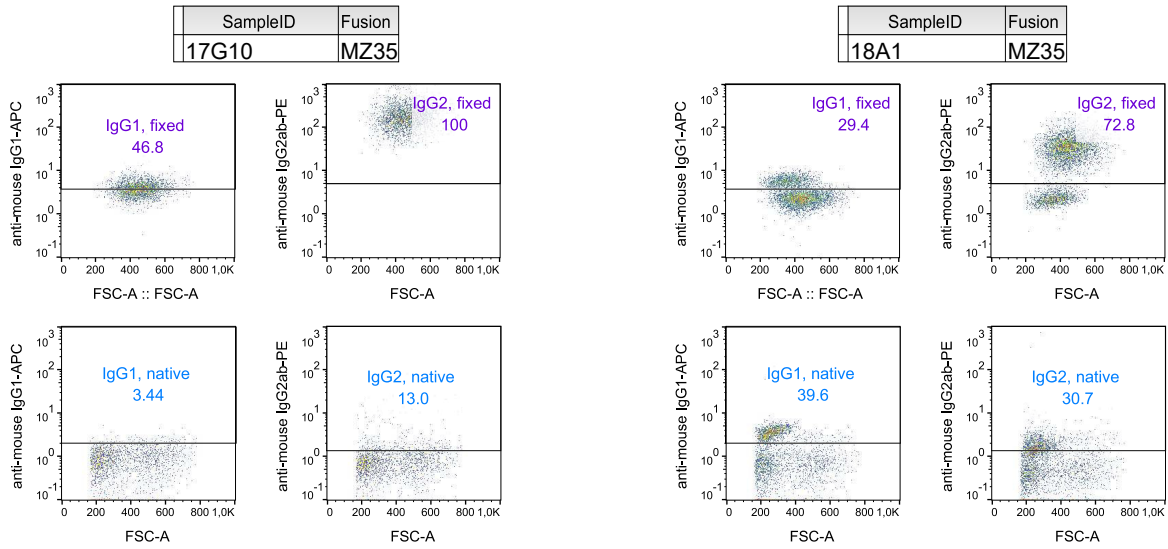


Figure S16. Flow cytometric results of the positive hybridoma supernatants 17G10 and 18A1 from fusion MZ35 identified in the first screening using native and FF90-fixed 3T3/Gag/trNGFR cells. The anti-mouse IgG1 vs. forward scatter area (FSC-A) plot as well as the anti-mouse IgG2ab vs. FSC-A plot of FF90 3T3/Gag/trNGFR cells are shown in the upper panels (purple), whereas the dot plots for native 3T3/Gag/trNGFR cells are in the lower panels (blue).

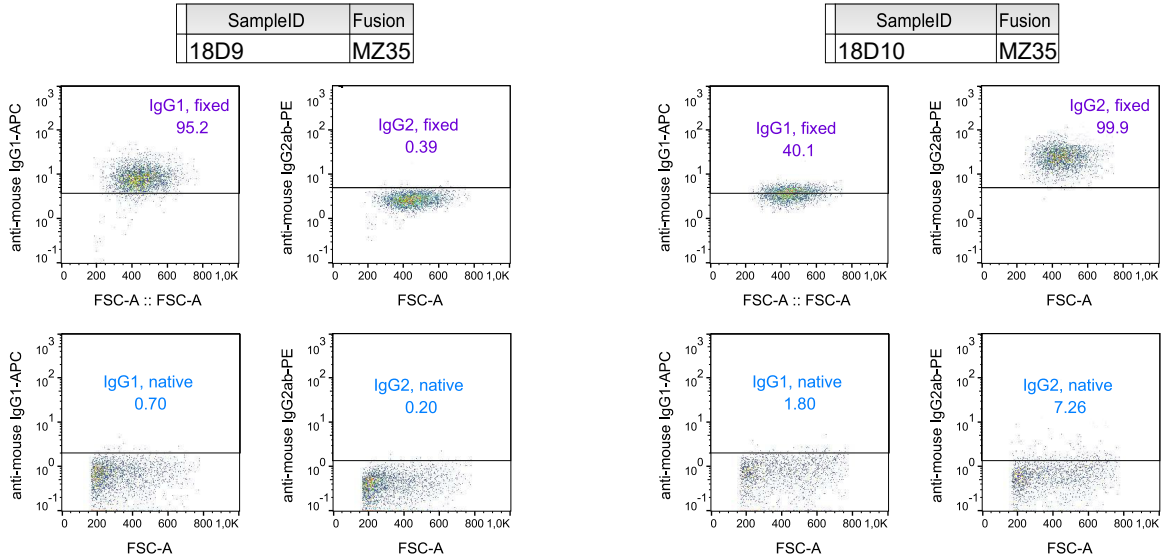


Figure S17. Flow cytometric results of the positive hybridoma supernatants 18D9 and 18D10 from fusion MZ35 identified in the first screening using native and FF90-fixed 3T3/Gag/trNGFR cells. The anti-mouse IgG1 vs. forward scatter area (FSC-A) plot as well as the anti-mouse IgG2ab vs. FSC-A plot of FF90 3T3/Gag/trNGFR cells are shown in the upper panels (purple), whereas the dot plots for native 3T3/Gag/trNGFR cells are in the lower panels (blue).

A. Supplementary data

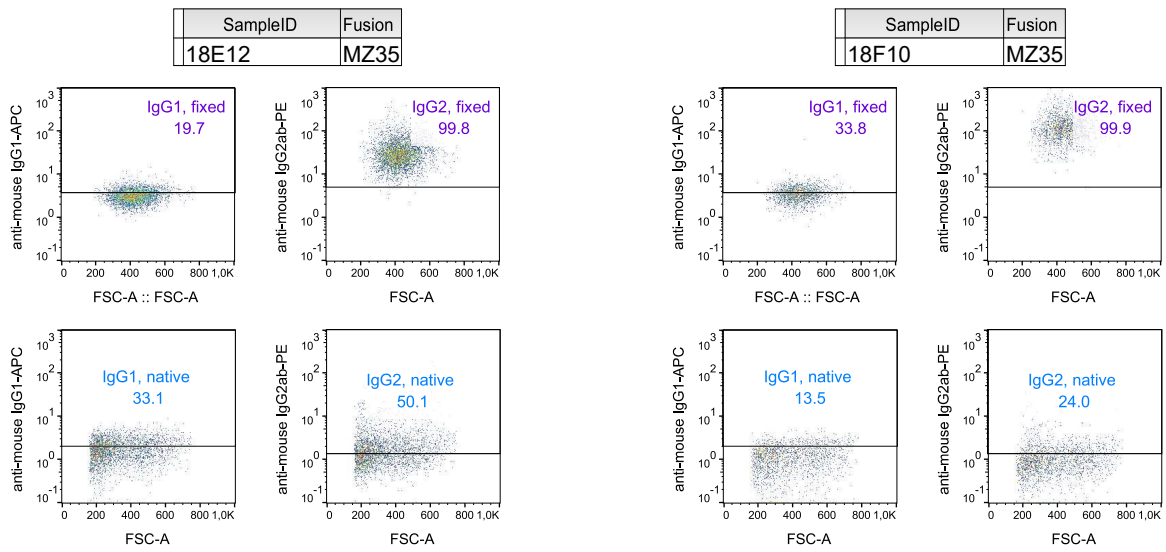


Figure S18. Flow cytometric results of the positive hybridoma supernatants 18E12 and 18F10 from fusion MZ35 identified in the first screening using native and FF90-fixed 3T3/Gag/trNGFR cells. The anti-mouse IgG1 vs. forward scatter area (FSC-A) plot as well as the anti-mouse IgG2ab vs. FSC-A plot of FF90 3T3/Gag/trNGFR cells are shown in the upper panels (purple), whereas the dot plots for native 3T3/Gag/trNGFR cells are in the lower panels (blue).

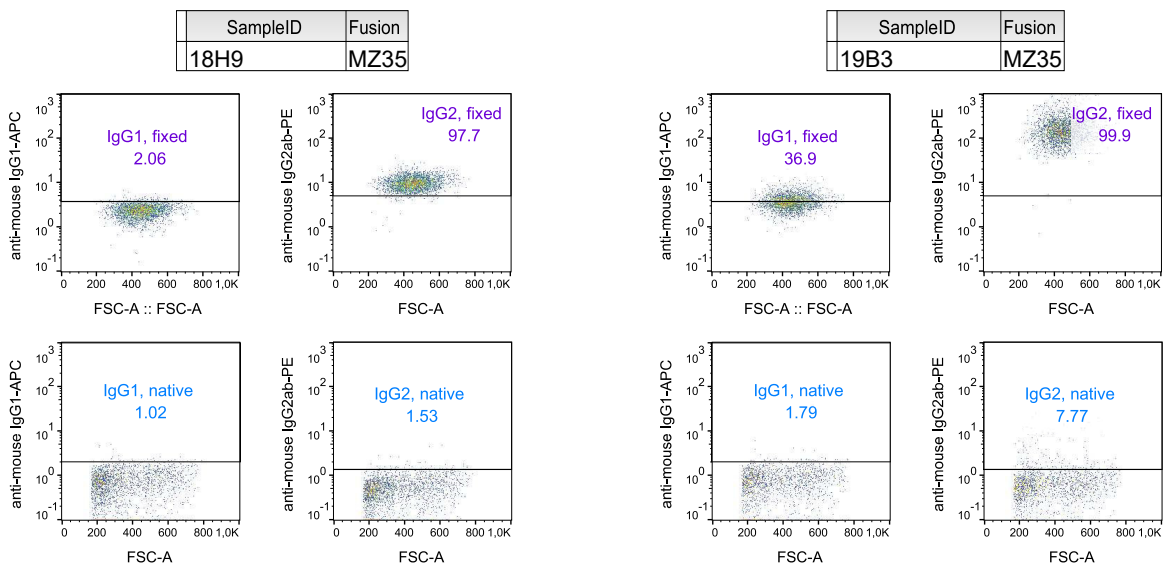


Figure S19. Flow cytometric results of the positive hybridoma supernatants 18H9 and 19B3 from fusion MZ35 identified in the first screening using native and FF90-fixed 3T3/Gag/trNGFR cells. The anti-mouse IgG1 vs. forward scatter area (FSC-A) plot as well as the anti-mouse IgG2ab vs. FSC-A plot of FF90 3T3/Gag/trNGFR cells are shown in the upper panels (purple), whereas the dot plots for native 3T3/Gag/trNGFR cells are in the lower panels (blue).

A. Supplementary data

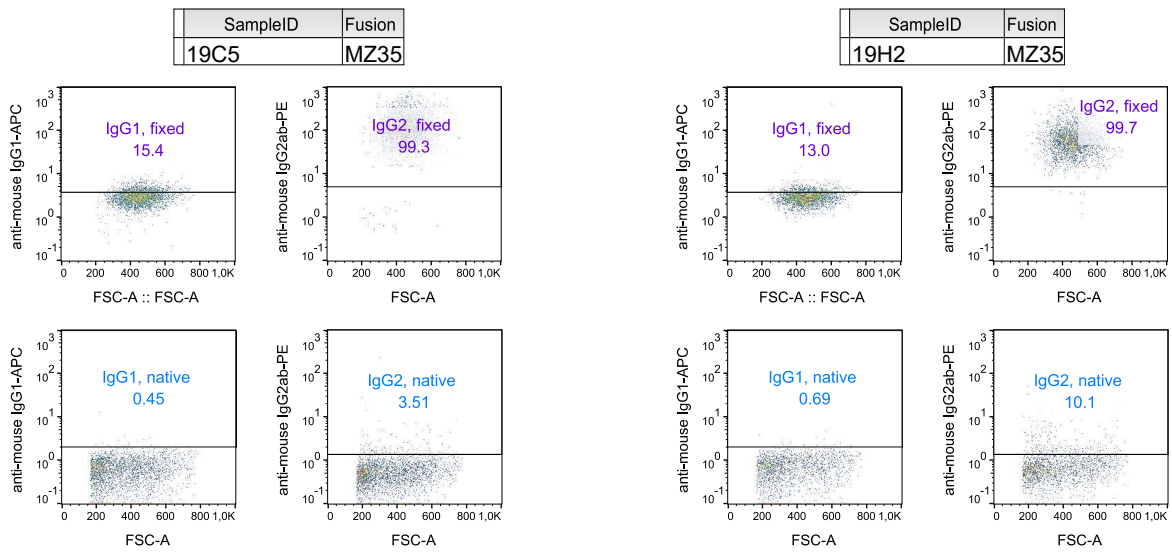


Figure S20. Flow cytometric results of the positive hybridoma supernatants 19C5 and 19H2 from fusion MZ35 identified in the first screening using native and FF90-fixed 3T3/Gag/trNGFR cells. The anti-mouse IgG1 vs. forward scatter area (FSC-A) plot as well as the anti-mouse IgG2ab vs. FSC-A plot of FF90 3T3/Gag/trNGFR cells are shown in the upper panels (purple), whereas the dot plots for native 3T3/Gag/trNGFR cells are in the lower panels (blue).

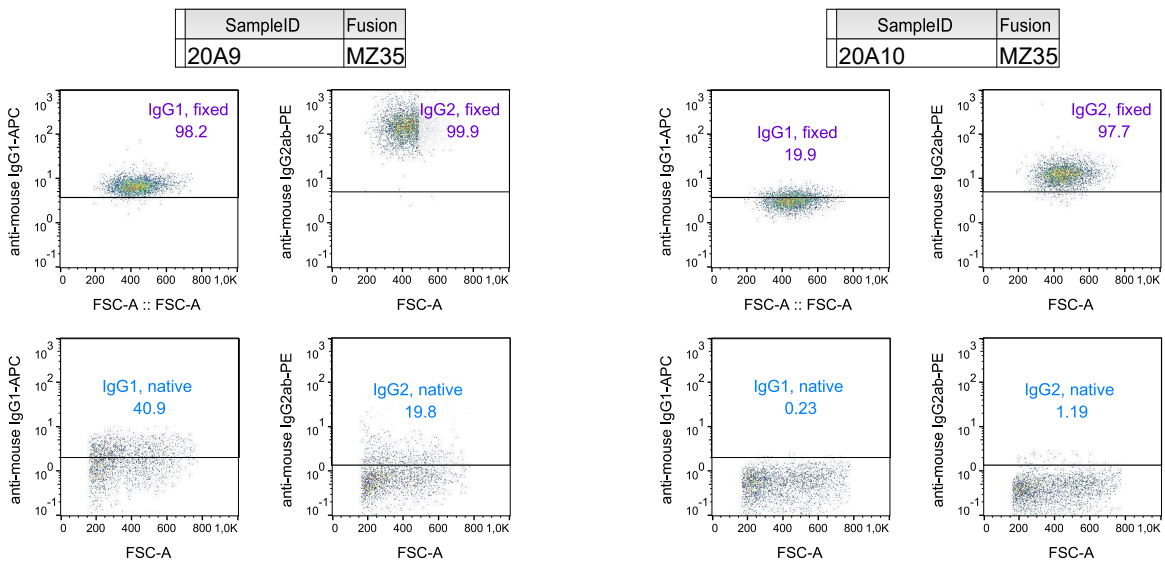


Figure S21. Flow cytometric results of the positive hybridoma supernatants 20A9 and 20A10 from fusion MZ35 identified in the first screening using native and FF90-fixed 3T3/Gag/trNGFR cells. The anti-mouse IgG1 vs. forward scatter area (FSC-A) plot as well as the anti-mouse IgG2ab vs. FSC-A plot of FF90 3T3/Gag/trNGFR cells are shown in the upper panels (purple), whereas the dot plots for native 3T3/Gag/trNGFR cells are in the lower panels (blue).

A. Supplementary data

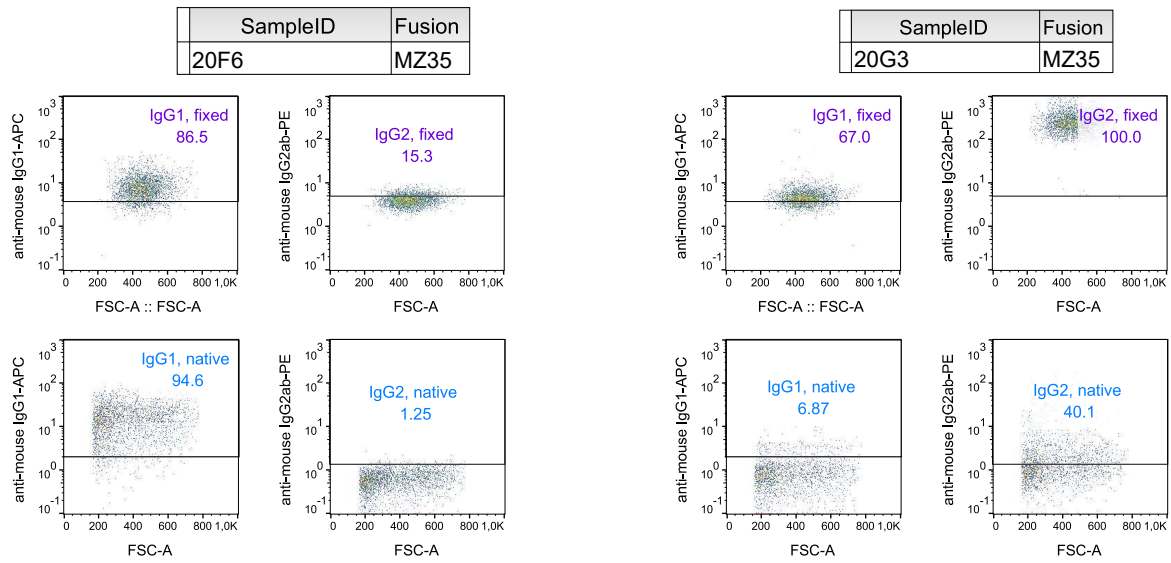


Figure S22. Flow cytometric results of the positive hybridoma supernatants 20F6 and 20G3 from fusion MZ35 identified in the first screening using native and FF90-fixed 3T3/Gag/trNGFR cells. The mAb 20F6 bound to native and FF90 cells. The anti-mouse IgG1 vs. FSC-A plot as well as the anti-mouse IgG2ab vs. FSC-A plot of FF90 3T3/Gag/trNGFR cells are shown in the upper panels (purple), whereas the dot plots for native 3T3/Gag/trNGFR cells are in the lower panels (blue).

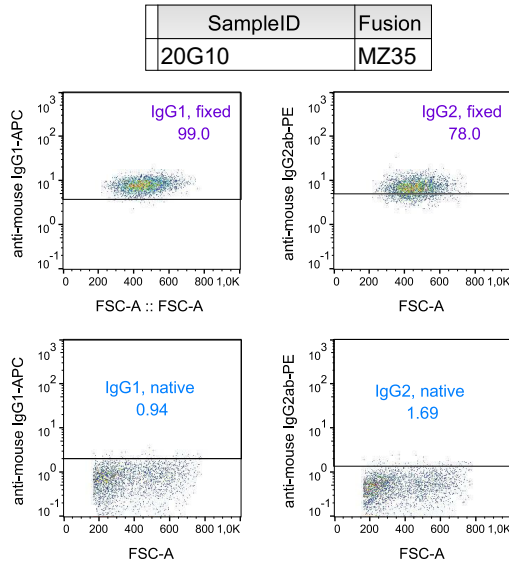


Figure S23. Flow cytometric results of the positive hybridoma supernatant 20G10 from fusion MZ34 identified in the first screening using native and FF90-fixed 3T3/Gag/trNGFR cells. The anti-mouse IgG1 vs. forward scatter area (FSC-A) plot as well as the anti-mouse IgG2ab vs. FSC-A plot of FF90 3T3/Gag/trNGFR cells are shown in the upper panels (purple), whereas the dot plots for native 3T3/Gag/trNGFR cells are in the lower panels (blue).

B. Standard lab protocols

B.1. SDS-PAGE

Lab Protocol	SDS-PAGE	09.09.2020
--------------	----------	------------

Potential hazards and safety precautions

Obtain special instructions by qualified lab personnel before starting work!

Wear personal protective equipment (lab coat, nitrile gloves, safety glasses).

Read the safety data sheets before starting work!

Dangerous (toxic, mutagenic, ..) substances you are going to work with:

- Acrylamide
- TEMED (N,N,N',N'-tetramethylethylenediamine)
- APS (ammoniumperoxodisulfate)
- Roti-Load 1, 4x conc. (Laemmli buffer)

LIMIT acrylamide work to designated areas (fume hood, laboratory Room 1303). Coat work bench with absorbent bench paper prior to working with acrylamide to prevent contamination of non-disposable surfaces. Change this paper layer frequently (eg. weekly or monthly, depending on work intensity) and especially after spilling liquids.

Know the location of spill kits, eyewashes, safety showers before starting work.

Disposal: Solutions containing acrylamide and the resultant polyacrylamide gels must be disposed of as hazardous chemical wastes (blue barrels labeled "Chemikalenabfall").

Handcasting of polyacrylamide gels

Materials

- ROTIPHORESE® gel 30 (37.5:1) (Carl Roth, Germany)
- TEMED (N,N,N',N'-tetramethylethylenediamine; Carl Roth, Germany)

- APS (ammoniumperoxodisulfate; Carl Roth, Germany)
- SDS (sodiumdodecylsulfate; Carl Roth, Germany)
- Tris (Carl Roth, Germany)
- HCl (Carl Roth, Germany)
- isopropanol (Carl Roth, Germany)
- casting module (Mini-PROTEAN Tetra cell equipment, Bio-Rad, USA)

Recipes for buffers and working solutions

1.5 M Tris-HCl pH 8.8 Dissolve 181.71 g Tris in 800 mL dH₂O. Adjust the pH to 8.8 using 1 M HCl. Adjust the volume to 1000 mL with H₂O.

0.5 M Tris-HCl pH 6.8 Dissolve 60.6 g Tris (Carl Roth, Germany) in 800 mL H₂O. Adjust the pH using 1 M HCl. Adjust the volume to 1000 mL with H₂O.

10 % (w/v) SDS Dissolve 10 g SDS in 100 mL H₂O. (Fume hood!)

10 % (w/v) APS Dissolve 10 g APS in 100 mL H₂O. (Fume hood!)

Handcasting procedure

The following recipe is for casting two 12 % polyacrylamide gels.

Ingredients	2x separating gel	2x stacking gel
H ₂ O	6.8 mL	3 mL
1.5 M Tris-HCl pH 8.8	5 mL	-
0.5 M Tris-HCl pH 6.8	-	1.25 mL
10 % SDS	200 µL	50 µL
ROTIPHORESE [®] gel 30	8 mL	670 µL
TEMED	10 µL	5 µL
10 % (w/v) APS	100 µL	25 µL

1. Put on your PPE as described above. Avoid ALL contact with acrylamide solutions or polyacrylamide gels - do not handle gels without gloves on!
2. Assemble the casting module.

3. Prepare separating and stacking gel by mixing water, Tris-HCl buffer, SDS and acrylamide solution in a tube. Water, Tris-HCl and SDS can be mixed outside the designated areas for working with acrylamide. Before adding acrylamide transfer the tube into designated area for acrylamide handling (fume hood).
4. Continue preparing the separating gel by adding TEMED and APS to start the polymerization reaction. Mix and cast the separating gel immediately. Fill to the green bar. Add isopropanol on top and wait until the gel is solid (usually 20-30 min).
5. Decant isopropanol and remove residual alcohol using the filter papers.
6. Add TEMED and APS to the stacking gel. Mix and immediately cast the stacking gel on top of the separating gel. Carefully insert the combs. Caution: Risk of splashing! Wait until the gel is solid.
7. Remove the comb and rinse the gel with water. Wrap the gel in moist paper tissues and put it into a plastic bag. The gel can be stored at 4 °C for about 1-2 weeks. Don't forget to label the bag with your name, date of preparation and the percentage of the gel.
8. Clean the working area.

Electrophoresis

Materials

- Roti-Load 1, 4x conc. (Laemmli buffer; Carl Roth, Germany)
- pre-stained protein size marker (e.g. PAGE Ruler, Thermo Fisher Scientific, USA)
- heat block (placed under the fume hood!)
- polyacrylamide gel
- buffer dam (if only one gel is run)
- gel electrophoresis chamber (Mini-PROTEAN Tetra cell equipment, Bio-Rad, USA)
- 10x ROTIPHORESE® 10x SDS-PAGE stock solution (Carl Roth, Germany)
- samples and controls

Procedure

1. If the 1x SDS running buffer is empty, dilute 10x SDS-PAGE stock solution to 1x. Mix 4.5 L water with 500 mL stock solution (stored at room temperature).

B. Standard lab protocols

2. Assemble the running module. If only one gel is run, use the buffer dam. The short plate of the casted gels faces the inside of the module.
3. Fill the running module with 1x running buffer. The wells are covered in buffer completely.
4. Prepare your samples: Work under the fume hood! Mix your protein samples with Laemmli buffer (ratio of 3:1). Incubate your samples for 5 min at 95 °C. Let them cool down before loading them onto the gel.
5. Check if the running module is tight. If, not reassemble it.
6. When the running module is tight, fill the chamber with 1x running buffer up to the marker.
7. Load 7.5 µL protein marker into well #1. Load 10 µL to 30 µL denatured protein sample into the remaining wells.
8. Place the lid onto the chambers. Ensure the lid is firmly on.
9. Turn the power supply on. Set voltage to a constant 130 V, and timer to 60 minutes. (Alternative: Set voltage to 80 V until the protein sample has passed the stacking gel. Then increase voltage to 130 V.)
10. Press run on power supply. You will know everything is connected properly if bubbles can be seen moving up from the electrode strip.
11. After 60 min the run is automatically stopped. Restart the run if the dye front hasn't reached the bottom of the gel yet.
12. Remove the gel cassette from the tank. Rinse it with water.
13. To open the cassette, insert the green opener into the slit and lever the glass plates apart.
14. Remove and discard the stacking gel. Gently remove the gel from the plate and put into tank filled with water for rinsing.
15. Continue with Coomassie staining or Western blotting.
16. Don't forget to clean the work space. (This includes wiping the surfaces with water.)

B.2. Blotting

Lab Protocol	Western blot transfer	09.09.2020
--------------	-----------------------	------------

This protocol describes the blotting procedure for transferring proteins separated by SDS-PAGE onto a PVDF membrane.

Potential hazards and safety precautions

Before starting work:

Obtain special instructions by qualified lab personnel.

Put on personal protective equipment (lab coat, nitrile gloves, safety glasses).

Read the safety data sheets.

Know the location of spill kits, eyewashes, safety showers.

Dangerous (toxic, flammable, ..) substances you are going to work with:

- Methanol

Disposure: Solutions containing methanol must be disposed into the liquid chemical waste container ("Flüssiger Chemikalienabfall"; fume hood, R1304). The polyacrylamide gels must be disposed of as hazardous chemical waste (blue barrels labeled "Fester Chemikalienabfall").

Materials

- SDS-PA gel containing separated protein samples
- dH₂O (VE-Wasser)
- Tris (Carl Roth, Germany)
- methanol, blotting grade (Carl Roth, Germany)
- glycine (Carl Roth, Germany)
- ROTI[®]PVDF membrane 0.45 (Carl Roth, Germany)
- gel blotting papers (Whatman GB005 Thickness 1.5 mm)
- blotting roller
- Trans-Blot Turbo system (Bio-Rad, USA)

Buffer recipes

Towbin blotting buffer

10x stock solution contains 250 mM Tris, 1.9 M glycine. Dissolve 30.3 g Tris and 142.6 g glycine in 1 L dH₂O. Stock solution is stored at room temperature.

1x Towbin blotting buffer contains 25mM Tris, 190mM glycine and 20 % (v/v) methanol. The buffer's pH will range between pH 8.1 to 8.5 depending on the quality of Tris, glycine, methanol and dH₂O used. For preparation of 250 mL 1x Towbin blotting buffer mix 25 mL 10x stock solution, 50 mL methanol and 175 mL dH₂O. Blotting buffer is stored at 4 °C.

Procedure

1. Prepare one tray containing methanol and two trays filled with 1x Towbin blotting buffer. Place the trays under the fume hood!
2. Equilibrate the gel in blotting buffer for 5 min.
3. Soak two blotting papers in blotting buffer and place them in the blotting cassette.
4. Pre-wet the PVDF membrane in methanol, then soak in 1x blotting buffer.
5. Assemble the blotting sandwich: two layers of soaked blotting paper, soaked PVDF membrane, equilibrated gel, one or two layers of soaked blotting paper.
6. Ensure removal of bubbles between gel and blotting paper using the blotting roller.
7. Close the blotting cassette and slot the cassette into to blotting device.
8. Run the transfer at 1 A, 25 V for 60 min.
9. Label the membrane orientation by placing an X at the upper right corner of the membrane.
10. Continue with Ponceau S or Western blot staining.

C. Acknowledgements

I would like to express my deepest gratitude to the following individuals for their invaluable support and guidance throughout my academic journey:

My mentor, Prof. Dr. Jörn Stitz, from the TH Köln for his expert advice, support and dedication to my research. His mentorship and feedback have been instrumental in shaping this work.

Prof. Dr. Thomas Scheper from the Leibniz University Hannover, for being my supervisor and supporting my work. Prof. Dr. Sascha Beutel and PD Dr. Ulrich Krings for reading and evaluating my thesis.

The staff of Miltenyi Biotec, especially Dr. Ian Johnston, Dr. Benjamin Theek and Lena Willnow, for providing a conducive research environment and access to resources that have enriched my study. Special thanks go to Monika Winkels for performing the excellent hybridoma fusion.

My dear colleagues at TH Köln, especially Natalie, Jamila, Yasemin, Anna and Tobias, for their stimulating discussions and support in keeping me motivated during the ups and downs of this research journey. Your companionship has made this experience more enjoyable.

My partner Dennis and my family, for their unconditional love, encouragement and understanding during this challenging academic pursuit. Your belief in me has been a constant motivation.

Lastly, I would like to express my heartfelt appreciation to my friends and my fellow volunteers from btS – Life Sciences Studierendeninitiative, who have indirectly contributed to this thesis. Your support and encouragement have been significant in my entire academic journey.

D. Curriculum vitae

Stefanie Schatz

geboren in Gummersbach, Deutschland

Ausbildung

- 04.2020–01.2024 **Promotionsstudiengang Chemie** an der Gottfried Wilhelm Leibniz Universität Hannover
- 04.2017–04.2019 **Master of Science in Molekularer und angewandter Biotechnologie** an der Rheinisch-Westfälischen Technischen Hochschule (RWTH) Aachen
- 10.2013–02.2017 **Bachelor of Science in Molekularer und angewandter Biotechnologie** an der RWTH Aachen
- 08.2006–08.2009 **Berufsausbildung zur Medizinisch-Technischen Laboratoriumsassistentin** an der Schule für Medizinisch-Technische Laboratoriumsassistenten, Uniklinikum Münster

Berufserfahrung

- 01.2023–04.2023 **Wissenschaftliche Mitarbeiterin** an der Fakultät für Angewandte Naturwissenschaften der Technischen Hochschule Köln
- 04.2019–07.2022 **Wissenschaftliche Hilfskraft** am Fraunhofer-Institut für Molekularbiologie und Angewandte Ökologie (IME), Aachen
- 02.2017–03.2017 **Forschungspraktikantin & wissenschaftliche Hilfskraft** am Institut für Anorganische Chemie, RWTH Aachen
- 05.2017–07.2017 **Forschungspraktikantin & wissenschaftliche Hilfskraft** am Institut für Anorganische Chemie, RWTH Aachen
- 12.2009–09.2013 **Medizinisch-Technische Laboratoriumsassistentin** am Universitätsklinikum Bonn

Ehrenamtliches Engagement

10.2019–10.2021 **Vorstand** der btS – Life Sciences Studierendeninitiative e.V. in Köln

03.2018–11.2018 **Projektleiterin** Organisation der Jahreshauptversammlung der btS –
Life Sciences Studierendeninitiative e.V.

E. List of publications

1. **Schatz, S. (70%)**; Willnow, L.; Winkels, M.; Rosengarten, J.F.; Theek, B.; Johnston, I.C.D.; Stitz, J. (2023), Generation of Antibodies Selectively Recognizing Epitopes in a Formaldehyde-Fixed Cell-Surface Antigen Using Virus-Like Particle Display and Hybridoma Technology. *Antibodies*, 12(3):57, doi: 10.3390/antib12030057
2. **Schatz, S. (75%)**; van Dijk, F.H.; Dubiel, A.E.; Cantz, T.; Eggenschwiler, R.; Stitz, J. (2023). Generation of Human 293-F Suspension NGFR Knockout Cells Using CRISPR/Cas9 Coupled to Fluorescent Protein Expression. In: Zielonka, S., Krah, S. (eds) *Genotype Phenotype Coupling. Methods in Molecular Biology*, vol 2681. Humana, New York, NY., doi: 10.1007/978-1-0716-3279-6_20
3. Rosengarten*, J.F.; **Schatz*, S. (47.5%)**; Stitz, J. (2022) Detection of Neutralization-sensitive Epitopes in Antigens Displayed on Virus-Like Particle (VLP)-Based Vaccines Using a Capture Assay. *J. Vis. Exp.*, (180), e63137, doi: 10.3791/63137
*both, J.F.R. and S.S., contributed equally
4. van Heuvel, Y.; **Schatz, S (10%)**; Hein, M.; Dogra, T.; Kazenmaier, D.; Tschorn, N.; Kupke, S.Y.; Reichl, U.; Genzel, Y.; Stitz, J. (2023) Novel suspension retroviral packaging cells generated by transposition using transposase encoding mRNA advance vector yields and enable production in bioreactors. *Front. Bioeng. Biotechnol.*, (11), doi: 10.3389/fbioe.2023.1076524
5. Rosengarten, J.F.; **Schatz, S. (15%)**; Wolf, T.; Barbe, S.; Stitz, J. (2022) Components of a HIV-1 vaccine mediate virus-like particle (VLP)-formation and display of envelope proteins exposing broadly neutralizing epitopes, *Virology*, 568, pp.41-48, doi: 10.1016/j.virol.2022.01.008
6. van Heuvel, Y.; **Schatz S. (10%)**; Rosengarten J.F.; Stitz, J. (2022) Infectious RNA: Human Immunodeficiency Virus (HIV) Biology, Therapeutic Intervention, and the Quest for a Vaccine. *Toxins*, 14(2):138, doi: 10.3390/toxins14020138